AFOSR-TR- 87-0819

Grant No: AFOSR-85-0218

BEHAVIOUR OF FIBRE-REINFORCED COMPOSITES UNDER DYNAMIC TENSION

K. Saka and J Harding
Department of Engineering Science
University of Oxford
Parks Road
OXFORD OX1 3PJ
UNITED KINGDOM

30 October 1986

Interim Report, 1st. May 1985 - 30th. April 1986

Approved for public release; distribution unlimited

Prepared for:

AFOSR/NA
Building 410
Bolling AFB
D. C. 20332

and

European Office of Aerospace
Research and Development
London
ENGLAND

PREFACE

This present interim report describes part of the third stage of an investigation into the mechanical properties of carbon/glass and carbon/kevlar fibre-reinforced composites under tensile impact loading. In the first stage, described in the Final Report on Grant No. AFOSR-82-0436 (issued August 1984), experimental equipment for the tensile impact testing of fibre-reinforced composite specimens was developed and the validity of the results obtained was confirmed. Composite specimens of various hybrid compositions were prepared and an initial series of tests was performed.

In the second stage* a microcomputing system was developed to allow rapid and accurate analysis of the experimental data, the gas gun and loading system was modified to permit easier access to the specimen and the accuracy of the elastic strain measurements was checked using strain gauges attached directly to the specimen. A complete set of results for impact tests at a rate of $\sim$1000/s on the five different carbon/glass hybrid lay-ups and a preliminary set of results on similar specimens at an intermediate rate of $\sim$10/s were presented and the broken specimens examined by optical and scanning electron microscopy. Analytical expressions relating the strength and stiffness of the hybrid specimens to the properties of the constituent plies and lamination parameters were derived.

This third report describes a continuation of the investigation, under Grant No. AFOSR-85-0218, for a period from 1st. May 1985 to 15th. November 1986, the present report relating to the first 12 months of this 18 month period.

*Described in the Final Report on Grant No. AFOSR-84-0092, issued September 1985.

unclassified

SECURITY CLASSIFICATION OF THIS PAGE

ADA182204

REPORT DOCUMENTATION PAGE

1a. REPORT SECURITY CLASSIFICATION: UNCLASSIFIED	1b. RESTRICTIVE MARKINGS
2a. SECURITY CLASSIFICATION AUTHORITY	3. DISTRIBUTION/AVAILABILITY OF REPORT: Approval for public release: distribution unlimited.
2b. DECLASSIFICATION/DOWNGRADING SCHEDULE	
4. PERFORMING ORGANIZATION REPORT NUMBER(S)	5. MONITORING ORGANIZATION REPORT NUMBER(S): AFOSR-TR- 87-0819
6a. NAME OF PERFORMING ORGANIZATION: Department of Engineering Science, University of Oxford	6b. OFFICE SYMBOL (If applicable): MIC
7a. NAME OF MONITORING ORGANIZATION: European Office of Aerospace Research and Development/LTS	
6c. ADDRESS (City, State and ZIP Code): Parks Road, Oxford OX1-3PJ, U.K.	7b. ADDRESS (City, State and ZIP Code): Box 14, FPO New York 09510
8a. NAME OF FUNDING/SPONSORING ORGANIZATION: AFOSR/NA	8b. OFFICE SYMBOL (If applicable): NA
8. PROCUREMENT INSTRUMENT IDENTIFICATION NUMBER: AFOSR 85-0218	
8c. ADDRESS (City, State and ZIP Code): Bolling AFB Bldg 410, Washington DC 20332	10. SOURCE OF FUNDING NOS.

PROGRAM ELEMENT NO.	PROJECT NO.	TASK NO.	WORK UNIT NO.
61102F	2302	B1	

11. TITLE (Include Security Classification): Behaviour of Fibre-Reinforced Composites under Dynamic Tension

12. PERSONAL AUTHOR(S): K. Sake and J. Harding

13a. TYPE OF REPORT	13b. TIME COVERED	14. DATE OF REPORT (Yr., Mo., Day)	15. PAGE COUNT
FINAL	FROM 1.5.85 to 30.4.86	1986 October 30	84

16. SUPPLEMENTARY NOTATION

17. COSATI CODES			18. SUBJECT TERMS (Continue on reverse if necessary and identify by block number)
FIELD	GROUP	SUB. GR.	
			Fibre-reinforced composites, DYNAMIC TENSION, Tensile impact testing, Hopkinson bar

19. ABSTRACT (Continue on reverse if necessary and identify by block number)

Epoxy specimens reinforced with plain-weave fabrics of either carbon or glass or with several hybrid combinations of the two in various layups, giving five different weight fractions of reinforcement from all-carbon to all-glass, have been tested in tension at an intermediate strain rate of ~10/s and a quasi-static strain rate of $\sim 10^{-3}$/s. Stress-strain curves are obtained and are compared with those derived in an earlier stage of the investigation at an impact strain rate of ~1000/s. The effect of both hybrid composition (volume fraction of carbon reinforced plies) and applied strain rate on the tensile modulus, the tensile strength and the strain to fracture is determined and a limited hybrid effect is observed in specimens with a carbon volume fraction in the approximate range 0.6 to 0.7 where, at all three strain rates, there is an enhancement of the failure strain over that for the all-carbon plies and an increased failure strength, most marked in the impact tests, over that predicted by the rule of mixtures. (KEYWORDS)

Two-dimensional stiffness matrices for the all-glass and the all-carbon reinforcing plies

20. DISTRIBUTION/AVAILABILITY OF ABSTRACT	21. ABSTRACT SECURITY CLASSIFICATION
UNCLASSIFIED/UNLIMITED ☒ SAME AS RPT. ☐ DTIC USERS ☐	

22a. NAME OF RESPONSIBLE INDIVIDUAL	22b. TELEPHONE NUMBER (Include Area Code)	22c. OFFICE SYMBOL
ANTHONY K AMOS	(202) 767-4937	AFOSR/NA

DD FORM 1473, 83 APR — EDITION OF 1 JAN 73 IS OBSOLETE.

UNCLASSIFIED

SECURITY CLASSIFICATION OF THIS PAGE

19. Abstract (continued)

have been determined under quasi-static loading. Previous analytical predictions for the hybrid moduli based on classical laminate theory and assuming the same properties in the warp and weft directions have been modified to allow for different moduli in these two directions. Using the experimentally determined stiffness matrices for the all-glass and all-carbon plies predicted hybrid moduli have been obtained and are found to agree well with both the experimental values of hybrid moduli and the rule of mixtures predictions.

CONTENTS

1. INTRODUCTION

Current concern with the poor impact resistance of advanced composites using carbon reinforcing fibres and with the marked degradation in their subsequent mechanical properties following micro-damage developed under sub-critical impact loading has strongly emphasised the need to obtain a full and accurate characterisation of the impact mechanical response of such materials. The present programme arose in response to this need and followed the successful development at Oxford of a tensile impact test for composite materials based on the split Hopkinson's pressure bar principle. Using this technique the tensile impact response of several different fibre-reinforced composites has been determined. The results obtained showed very little effect of strain rate on the behaviour of carbon-fibre-reinforced specimens but a very significant increase with strain rate in the modulus, strength and ability to absorb energy in glass-fibre-reinforced specimens.

Arising from these observations the primary aim of the present programme is to determine the room-temperature tensile stress-strain response of various hybrid composites of carbon and glass and carbon and kevlar and of their constituent plies over a range of strain rates from quasi-static ($\sim 10^{-3}$/s) to impact ($\sim$1000/s), to investigate by optical and scanning electron microscopy the operative micromechanisms of deformation and fracture and to determine how far hybridisation allows an optimisation of the mechanical properties under impact loading. The first two progress reports described the development of the experimental equipment and microcomputing system, the design of specimen and the various hybrid lay-ups and presented experimental results for tests at impact and intermediate rates of straining, $\sim$1000/s and $\sim$10/s respectively. In an appendix to the second report analytical expressions were developed relating the strength and stiffness of the hybrid specimens to the properties of the constituent plies and the lamination parameters.

The current report describes a continuation of this programme and presents a complete set of results for the carbon/glass hybrids tested in tension at three rates of strain, $\sim$1000/s, $\sim$10/s and a quasi-static rate of $\sim 10^{-3}$/s. The effect of hybrid weight fraction at each strain rate and of strain rate on specimens having a given hybrid weight fraction are determined. Tests have also been performed, at the quasi-static rate, to determine the two-dimensional stiffness matrix of both the glass-reinforced plies and the carbon reinforced plies and the results used to check the analytical expressions for the stiffness of the various hybrids as derived in the second progress report. To check the corresponding analytical expressions for hybrid strength the compressive strengths of the carbon and the glass plies need to be measured and apparatus to allow this under impact loading has been developed. During the remaining six months of the present grant period it is planned to determine the two-dimensional stiffness matrix of both the carbon and the glass plies under impact loading and to measure the compressive strengths of the two types of ply under both quasi-static and impact loading and hence to check the analytical expressions at the two rates. It is also hoped to complete the examination of the micromechanisms of failure at the three rates of loading by optical and scanning electron microscopy.

2. EXPERIMENTAL PROCEDURE

The first and second progress reports, references (1) and (2), issued August 1984 and September 1985, gave full details of the testing equipment used for tests at both impact and intermediate rates of strain, ∿1000/s and ∿10/s respectively. To complete the range of strain rates covered, tests have now been performed at a quasi-static rate of $\sim 10^{-3}$/s using a standard screw-driven Instron testing machine and a brief description of the experimental arrangement is given in section 2.1 below. This is followed by section 2.2 which describes the techniques used for determining the quasi-static two-dimensional stiffness matrix for the all-carbon and all-glass laminates on which the analytical predictions of the hybrid stiffnesses are based.

Although balanced plain-weave fabrics have been used for both the carbon and the glass reinforcement in the various hybrid specimens, results presented in the second progress report suggested that the mechanical properties in the warp and the weft directions might differ slightly. This was confirmed for the all-carbon and the all-glass laminates in the quasi-static tests referred to above. A series of tests was performed, therefore, at impact rates using the modified version of the gas gun described in the second progress report, on all-glass and all-carbon specimens to determine the effect of strain rate on the difference in the warp and the weft mechanical properties. These are the first test results to be reported on from the modified gas gun. Problems associated with the stress fluctuations on the loading pulse and their effect on the accuracy of the wave analysis during the early stages of the Hopkinson-bar analysis are discussed in section 2.3 below.

In connection with the analytical predictions of hybrid strength, described in the appendix to the second progress report, it is necessary to determine the compressive failure strength of the all-carbon and the all-glass laminates. An experimental rig for determining the impact compressive strength is described in section 2.4.

2.1 Quasi-Static Tests

For the quasi-static tests the same load cell, specimen grips and displacement measurement technique, employing the integrated output from two velocity transducers, as described in the second progress report for the intermediate rate tests, are again used, the only difference being that the load is applied more slowly using a screw-driven Instron testing machine. Again strain gauges attached to the specimen parallel gauge

---

(1) Saka, K. and Harding, J., "Behaviour of Fibre-Reinforced Composites under Dynamic Tension", Final Report on Grant No. AFOSR-82-0346, August 1984 (Oxford University Engineering Laboratory Report No. OUEL No. 1543/84).

(2) Saka, K. and Harding, J., "Behaviour of Fibre-Reinforced Composites under Dynamic Tension", Final Report on Grant No. AFOSR-84-0092, September 1985 (Oxford University Engineering Laboratory Report No. OUEL No. 1602/85.

section provide a check of the strain, and hence of the tensile modulus, while the deformation is elastic. Output signals from the load cell strain gauges, the velocity transducers and the specimen strain gauges are stored in two dual-channel transient recorders and are subsequently processed on a microcomputer to obtain two stress-strain curves derived from the load cell signal and either the velocity transducers or the specimen strain gauges. Two such curves for a test on an all-carbon specimen are compared in fig. 1 from which it is apparent that the velocity transducers overestimate the specimen strain, presumably because they also measure the deflection in the grips, and the specimen strain gauges fail well before final failure of the specimen. To obtain a corrected stress-strain curve for the test, therefore, the strain measured from the velocity transducers is reduced to give an initial slope to the stress-strain curve in agreement with that from the specimen strain gauges. In test on all-glass specimens, for which the initial tensile modulus is less than half that for the all-carbon specimens, the velocity transducers were found to underestimate the true specimen strain, see fig. 2, and the required correction is in the opposite direction. This is presumably because the specimen grips make a much less significant contribution to the overall displacement measured by the velocity transducers in tests on the more flexible all-glass specimens.

2.2 Determination of the Quasi-Static Stiffnes Matrix

For all the above quasi-static tests standard tensile specimens, waisted in the thickness direction as described in the earlier reports, (see fig. 2 of ref. (2)), were used. In determining the quasi-static stiffness matrix, however, although the same experimental set-up was employed, the test specimens were parallel sided coupons taken from the all-glass or all-carbon laminates and with the loading axis in either the warp or the weft directions or at 45^{o} to both warp and weft directions. Strain gauge rosettes were attached to either side of the specimens, as shown schematically in fig. 3, and a digital microvoltmeter was used to measure the strain gauge outputs as each specimen was loaded and unloaded several times within the elastic range. Finally each specimen was loaded through to failure, usually by pull-out of the specimen from the grips, the various load cell, velocity transducer and specimen strain gauge signals being stored in transient recorders in the usual way. Raw data from one such test on an unwaisted all-carbon specimen loaded in the warp (A) direction is shown in figs. 4a, b and c, for the load cell, the velocity transducer and the two specimen strain gauge directions respectively, each curve being a direct plot of the corresponding datafile as stored in the microcomputer. The derived variation of stress with strain in the loading direction determined from the specimen strain gauges is shown in fig. 5, the slope of which gives for the modulus in the warp direction a value of 47.6 GPa. By comparing the specimen strain gauge signals for the two orthogonal directions, longitudinal and transverse, see fig. 6, a Poisson's ratio, ν_{AB}, of 0.119 is obtained.

2.3 Tests using the Modified Gas Gun

Although the split Hopkinson's pressure bar (SHPB) test assembly de-

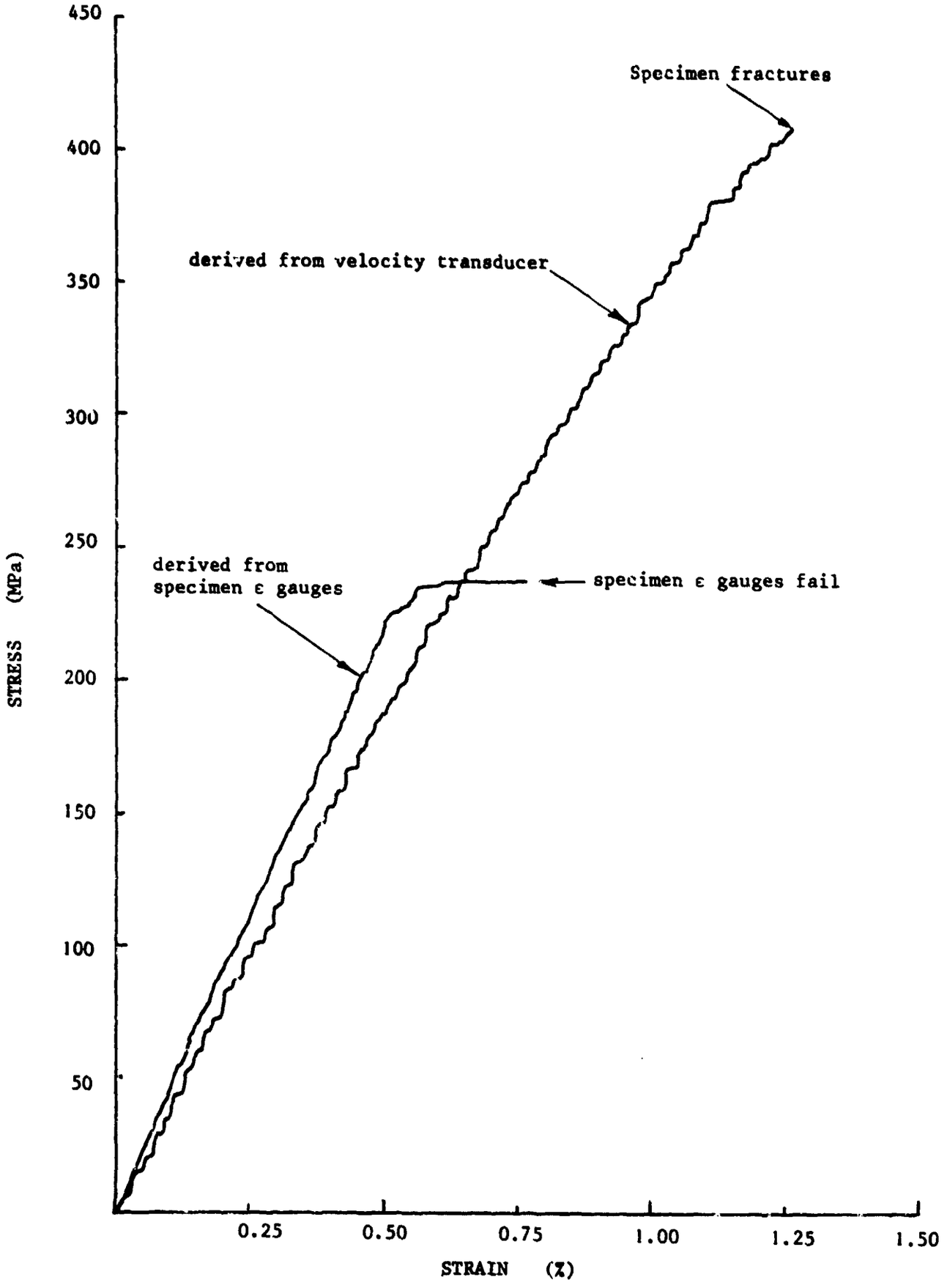

Fig.1 QUASI-STATIC STRESS-STRAIN CURVES FOR AN ALL-CARPON SPECIMEN

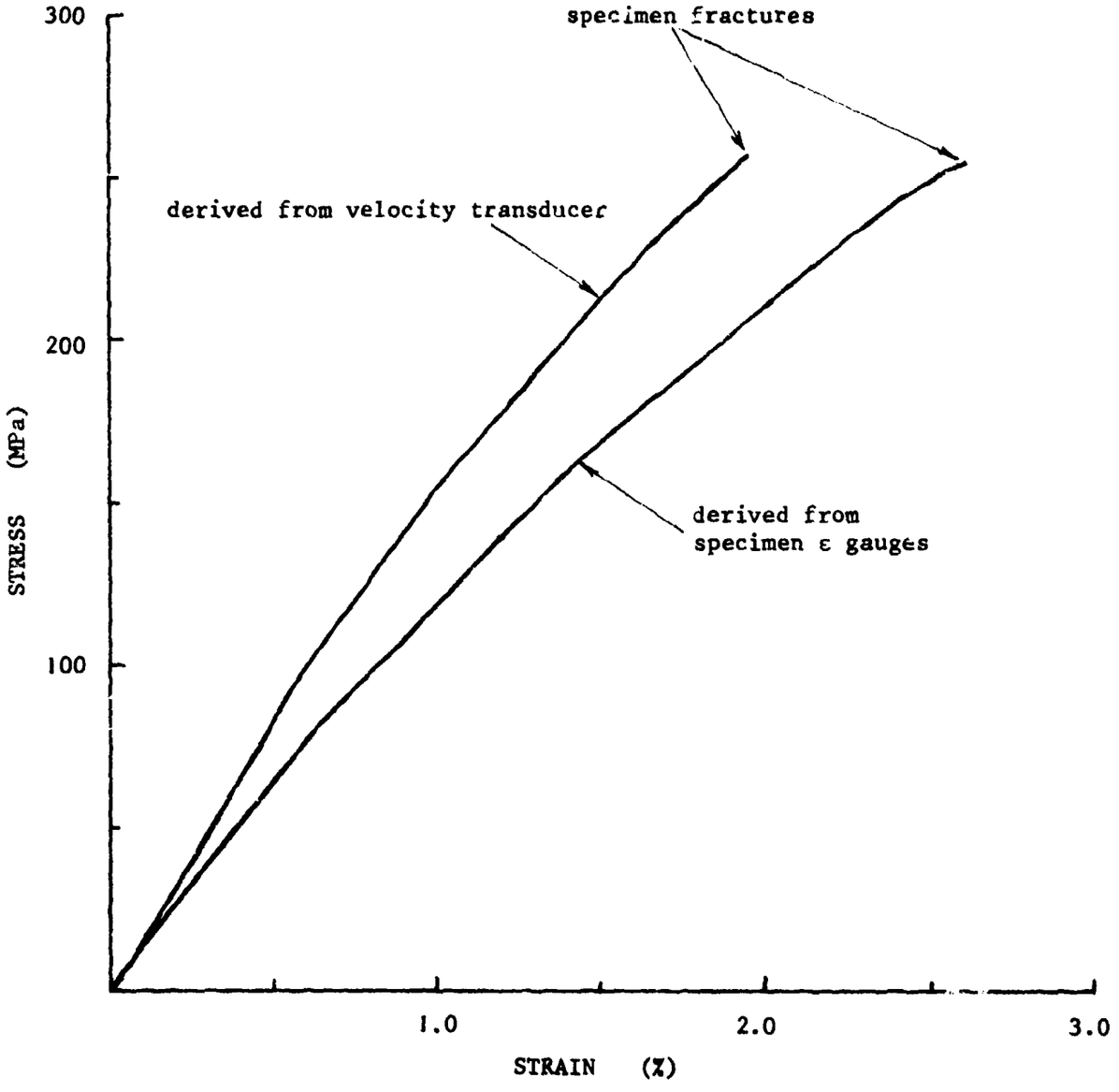

Fig.2 QUASI-STATIC STRESS-STRAIN CURVES FOR AN ALL-GLASS SPECIMEN

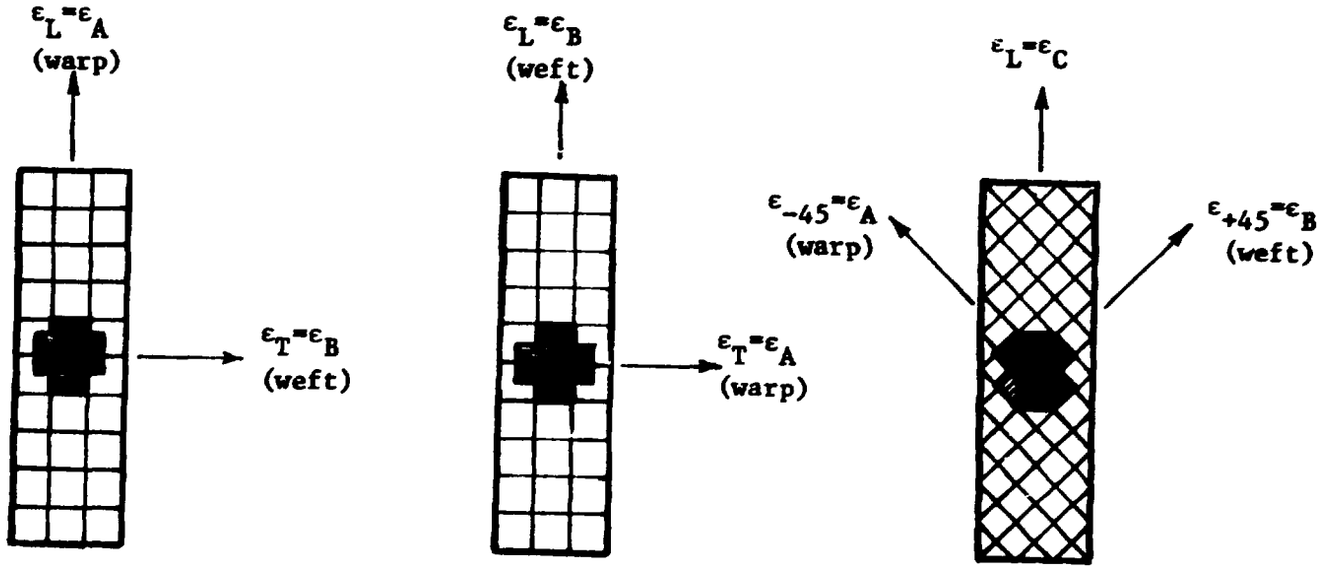

Fig. 3 TEST SPECIMENS FOR STIFFNESS MATRIX DETERMINATION

Fig.4 RAW DATA FOR ELASTIC TEST ON AN ALL-CARBON SPECIMEN LOADED IN THE WARP (A) DIRECTION

a) Load Cell Signal

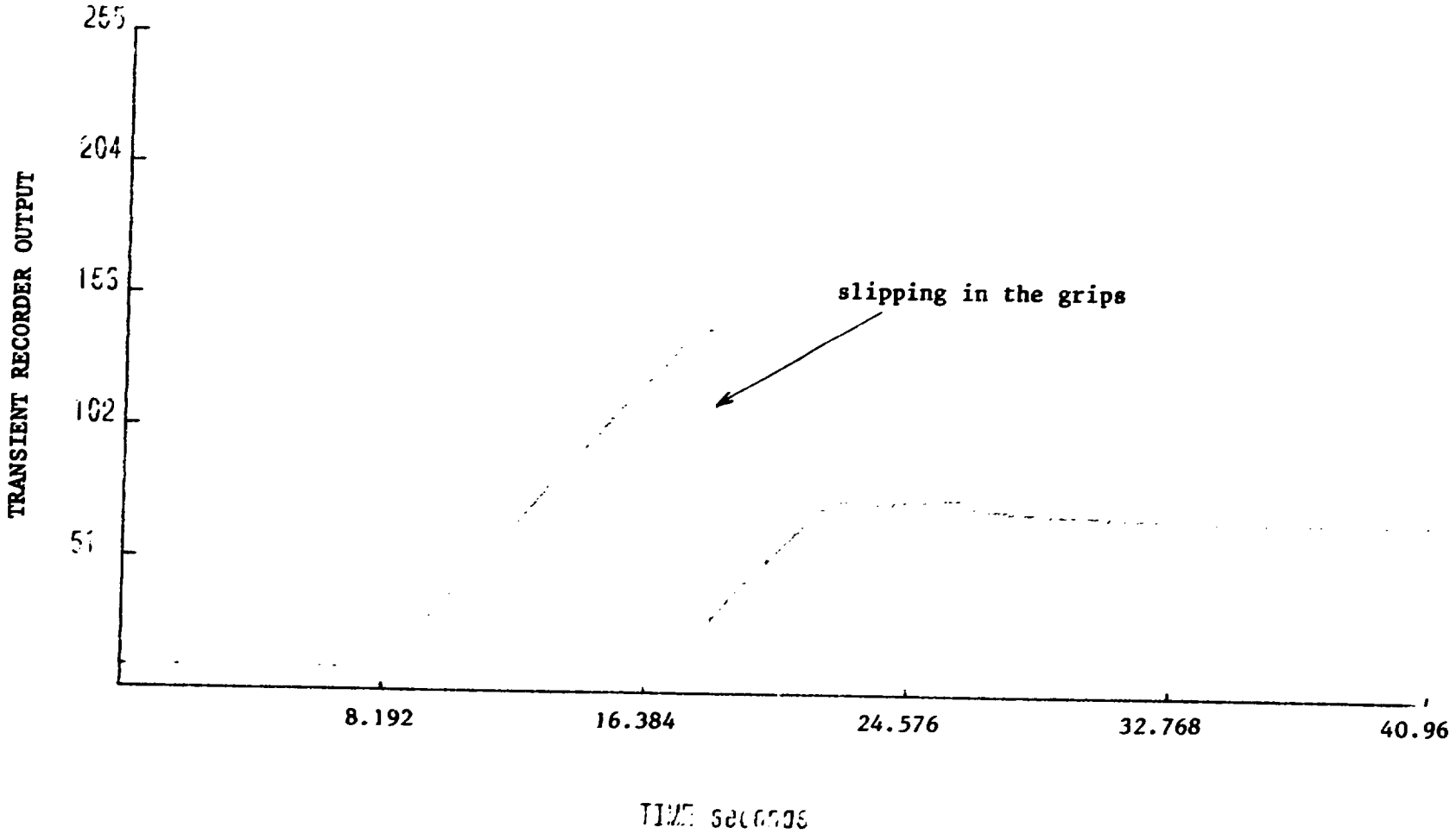

4b) Integrated Velocity Transducer Signal

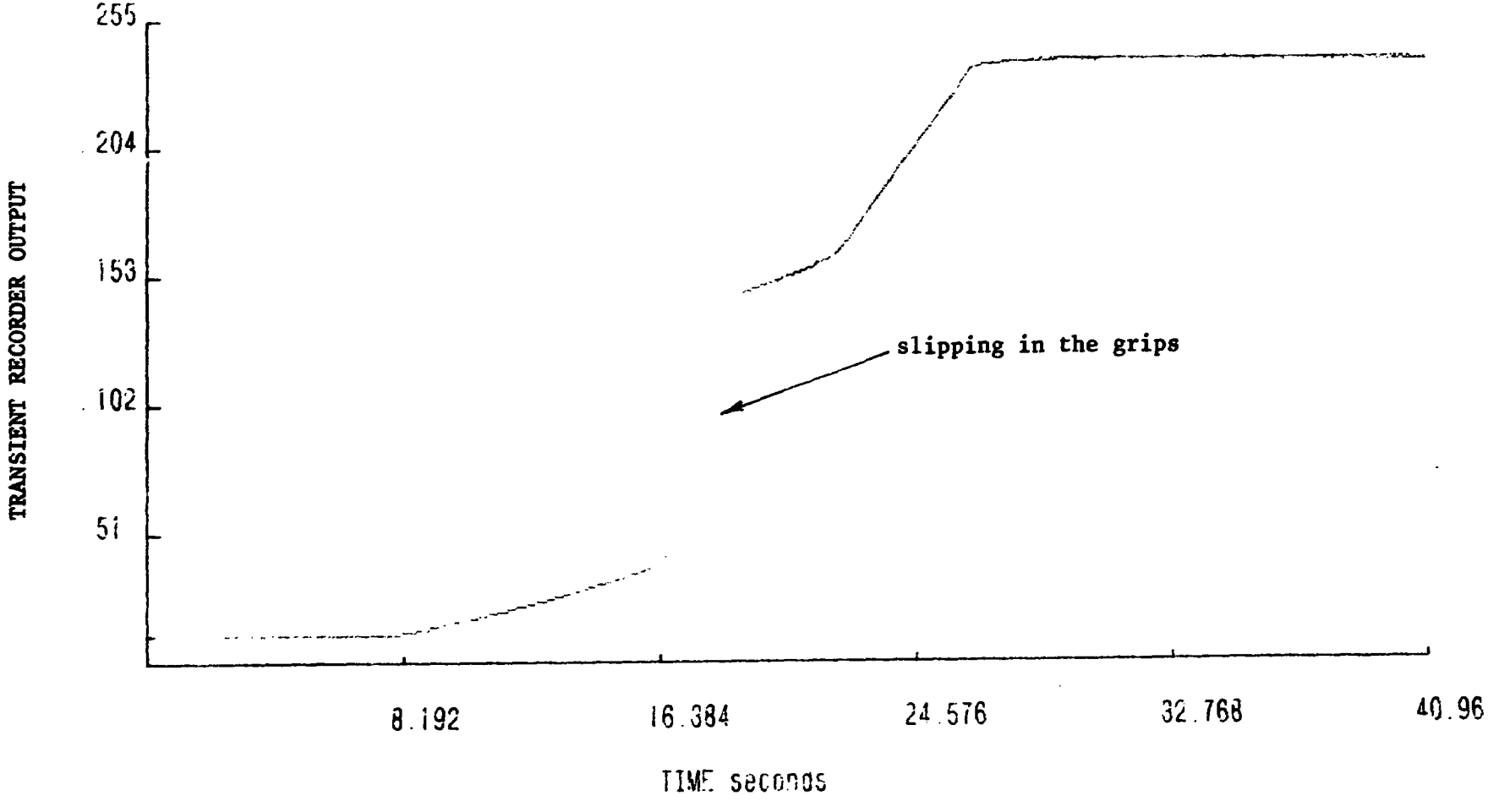

4c) Specimen Strain Gauge Signals

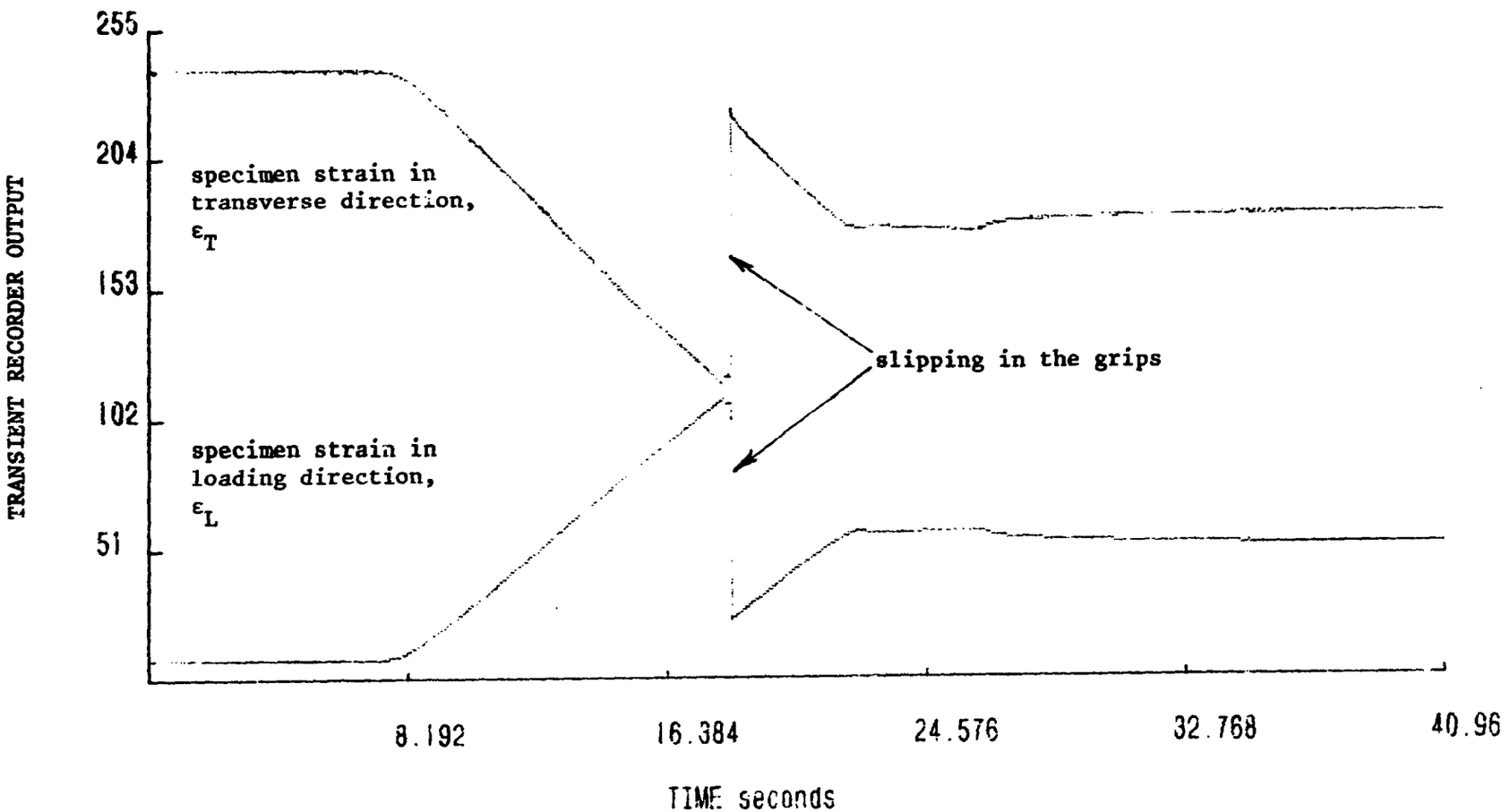

Fig.5 STRESS (σ) v. LONGITUDINAL STRAIN (ϵ_L) FOR TEST OF Fig.4

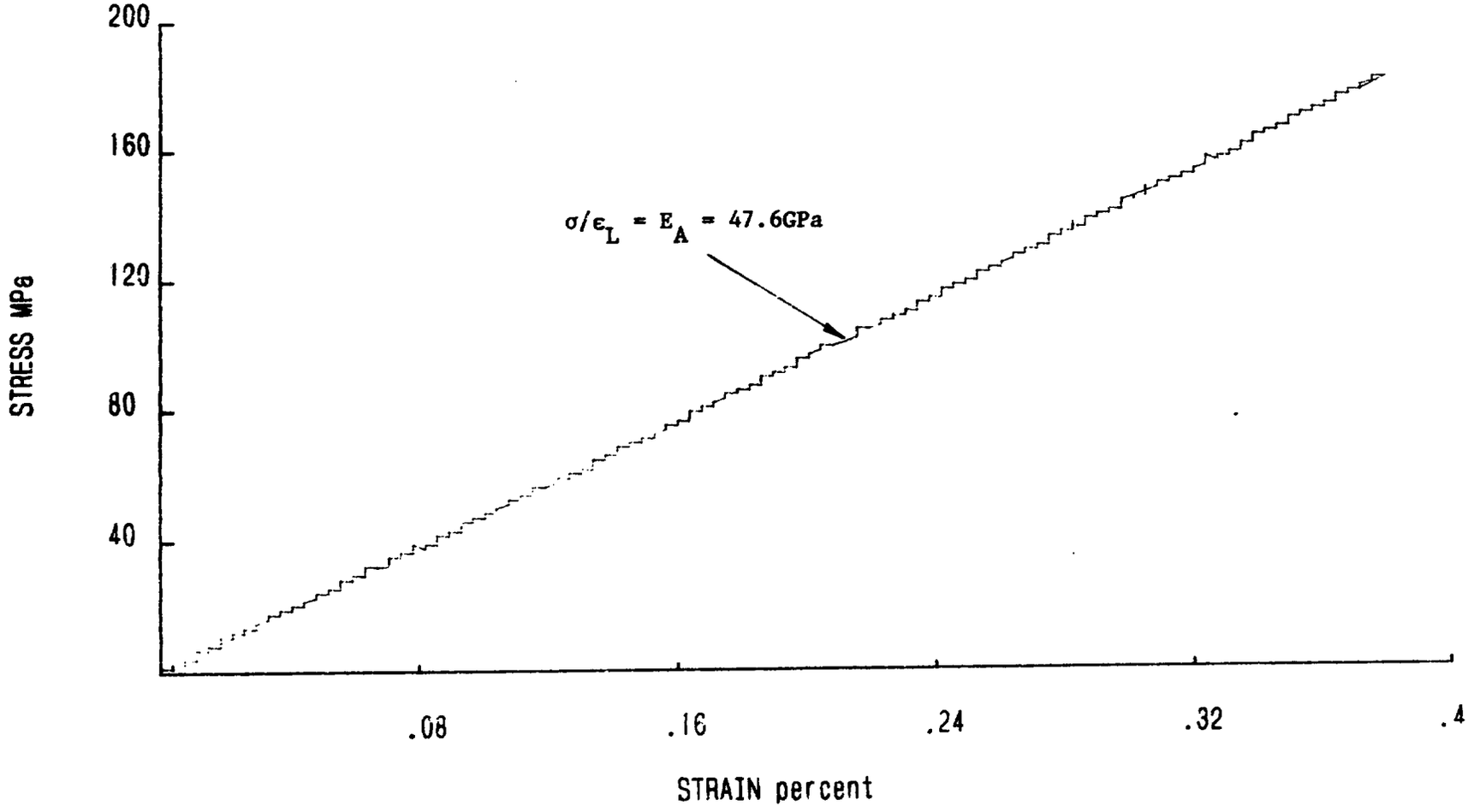

Fig.6 TRANSVERSE STRAIN (ϵ_T) v. LONGITUDINAL STRAIN (ϵ_L) FOR TEST OF Fig.4

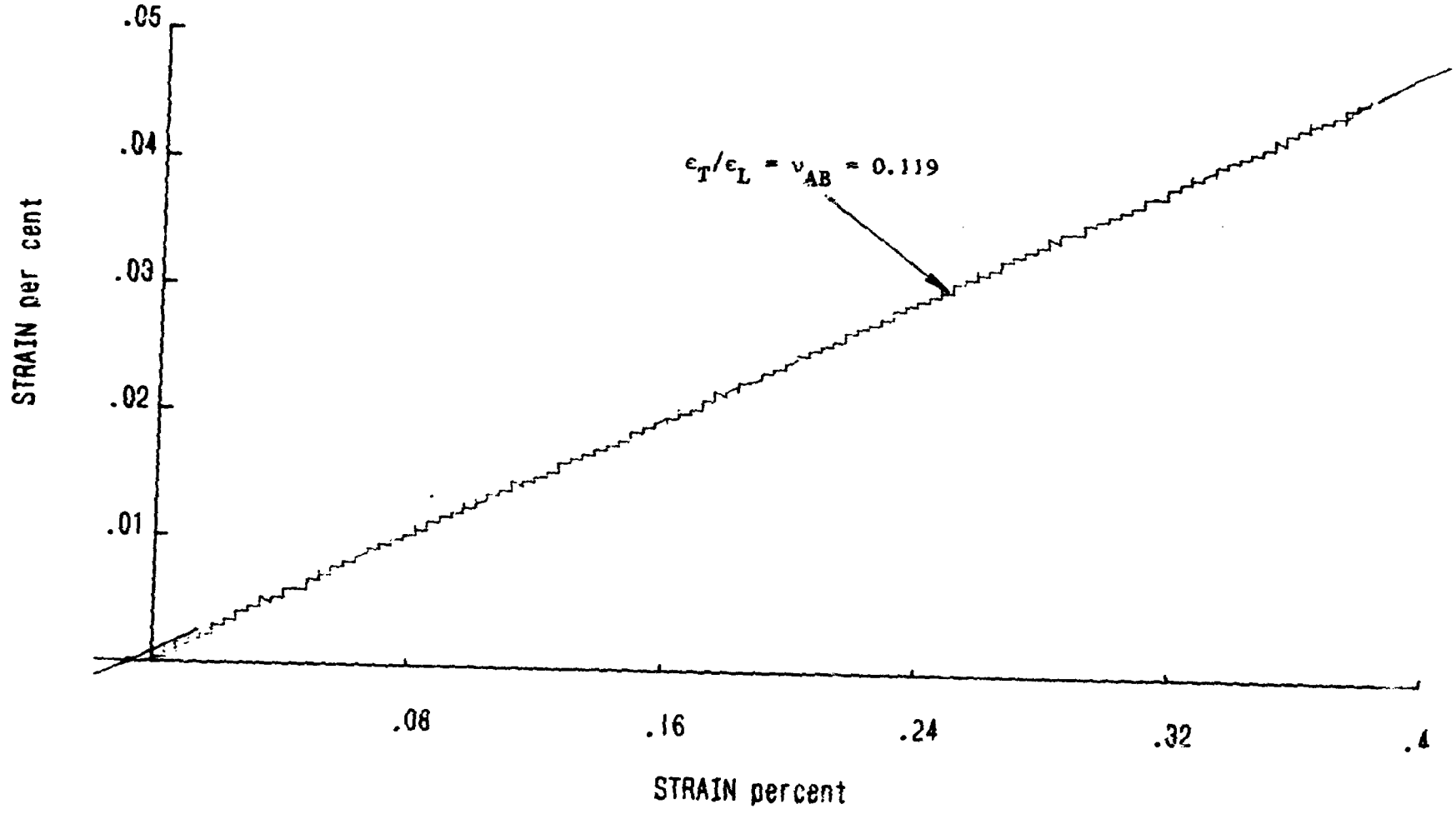

scribed previously, involving two 9.5mm diameter loading rods either side of the thin strip specimen, remains unaltered the method by which the incident loading wave is generated has changed in the development of the modified gas gun. In particular, a hollow cylindrical tube, rather than a solid cylindrical bar, is now used as the projectile and the impact is against a large diameter block attached to a solid loading bar, rather than a hollow tube within which the test assembly was previously contained. These differences have led to an incident loading pulse with rather stronger initial stress fluctuations than before, as may be seen in fig. 7 which shows the raw data, as stored in the microcomputer before processing, for gauge signals I (incident pulse) and II (reflected pulse) from a test at ∿10m/s on an all-carbon specimen. The corresponding signals from the output bar, gauge III, and the specimen strain gauges, ε_g, are shown in fig. 8.

The first part of the analysis converts the signals from gauges I and II to stress-time curves and adjusts them to the same time origin, as shown in fig. 9. The two curves should coincide up to the arrival of the reflected wave at the second gauge station, i.e. after a delay of 16.96 microseconds. They should then diverge as they are seen to do in fig. 9. The second stage of the analysis uses the difference between these two curves to derive the stress and velocity at the input end of the specimen and compares this stress with that at the output end of the specimen which is measured directly at gauge station III. Ideally these two stress measurements should show close agreement after the first few microseconds, during which time equilibrium across the specimen is being set up. In practice the stress derived at the input end is very sensitive to the difference between the two stress-time curves of fig. 9 and the fluctuating incident (gauge I) signal makes accurate determination of this stress very difficult. Consequently the agreement between the input and the output stresses, see fig. 10, is not as good as was generally found with the earlier loading system. While it is hoped that further modifications to the loading system will lead to an improved agreement it has, nevertheless, always been the practice to base all specimen stress calculations on the output bar stress signal since this is measured directly.

Also of importance is the accuracy with which the specimen strain can be determined. Previously (see fig.7 of the second progress report) very good agreement was obtained between the specimen strain as determined by the Hopkinson bar analysis with that derived from the specimen strain gauges. In the present tests, however, the Hopkinson bar analysis significantly overestimates the specimen strain leading, as shown in fig. 11, to an apparent initial modulus of 36.6GPa, much less than the value of 49.8GPa derived directly from the specimen strain gauges. Although the determination of the velocity at the input end of the specimen, on which the Hopkinson bar analysis of strain depends, is less sensitive than the stress to small variations in the gauge I and gauge II signals of fig. 9, the stress fluctuations on the gauge I signal are likely to be the cause of the overestimate of strain in the early stages of deformation and hence of the inaccurate measure of the initial modulus. In the light of the earlier impact results, described in the first and second progress reports, the final stress-strain curve for the test of fig. 11 is obtained by adjusting the initial linear region of the full Hopkinson-bar curve to have the increased slope given by the specimen strain gauges. The

Fig.7 RAW DATA FOR IMPACT TEST ON AN ALL-CARBON SPECIMEN

(Input bar strain gauge signals)

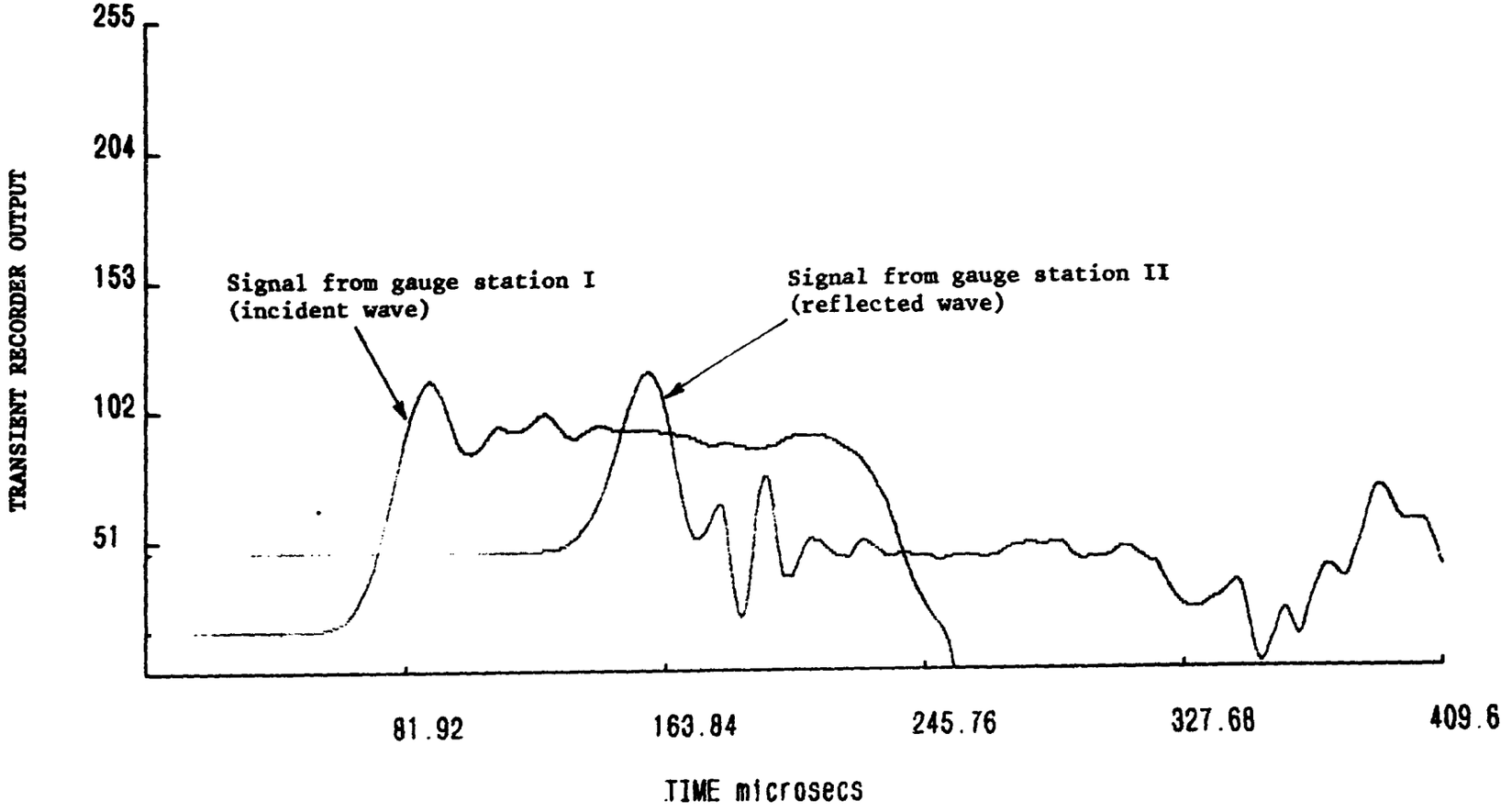

Fig.8 RAW DATA FOR IMPACT TEST ON AN ALL-CARBON SPECIMEN

(Specimen and output bar strain gauge signals)

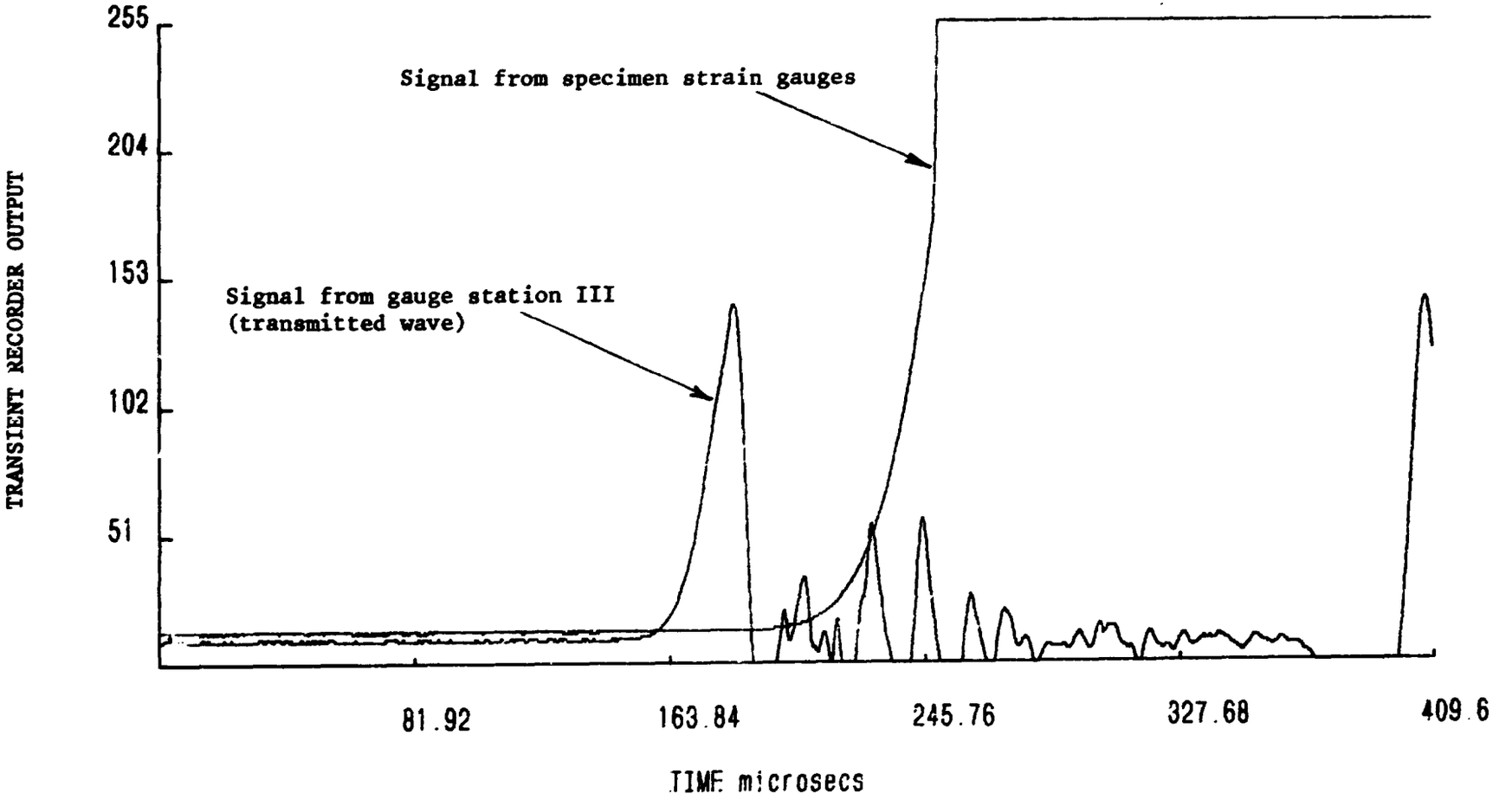

Fig.9 COMPUTED STRESS-TIME SIGNALS FOR GAUGES I AND II FROM DATA OF Fig.7

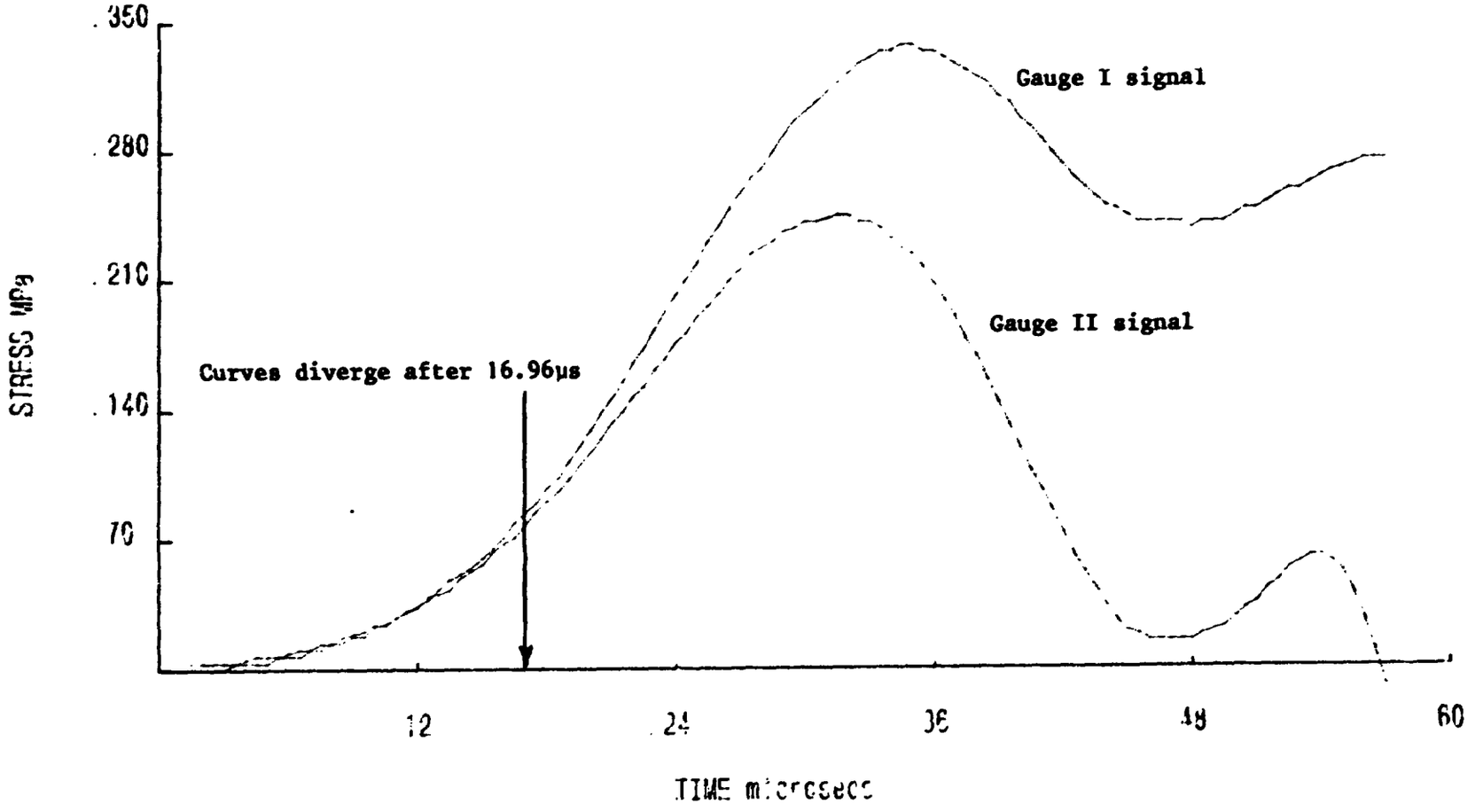

Fig.10 COMPUTED INPUT AND OUTPUT STRESS SIGNALS FROM DATA OF Figs.7 AND 8

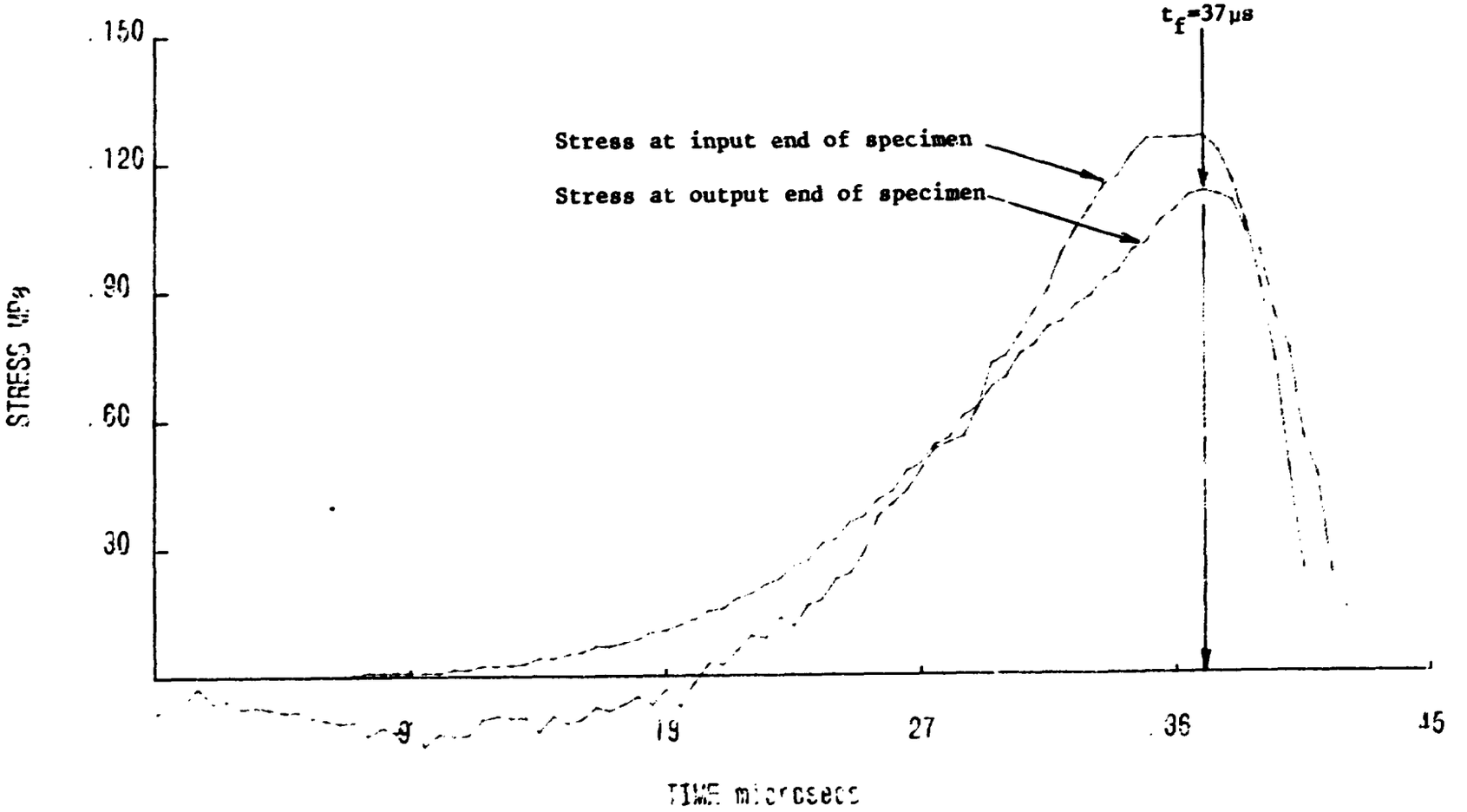

Fig.11 COMPUTED STRESS-STRAIN CURVES FROM DATA OF Figs.7 AND 8

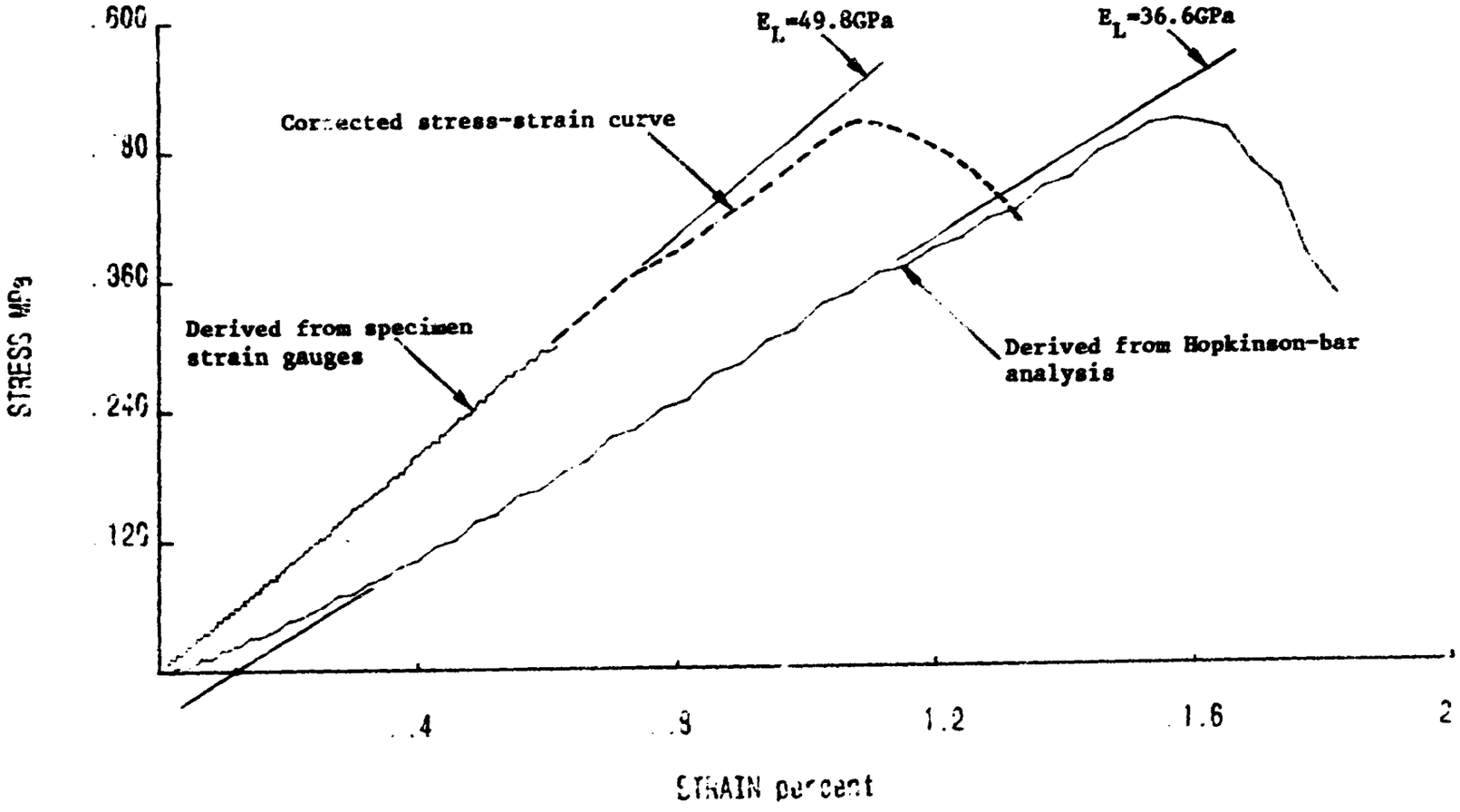

resulting stress-strain curve is shown dashed in fig. 11. In consequence the fracture strain, taken as the strain at maximum stress, is reduced from 1.58% to 1.10% and the mean strain rate, taken as the fracture strain divided by the time to fracture, as defined in fig. 10, from 427/s to 279/s.

2.4 Experimental Rig for Impact Compression Tests

Following the proposal in the second progress report to check analytical predictions for the moduli and strengths of the carbon/glass hybrids from measurements of the stiffness matrix and the tensile and compressive strengths for the all-glass and the all-carbon laminates it became necessary to design an experimental rig for determining the impact compressive strengths in both warp and weft directions for specimens cut from these laminates. In previous work on the impact compressive strength of reinforced plastic materials short cylindrical type specimens have normally been used (3,4). This, however, is not a recommended design of specimen for composites testing, being susceptible to frictional end effects which could mask the true material response. Nor could such specimens be prepared from the laminates used in the production of the standard tensile specimens. Since, however, the thin strip specimen waisted in the thickness direction is the recommended design for quasi-static compression, as well as tension, testing, it is proposed in the present impact compression tests to use specimens of identical dimensions to those tested in tension. The test assembly, which is shown schematically in fig. 12a, is impacted by a projectile of 12.5mm diameter by 330mm long fired from a small air-gun at velocities up to ~20m/s.

The compression loading rig shown in fig. 12a may also be used to apply a transverse impact loading to plate type specimens, see fig. 12b. A photograph illustrating the small air-gun and the transverse plate impact loading arrangement is shown in fig. 13. Under such a loading system a greater hybrid effect might well be expected if the glass-fibre reinforced plies are situated in those regions of the specimen experiencing the largest deformations. A few exploratory tests are planned, therefore, in which the same laminates as have been used in the preparation of the tensile test specimens are also subjected to controlled transverse impact loading.

---

(3) Sierakowski, R. L., Nevill, G. E., Ross, C. A. and Jones, E. R., "Dynamic compressive strength and failure of steel reinforced epoxy composites", J. Comp. Mat., 5, (1971), 362-377.

(4) Griffiths, L. J. and Martin, D. J., "A study of the dynamic behaviour of a carbon fibre composite using the split Hopkinson pressure bar", J. Phys. D., Appl. Phys., 7, (1974), 2329-2341.

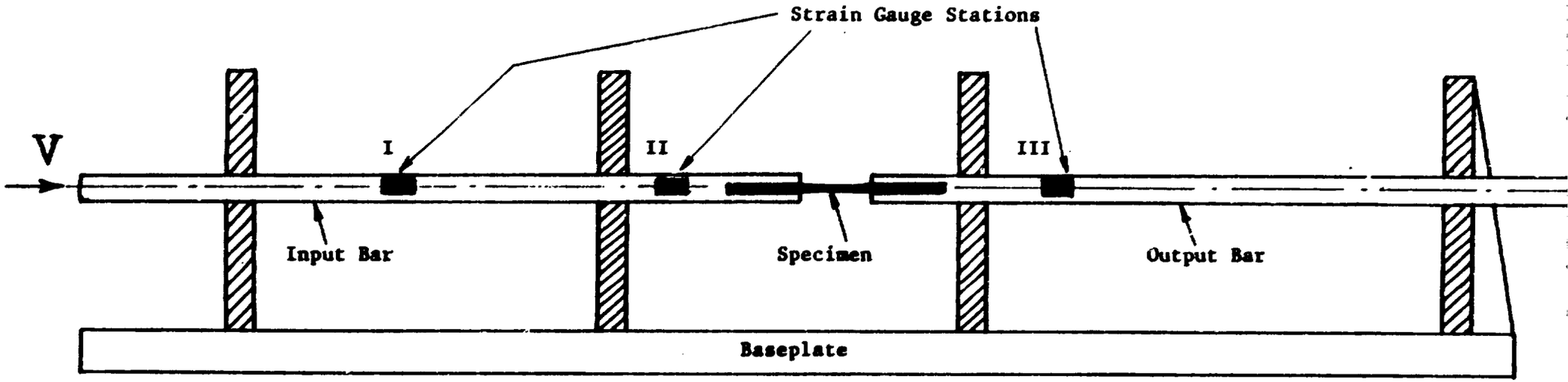

Fig.12a Test Rig for Impact Compression Tests

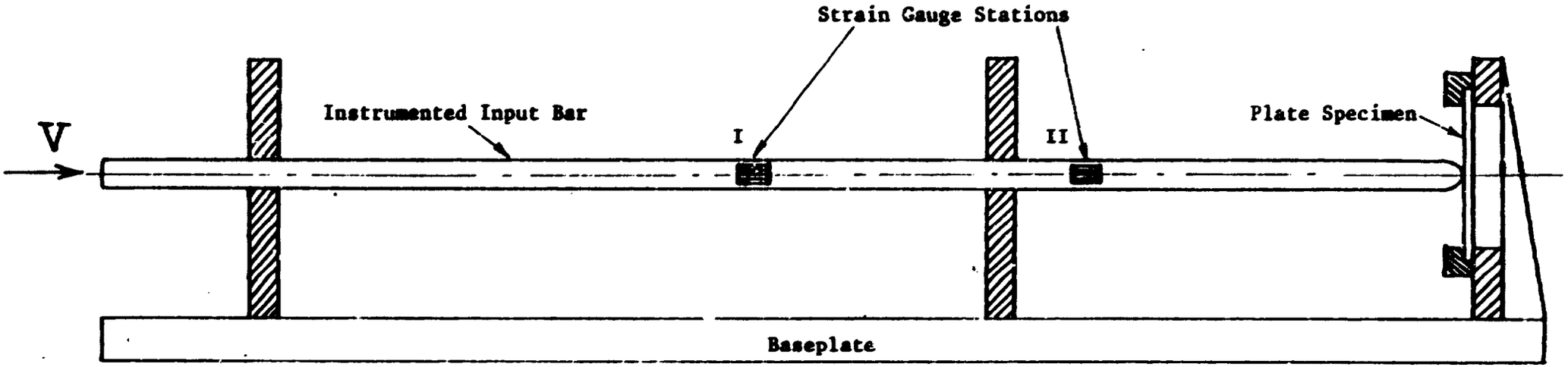

Fig.12b Test Rig for Transverse Impact Tests

Fig.13 SMALL AIR-GUN AND TRANSVERSE IMPACT TEST ASSEMBLY

3. EXPERIMENTAL RESULTS

The second progress report gave a complete set of results for impact tests on the all-glass, the all-carbon and the three hybrid specimen lay-ups. At the intermediate rate, however, only one test result was available for the all-carbon and the type 2a hybrid specimens and the corresponding stress-strain curves showed a somewhat anomalous behaviour in comparison with that for the other three types of specimen at this rate in the light of the behaviour found at impact rates. Further tests have now been performed at the intermediate rate on the all-carbon and type 2a hybrid specimens and these are described in section 3.1 below. To complete the range of strain rates covered these tests were followed by a complete set on all five specimen types at a quasi-static rate of $\sim 10^{-3}$/s. These are described in section 3.2. Also at the quasi-static rate, elastic tests were performed on the all-glass and the all-carbon laminates, on specimens cut with the tensile axis in either the warp or the weft directions, or at 45° to both these directions, to determine the two-dimensional stiffness matrix required for predicting the elastic properties of the hybrid specimens. These results are presented in section 3.3.

The previous suggestion, in the second progress report, that the mechanical properties of the laminates might be different in the warp and weft directions, is strengthened by the results described in section 3.1 and confirmed by the results reported in section 3.3. A further set of impact tests, therefore, was performed on the all-glass specimens in both warp and weft directions and on the all-carbon specimens in the weft direction, using the modified gas-gun. Whereas it was known that in the first set of impact tests on the all-carbon material, the specimens had been loaded in the warp direction, there was a suspicion that the first set of impact tests on the all-glass material had used a mixture of specimens cut in both warp and weft directions, since at this stage it had not been realised that the difference might be important. The results of the impact tests on the modified gas-gun are presented in section 3.4.

3.1 Intermediate-Rate Tests

Three more tests were performed on all-carbon specimens at a strain rate of ~8/s. These specimens were cut with the tensile axis in the weft direction and the resulting stress-strain curves all agreed closely with the single result given earlier in the second progress report. The four stress-strain curves are compared in fig. 14. Further tests were also performed on the type 2a hybrid specimens. Stress-strain curves for five such tests at a strain rate of ~11/s are shown in fig. 15. Although the scatter between individual tests is a little greater here it is not too great to mask a significant difference between the present results, for specimens thought to have been loaded in the warp direction, and the earlier single test on a specimen thought to have been loaded in the weft direction, which had a lower strength and a lower strain at failure. This curve is also shown in fig. 15.

Mean stress-strain curves for the five types of specimen tested at the intermediate rate are compared in fig. 16. Although the general behaviour shown is similar to that observed at impact rates with, for ex-

Fig.14 INTERMEDIATE RATE STRESS-STRAIN CURVES FOR ALL-CARBON SPECIMENS

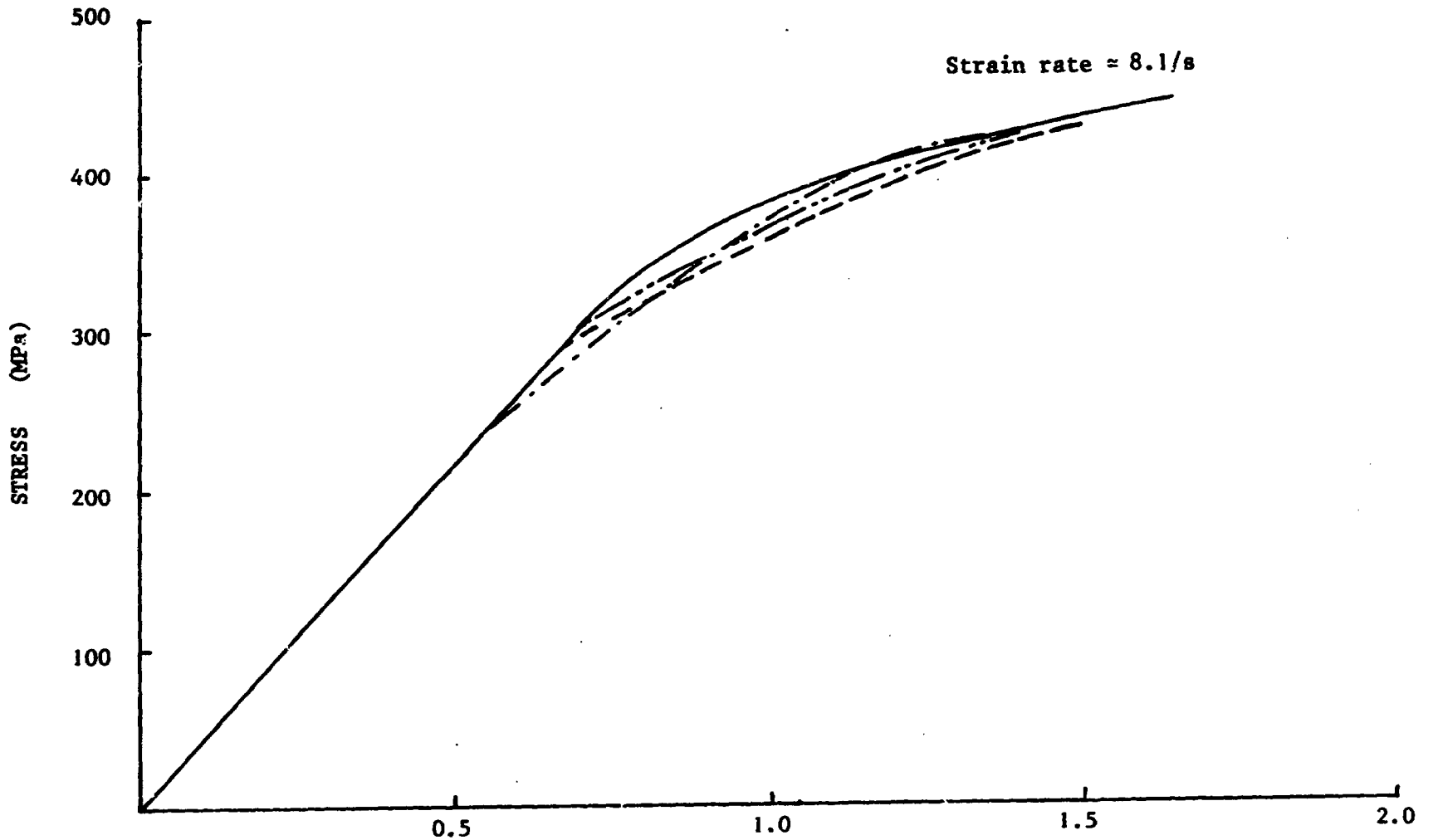

Fig.15 INTERMEDIATE RATE STRESS-STRAIN CURVES FOR TYPE 2a HYBRID SPECIMENS

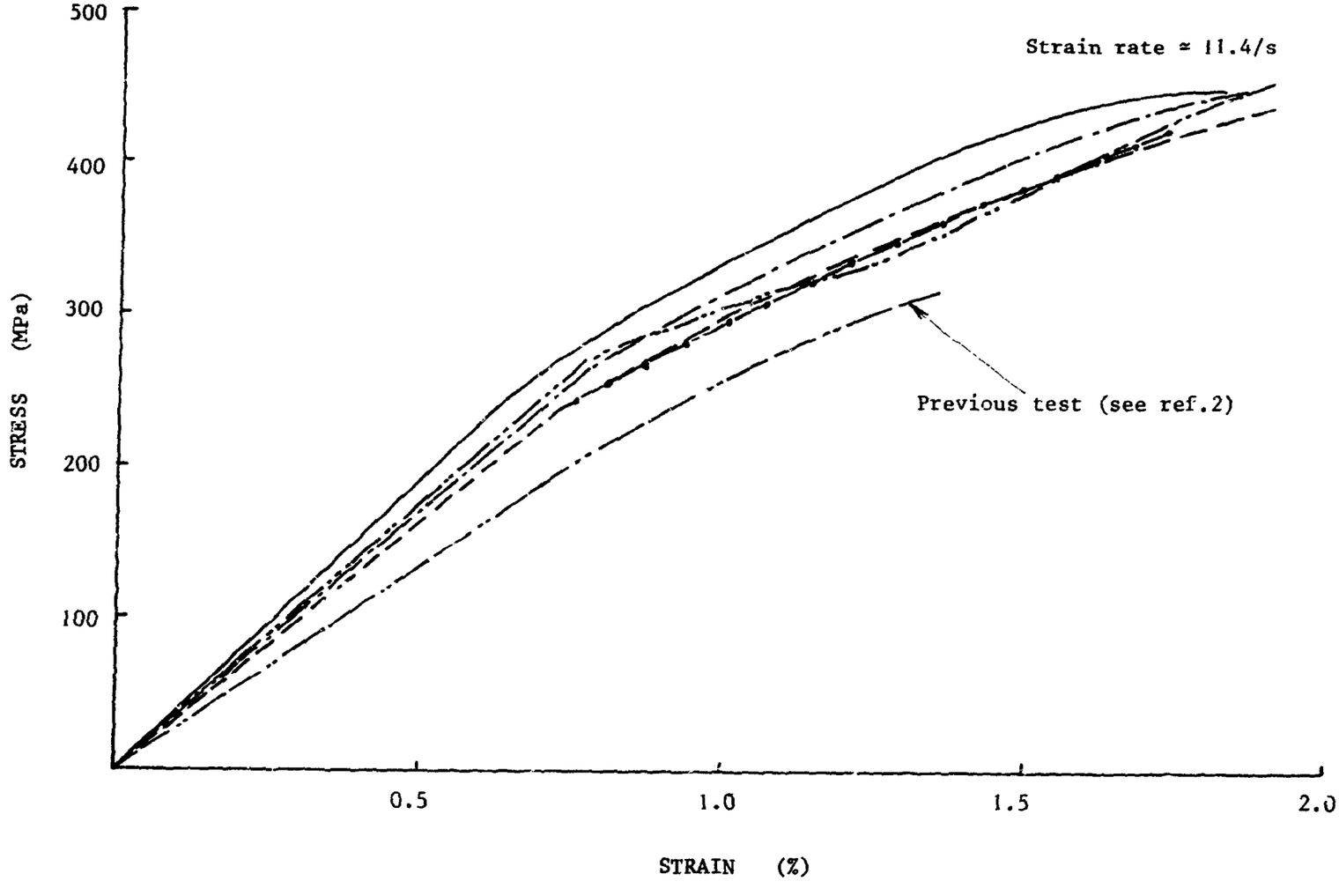

Fig.16 EFFECT OF HYBRID COMPOSITION ON MEAN INTERMEDIATE RATE STRESS-STRAIN CURVES

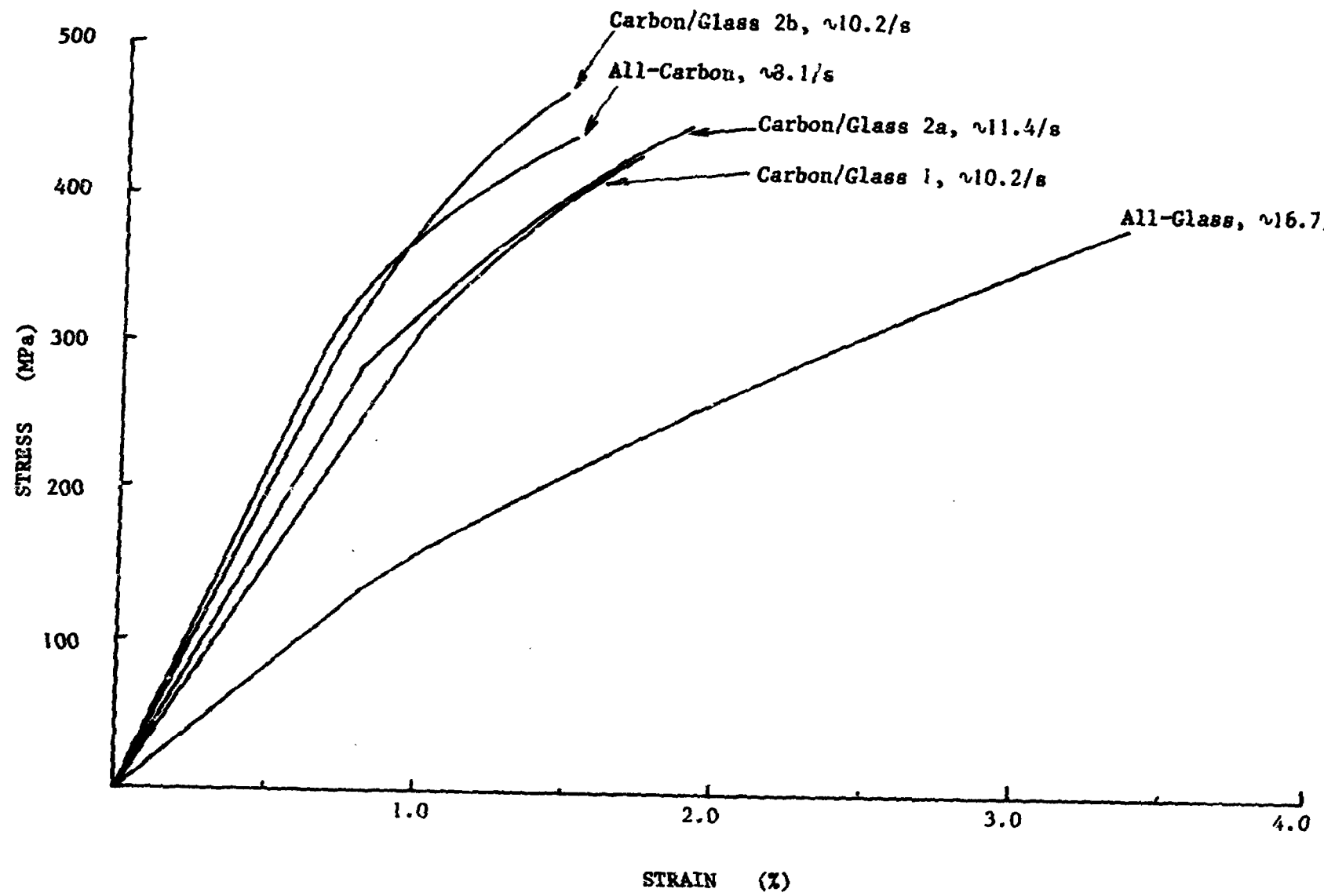

ample, a continuously increasing initial modulus with carbon weight fraction and, in the main, a continuously reducing strain at failure, some anomalies are observed, in particular the lower failure strength of the all carbon, as compared with the type 2b hybrid, specimens, the latter having only a 0.75 weight fraction of carbon fibres. Some of these anomalies may be due to the different mechanical behaviour found in the warp and weft directions since, although the results in fig. 16 for the all-carbon and the all-glass specimens are for loading in the weft direction, some uncertainty remains as to which are the warp and the weft directions in the hybrid specimens and a check on this still has to be performed.

3.2 Quasi-Static Tests

Stress-strain curves for quasi-static tests at a mean strain rate of $\sim 10^{-3}$/s on the all-carbon, carbon/glass hybrids type 2b, 2a and 1 and the all-glass specimens are shown in figs. 17, 18, 19, 20 and 21 respectively. Results are presented for four tests on each material, except fot the all-glass laminate where only three specimens were tested. For the type 1 and 2b hybrids and the all-glass specimens the scatter between individual results was very small. In the type 2a hybrid tests one specimen appeared significantly stronger than the other three. Again this may be due to the difference between the warp and the weft directions. One of the all-carbon specimens pulled out of the grips so a tensile failure load and a corresponding tensile failure strain could not be determined.

Mean stress-strain curves from each of these five series of tests are compared in fig. 22. As at the intermediate rate the fracture strength of the type 2b hybrid exceeds that of the all-carbon specimens. Otherwise the behaviour is in agreement with that observed under impact loading, with a continuously increasing initial modulus and decreasing failure strain the higher the carbon weight fraction.

All the specimens used in obtaining the stress-strain curves of figs. 17 to 22 were thought to have been loaded in the weft direction, although in the case of the type 2a hybrids some uncertainty still remains. In order to check this for the all-glass and the all-carbon specimens, and as a first step towards determining the stiffness matrix for these two materials, two further series of quasi-static tests were performed on all-glass and all-carbon specimens cut with their axes perpendicular to the axes of the specimens used in the earlier tests. The stress-strain curves obtained are shown in fig. 23, for three tests on all-glass specimens, and in fig. 24, for three tests on all carbon specimens. In two of the latter tests a sudden small drop in load was observed shortly before final failure. This was accompanied by a corresponding sudden increase in displacement across the specimen as a whole, as recorded on the velocity transducers. Since the specimen strain gauges had failed before this point was reached, it was not possible to determine unambiguously whether the drop in load was due to a sudden increase in specimen extension or to a sudden small slippage in the grips. The latter, however, was not thought to be very likely since, when it does occur, which is only very infrequently, it is accompanied by almost complete unloading, see fig. 17, and by an observable displacement between the grips and the specimen. If, on the other hand, the load drop is due

Fig.17 QUASI-STATIC STRESS-STRAIN CURVES FOR ALL-CARBON SPECIMENS

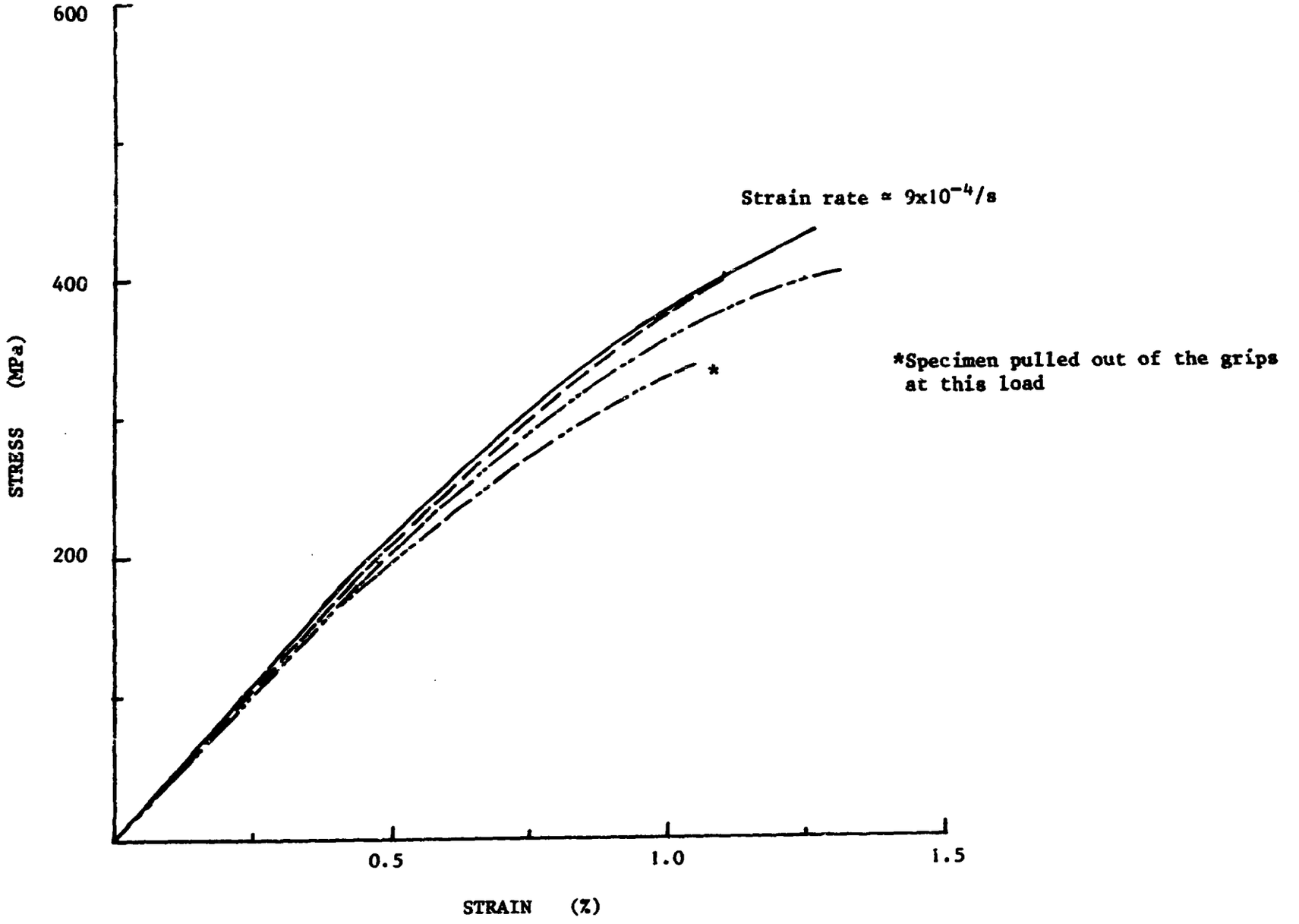

Fig.18 QUASI-STATIC STRESS-STRAIN CURVES FOR TYPE 2b HYBRID SPECIMENS

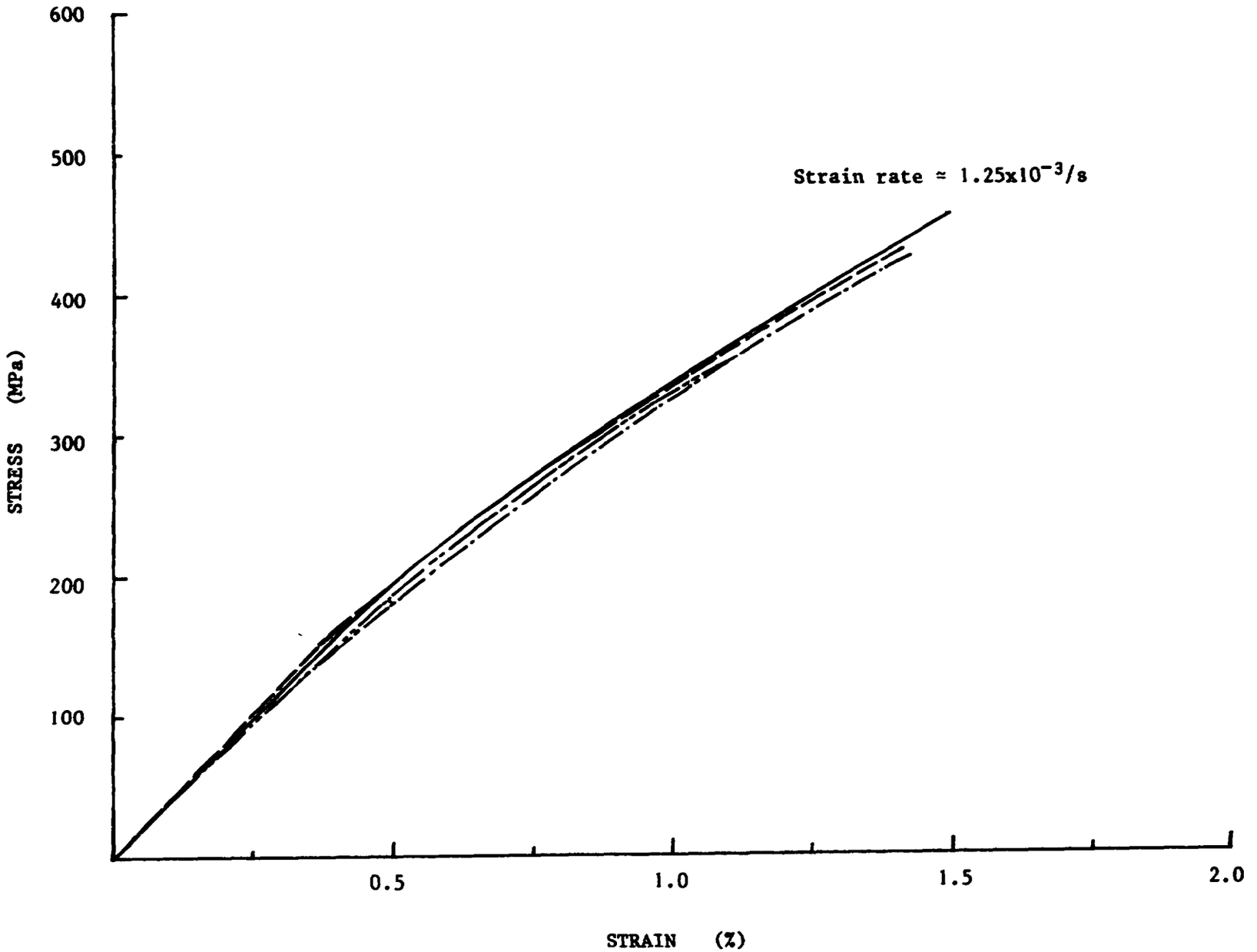

Fig.19 QUASI-STATIC STRESS-STRAIN CURVES FOR TYPE 2a HYBRID SPECIMENS

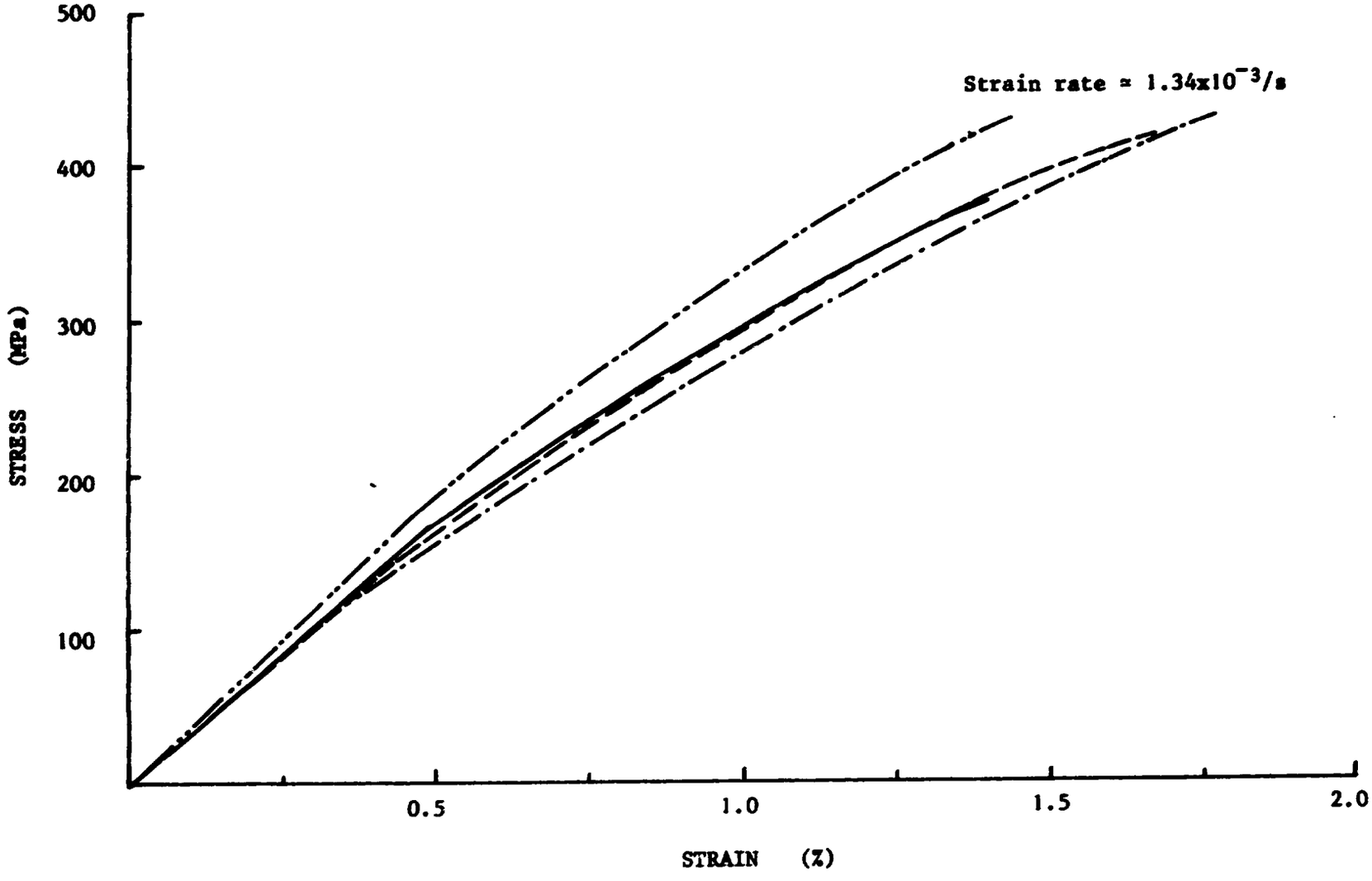

Fig.20 QUASI-STATIC STRESS-STRAIN CURVES FOR TYPE 1 HYBRID SPECIMENS

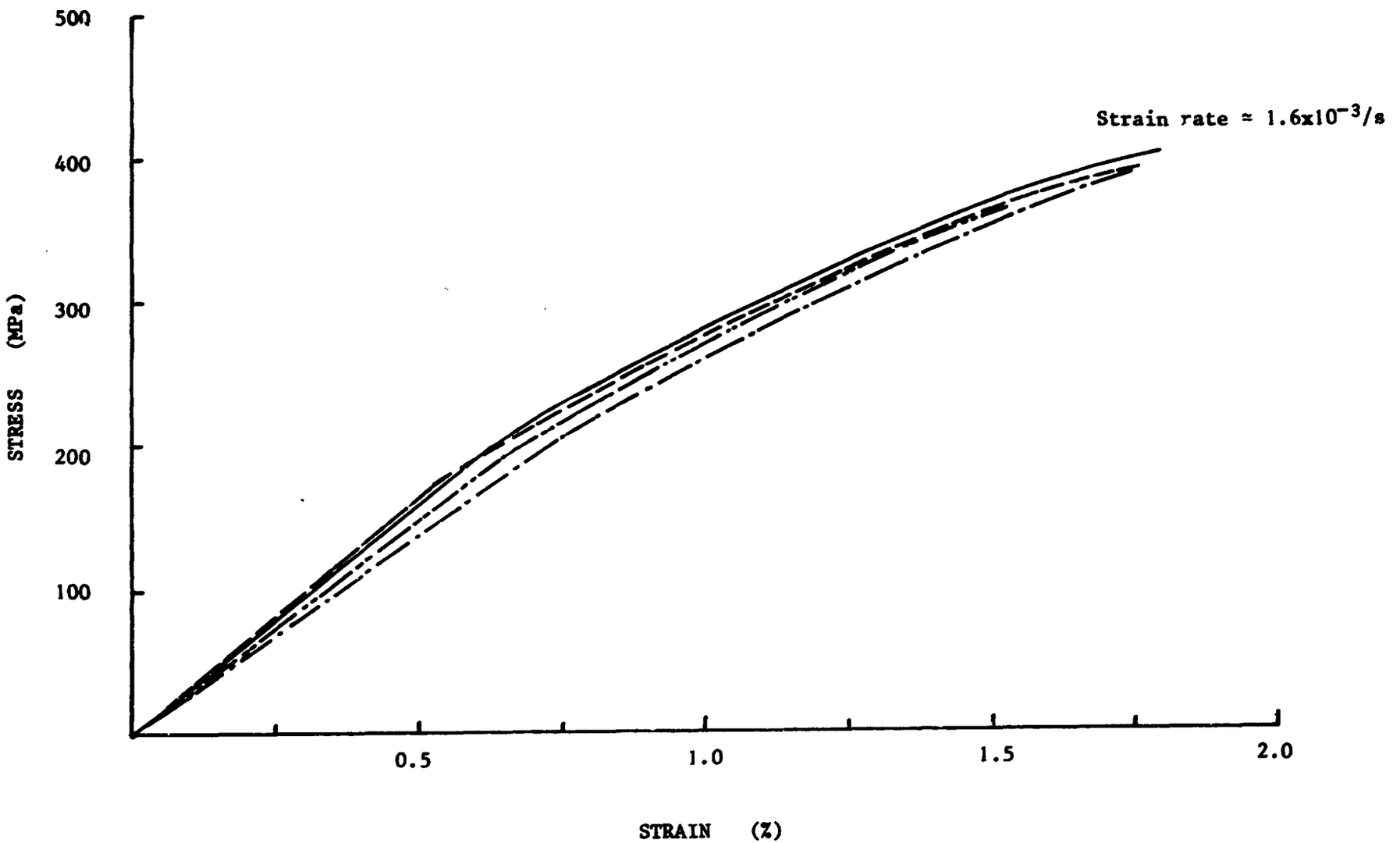

Fig.21 QUASI-STATIC STRESS-STRAIN CURVES FOR ALL-GLASS SPECIMENS

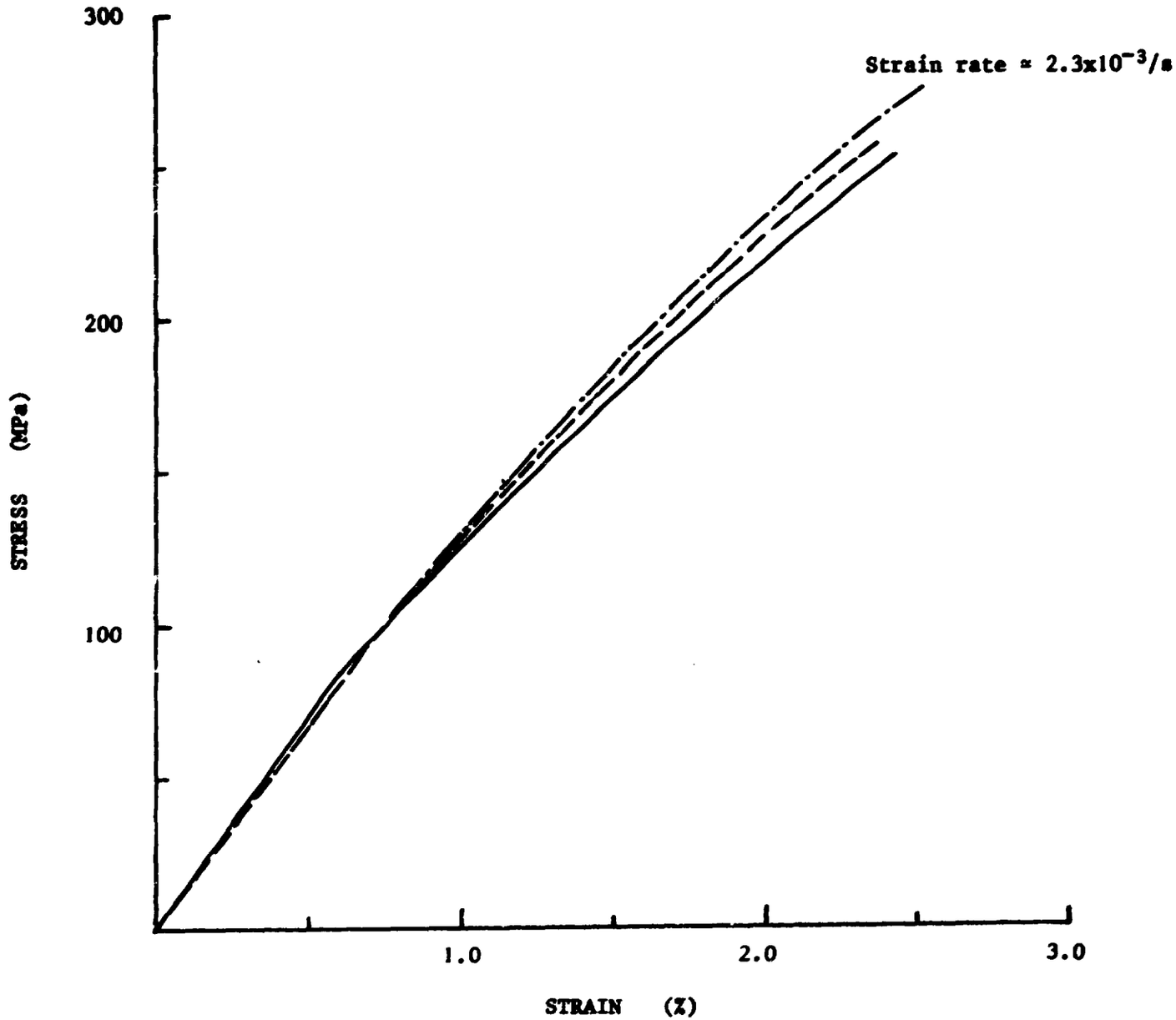

Fig.22 EFFECT OF HYBRID COMPOSITION ON MEAN QUASI-STATIC STRESS-STRAIN CURVES

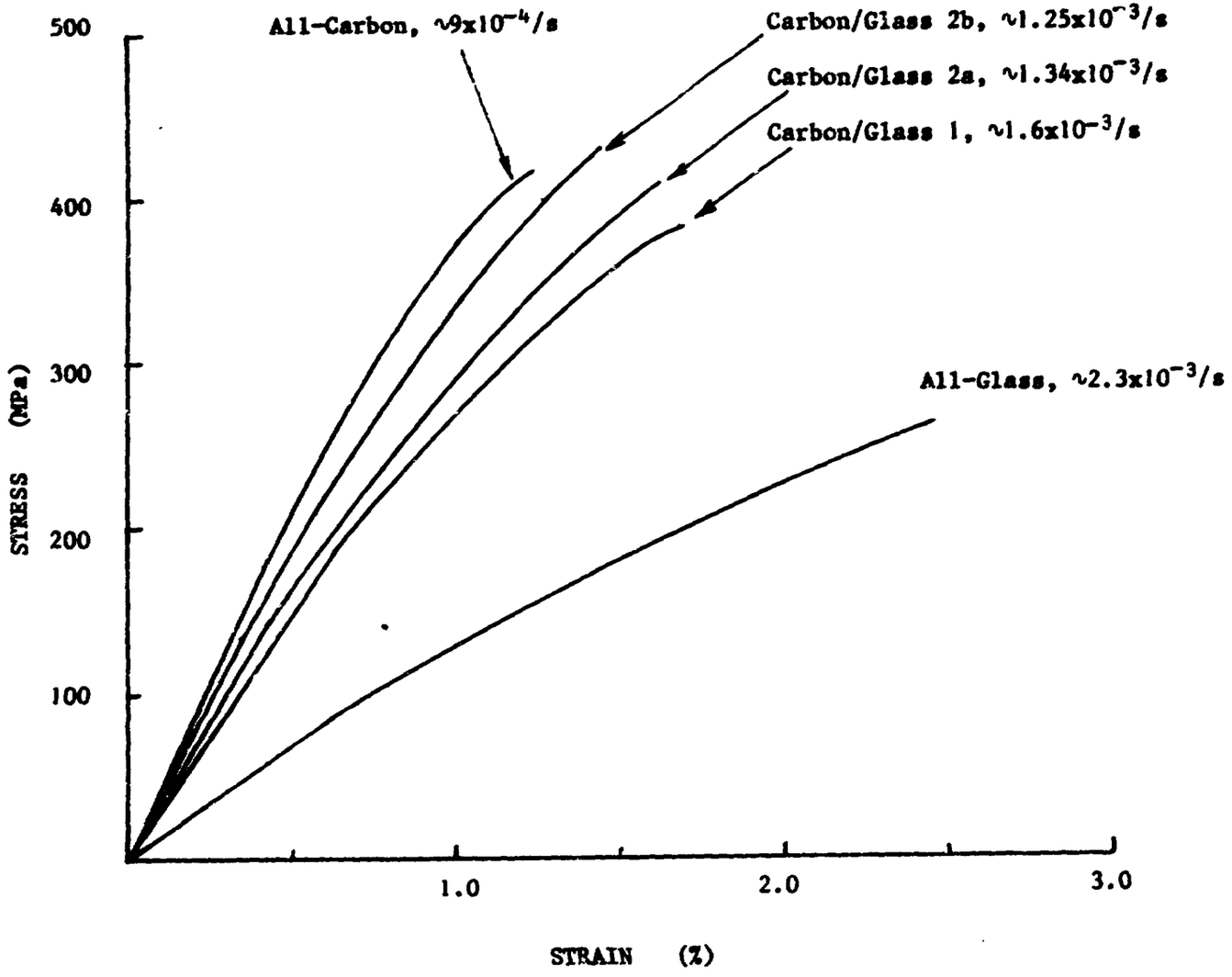

Fig.23 QUASI-STATIC STRESS-STRAIN CURVES FOR ALL-GLASS SPECIMENS LOADED IN THE WARP DIRECTION

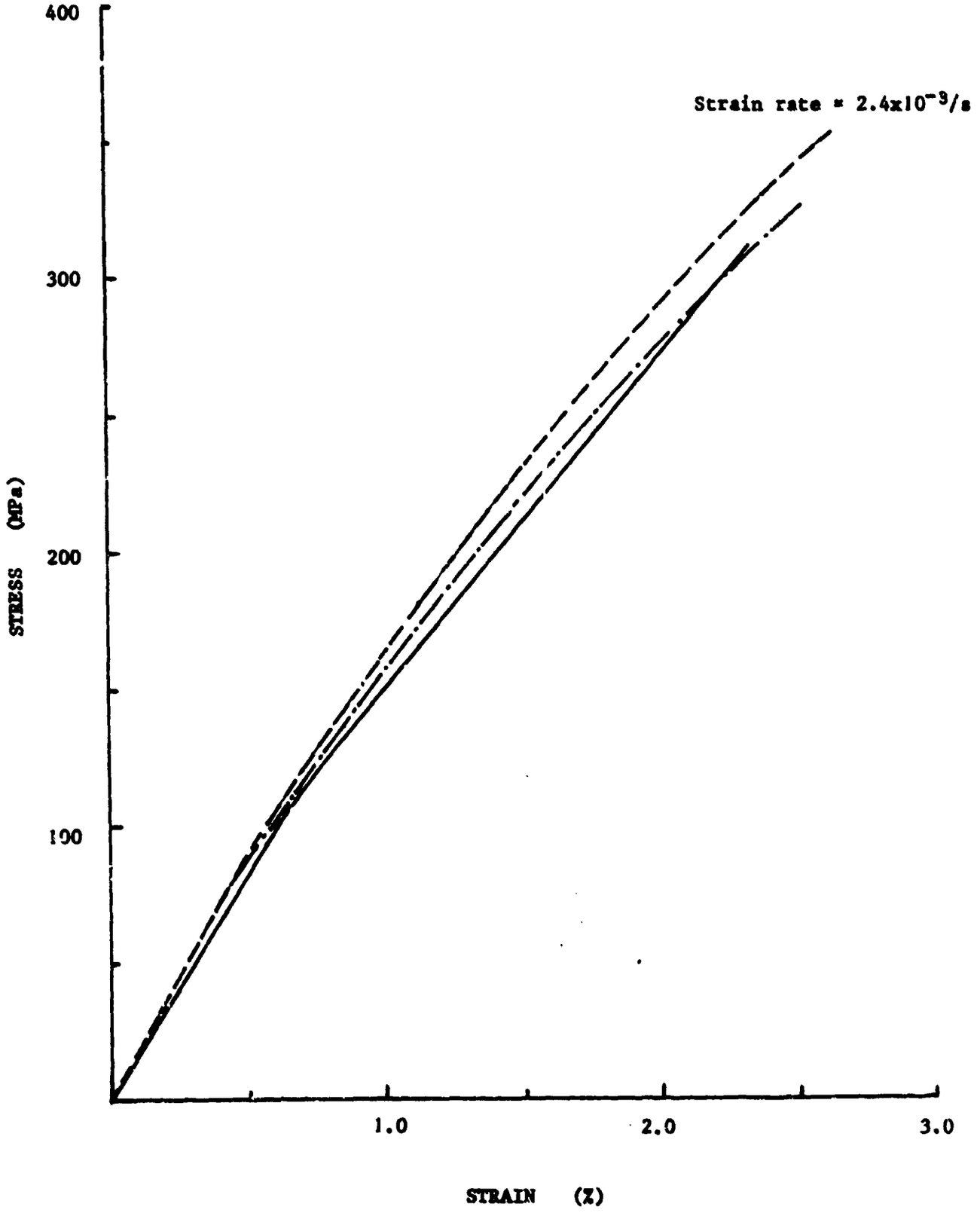

Fig.24 QUASI-STATIC STRESS-STRAIN CURVES FOR ALL-CARBON SPECIMENS LOADED IN THE WARP DIRECTION

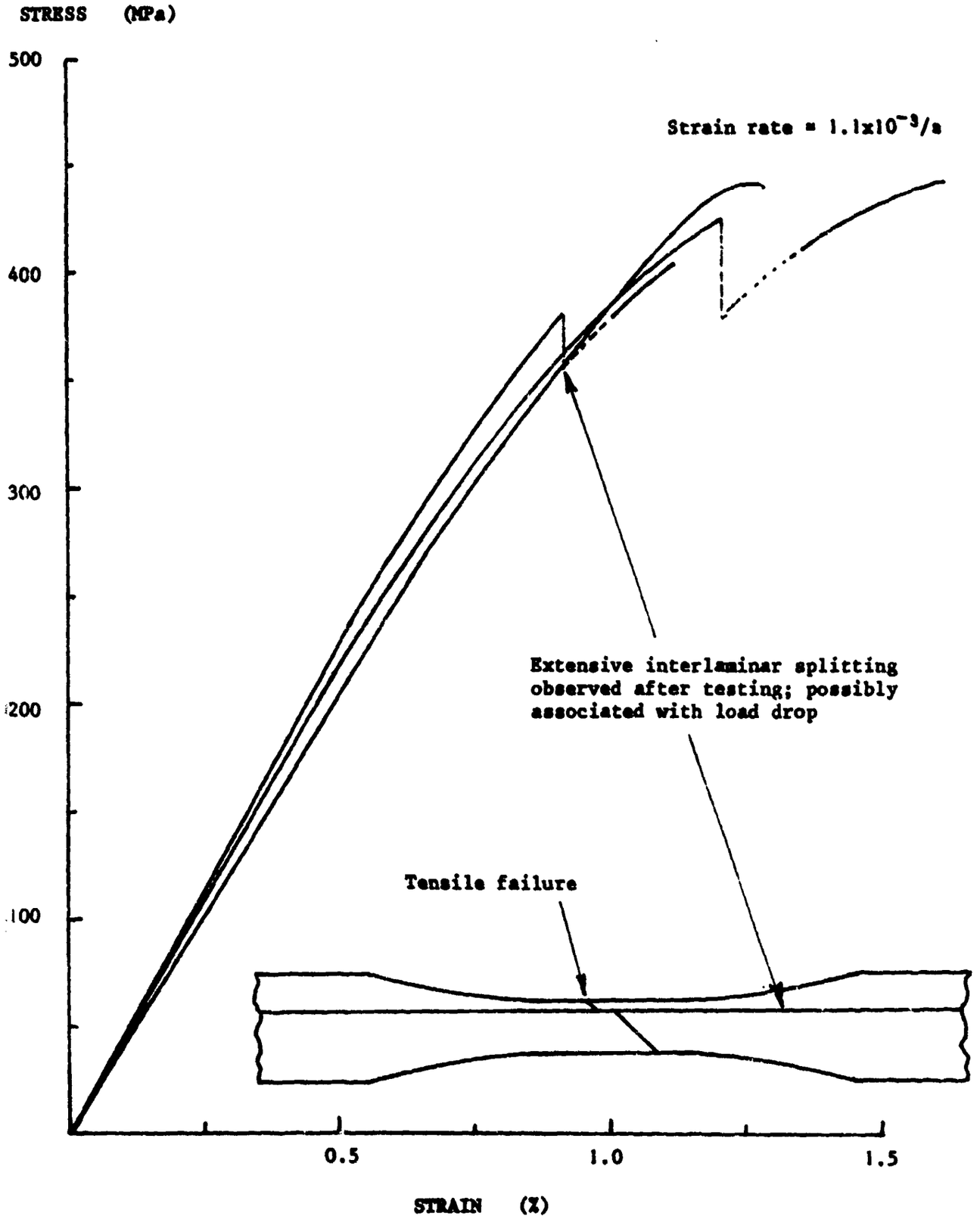

to a genuine increase in specimen extension then it is necessary to suggest a possible damage mechanism by which this could happen. In one of the two cases illustrated in fig. 24 where a load drop was observed the specimen was found to have delaminated extensively between two neighbouring plies, as sketched in fig. 24, so fracture could have taken place in two stages with delamination interrupting the process. It was less clear whether a similar process could have been the cause of the load drop in the second specimen.

Figures 25 and 26 compare the mean stress-strain curves from figs. 23 and 24, respectively, with the corresponding curves for all-glass and all-carbon specimens shown in fig. 22. It is confirmed that the earlier tests (figs. 17 and 21) were for specimens loaded in the weft (lower strength) direction and the current tests (figs. 23 and 24) for specimens loaded in the warp (higher strength) direction. A fuller comparison of the mechanical properties in the two directions is given in Table I below, where orientation 'A' implies loading along the warp direction and 'B' loading along the weft direction.

TABLE I Comparison of Mechanical Properties in Warp and Weft Directions for All-Glass and All-Carbon Specimens (Quasi-static tests)

Material	Orientation	E (GPa)	σ_{max} (MPa)	ε_f (%)	σ_y (MPa)	ε_y (%)
All-glass	Warp (A)	16.7	328	2.53	92	0.55
	Weft (B)	13.7	262	2.45	87	0.63
All-carbon	Warp (A)	43.3	428	1.35	240	0.55
	Weft (B)	42.5	416	1.24	172	0.40

where E is the initial modulus in the loading direction, σ_m is the maximum stress supported by the specimen and ε_f the corresponding strain and σ_y and ε_y are the stress and strain at the limit of the linear elastic response of the specimen.

A small difference in properties for the two directions is apparent in the all-carbon specimens and a more significant difference in the all-glass specimens. This is not surprising since for the glass reinforcing mat there were more ends (252) than picks (173) per 10cm whereas for the much coarser carbon mat there was the same number (47) in each direction.

3.3 Determination of Quasi-Static Stiffness Matrix

To allow a determination of the full two-dimensional stiffness matrix, tests were performed on parallel-sided coupons cut from the all-glass and all-carbon laminates with the loading axis along the warp (A) or the weft (B) directions or at 45° to both warp and weft directions (C). Strain gauges were attached to the specimens as shown earlier (fig. 3) and each coupon was loaded and unloaded several times, remaining within the elastic range. Results obtained in this way for an all-glass coupon load-

Fig.25 COMPARISON OF QUASI-STATIC STRESS-STRAIN CURVES FOR ALL-GLASS SPECIMENS LOADED IN WARP AND WEFT DIRECTIONS

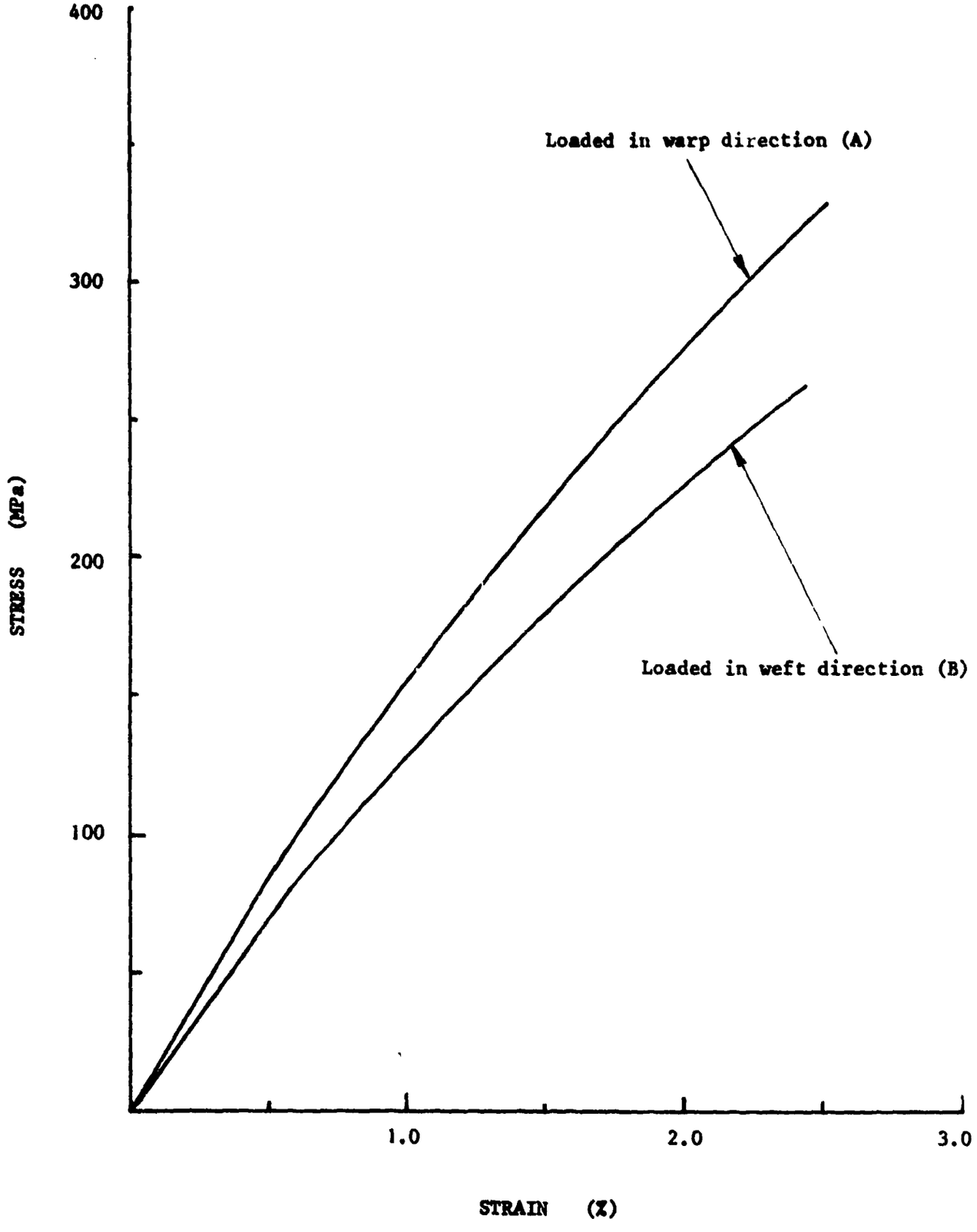

Fig.26 COMPARISON OF QUASI-STATIC STRESS-STRAIN CURVES FOR ALL-CARBON SPECIMENS LOADED IN WARP AND WEFT DIRECTIONS

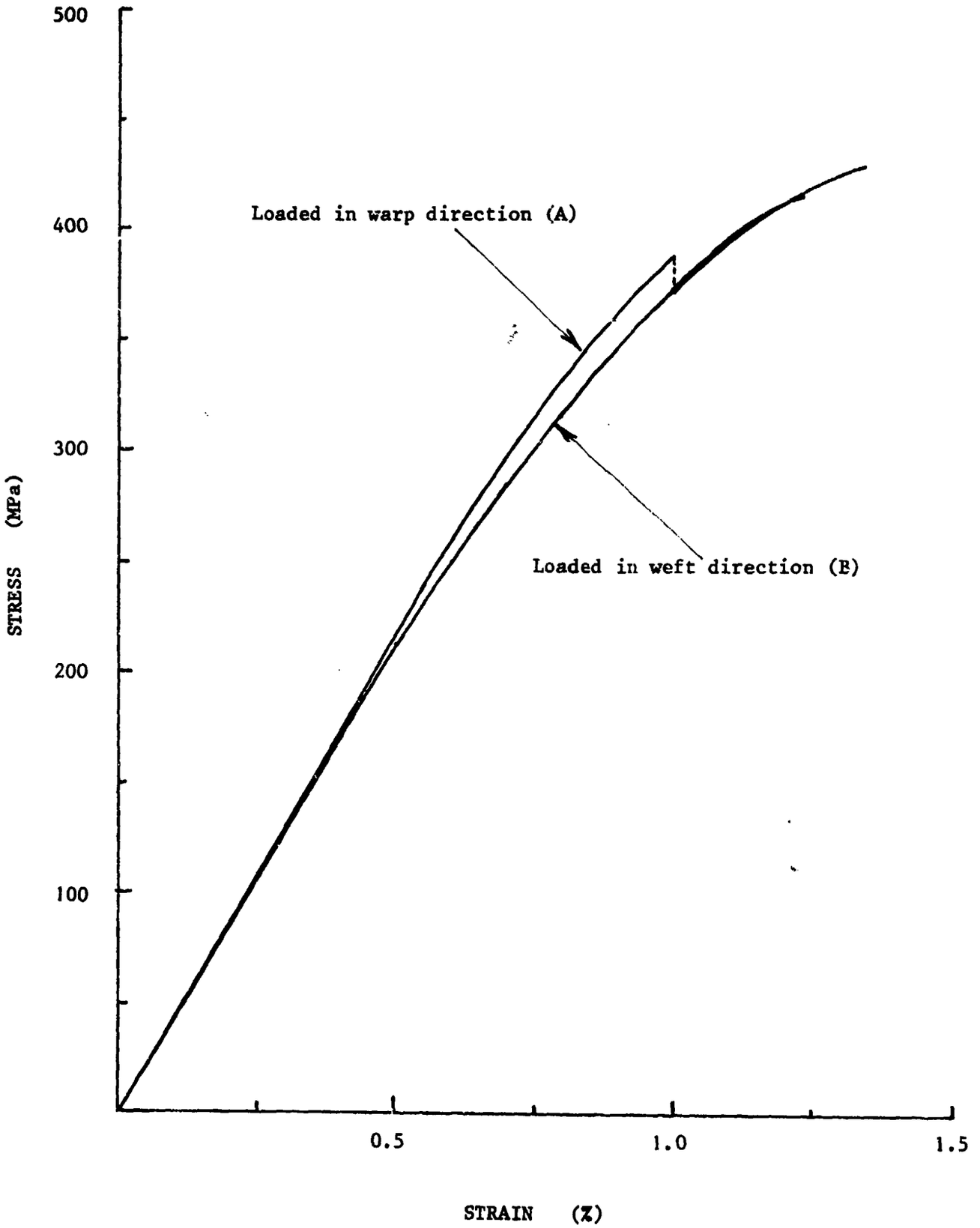

ed in the warp direction are shown in fig. 27, the scatter band indicated at each load being for six measurements, three during loading and three during unloading. The resulting modulus in the loading direction, E_A, was found to be 16.35GPa, which compares with the value of 16.7GPa given in Table I from the earlier tests on standard tensile specimens. Similar results for a coupon loaded in the weft direction gave 13.8GPa, compared with 13.7GPa in Table I. To obtain Poisson's ratio strain gauge signals in the loading and transverse directions (ε_L and ε_T) are compared for the same three loading cycles, results obtained in this way for all-glass coupons loaded in the weft direction being shown in fig. 28. The mean slope in fig. 28 gives a Poisson's ratio, ν_{BA}, of 0.141. Similar results for an all-glass coupon loaded in the warp direction gave $\nu_{AB} = 0.164$. For an orthotropic laminate it may be shown that

$$E_A\nu_{BA} = E_B\nu_{AB} \qquad (1)$$

The present results satisfy this relationship with an accuracy greater than ±1%.

A similar series of tests was performed on coupons cut from the all-carbon laminate. Here, however, a difference in behaviour was observed between loading and unloading as may be seen from the results listed in Table II. When fitted to equation (1) these show a discrepancy of ±20% when the loading line results are used reducing to ±5% when the unloading line results are tested. In fact, failure of the symmetry hypothesis is not unusual and has been reported by many other investigators, for example Lempriere (5) and Bert, Mayberry and Ray (6). A non-conservative behaviour of some constituent of the composite is usually postulated as the cause, possibly in this case the non-conservative microcracking of the epoxy resin during 'elastic' loading of the woven carbon fibre reinforced specimens. It is usual in such cases to define ν_{BA} in terms of equation (1) as $E_B\nu_{AB}/E_A$.

TABLE II Elastic Constants for the All-Carbon Laminate
(Quasi-static tests)

	E_A (GPa)	E_B (GPa)	ν_{AB}	ν_{BA}
Loading	46.4	43.6	0.144	0.088
Unloading	44.5	43.6	0.091	0.081

To determine the shear modulus similar reloading tests were performed on coupons cut at 45° to the warp and weft directions. For the strain

(5) Lempriere, B. M., "Uniaxial Loading of Orthotropic Materials", AIAA Journal, 6, (1968), 365-368.

(6) Bert, C. W., Mayberry, B. L. and Ray, J. D., "Behaviour of Fibre-Reinforced Plastic Laminates under Biaxial Loading", ASTM STP 460, (1969), 362-380.

Fig.27 QUASI-STATIC 'ELASTIC' RELOADING TESTS FOR AN ALL-GLASS SPECIMEN LOADED IN THE WARP DIRECTION

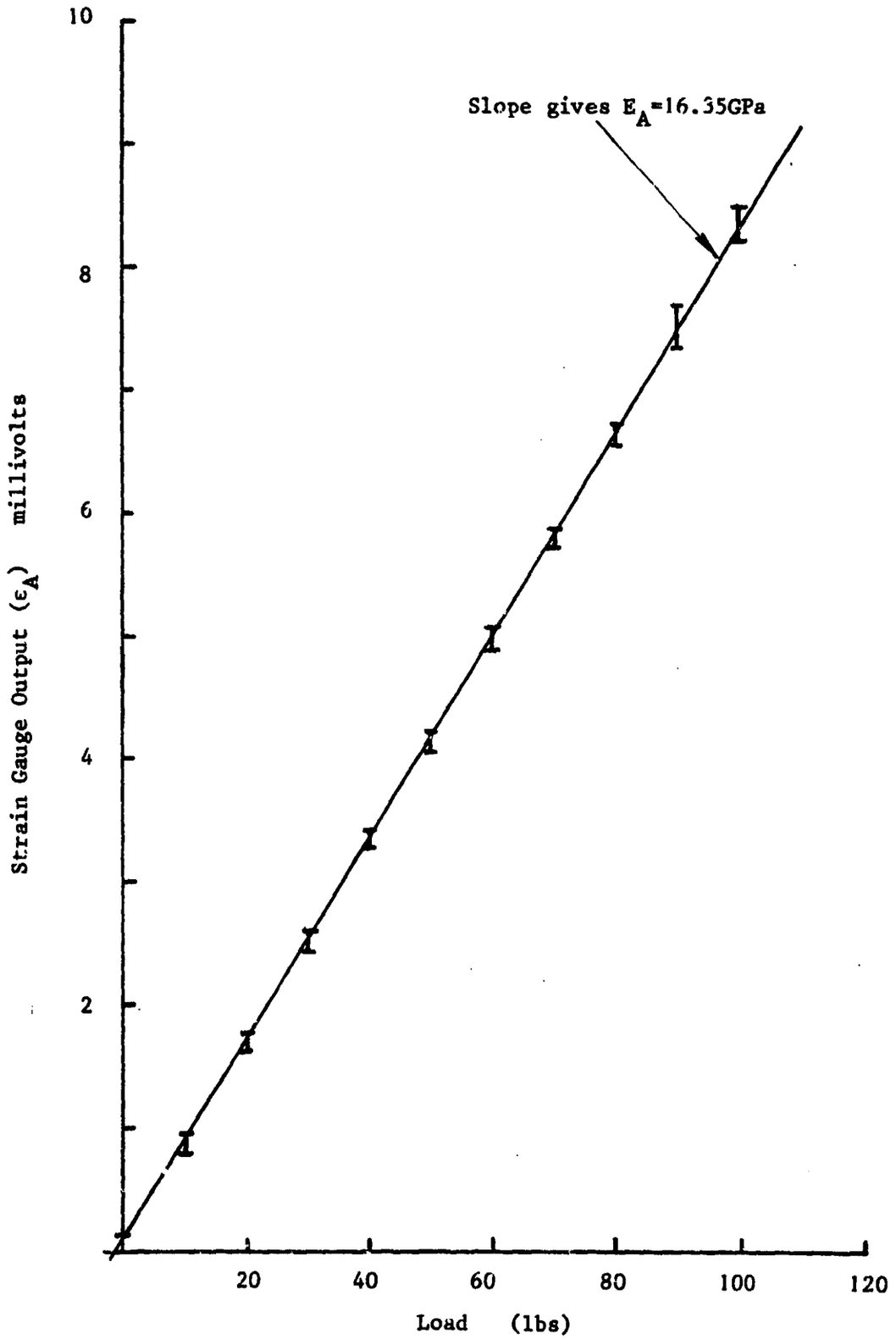

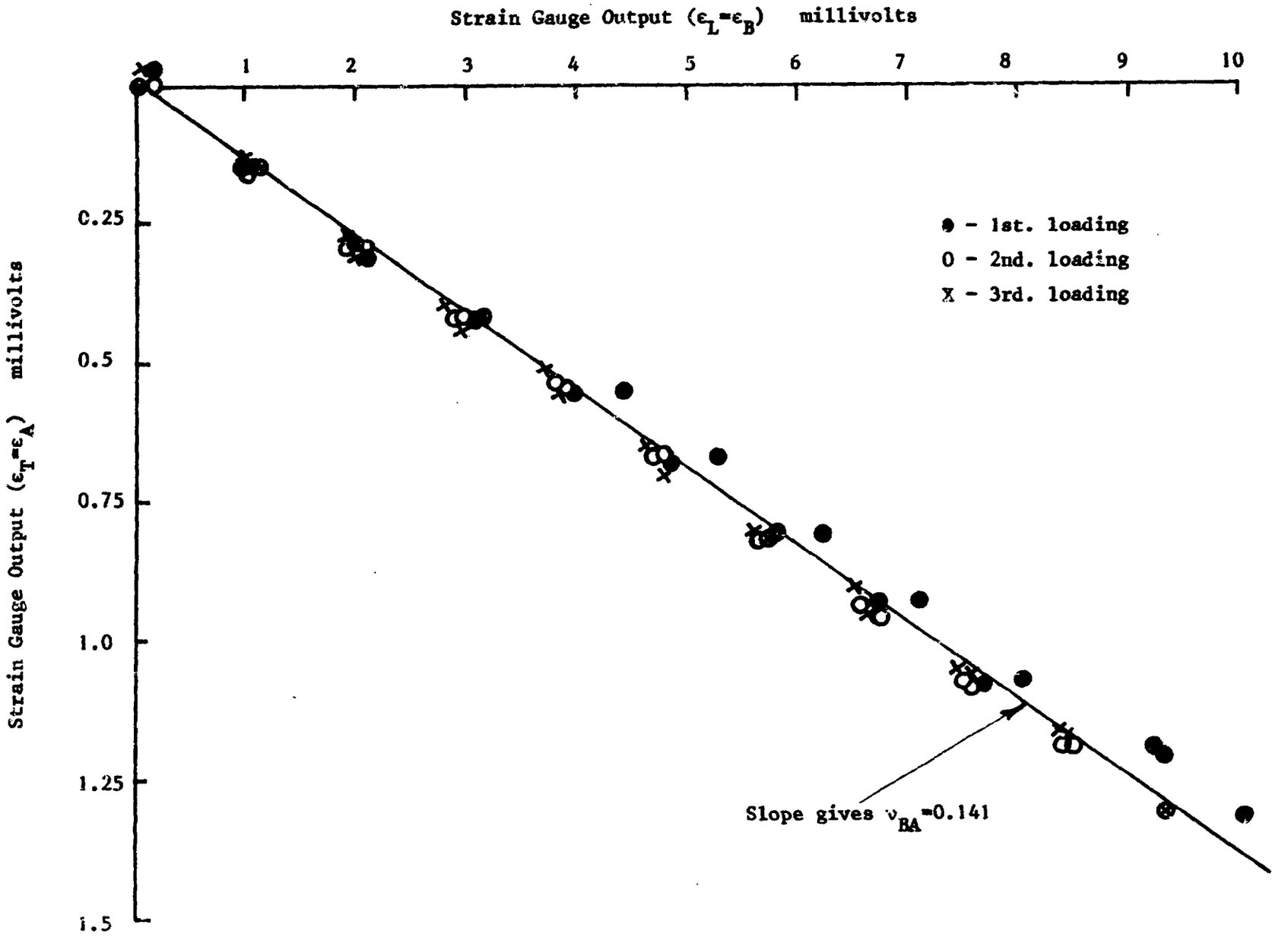

Fig.28 QUASI-STATIC 'ELASTIC' RELOADING TESTS FOR AN ALL-GLASS SPECIMEN LOADED IN THE WEFT DIRECTION

gauges aligned with the loading direction a discrepancy between the loading and unloading behaviour was again observed, more marked here for the all-glass than the all-carbon material and appearing as a lag in the strain gauge response on unloading, see fig. 29. There was little difference, however, between the slopes of the loading and unloading lines and an average result for the modulus in the 45° direction, E_C, of 5.39 GPa (±5%) is obtained. For the all-carbon specimens the corresponding result was 9.58GPa (±0.5%).

The required shear modulus, G_{AB}, may be obtained from the orthotropic transformation equation

$$1/E_C = (1/E_A)\cos^4\theta + \{(1/G_{AB}) - (2\nu_{AB}/E_A)\}\sin^2\theta\cos^2\theta + (1/E_B)\sin^4\theta$$

where θ is the angle between the warp tows, in the A direction, and the applied tension in the C direction. For $\theta = 45^o$ this reduces, see ref. 7, to the form

$$G_{AB} = \{(4/E_C) - (1/E_A) - (1/E_B) + (2\nu_{AB}/E_A)\}^{-1} \qquad (2)$$

Using this equation and taking E_C = 5.39GPa, E_A = 16.35GPa, E_B = 13.77 GPa and ν_{AB} = 0.164 gives for the all-glass laminate a shear modulus of G_{AB} = 1.59GPa. A similar calculation for the all-carbon laminate, taking E_C = 9.58GPa, E_A = 45.5GPa, E_B = 43.6GPa and either ν_{AB} = 0.144 (loading) or 0.091 (unloading) gives for the shear modulus values of either 2.64GPa or 2.66GPa, respectively, a negligible difference.

An alternative method for determining the shear modulus was proposed by Petit (ref. 8) using a single tension test on a $[\pm 45^o]_s$ laminate. In the simplified form developed by Rosen (ref. 9) this gives

$$G_{AB} = \sigma_x/2(\varepsilon_x - \varepsilon_y) \qquad (3)$$

where the x-direction, the direction of loading, is at 45° to the reinforcing directions so that the shear stress and strain are given by

$$\tau_{AB} = \sigma_x/2 \quad \text{and} \quad \gamma_{AB} = \varepsilon_x - \varepsilon_y.$$

In the present tests ε_y was not measured directly but may be determined, using the Mohr's circle for strain, from the strain gauge readings in the two reinforcing directions, ε_α and ε_β corresponding to ε_{-45} and ε_{+45} in fig. 3, giving

---

(7) Yeow, Y. T. and Brinson, H. F., "A Comparison of Simple Shear Characterisation Methods for Composite Laminates", Composites, 9, (1978), 49-55.

(8) Petit, P. H., "A Simplified Method of Determining the Inplane Shear Stress-Strain Response of Unidirectional Composites", ASTM STP 460, (1969), 83-93.

(9) Rosen, B. W., "A Simple Procedure for Experimental Determination of the Longitudinal Shear Modulus of Unidirectional Composites", J. Composite Mater., 6, (1972), 552-554.

Fig.29 QUASI-STATIC 'ELASTIC' RELOADING TESTS FOR AN ALL-GLASS SPECIMEN LOADED IN THE 45° DIRECTION

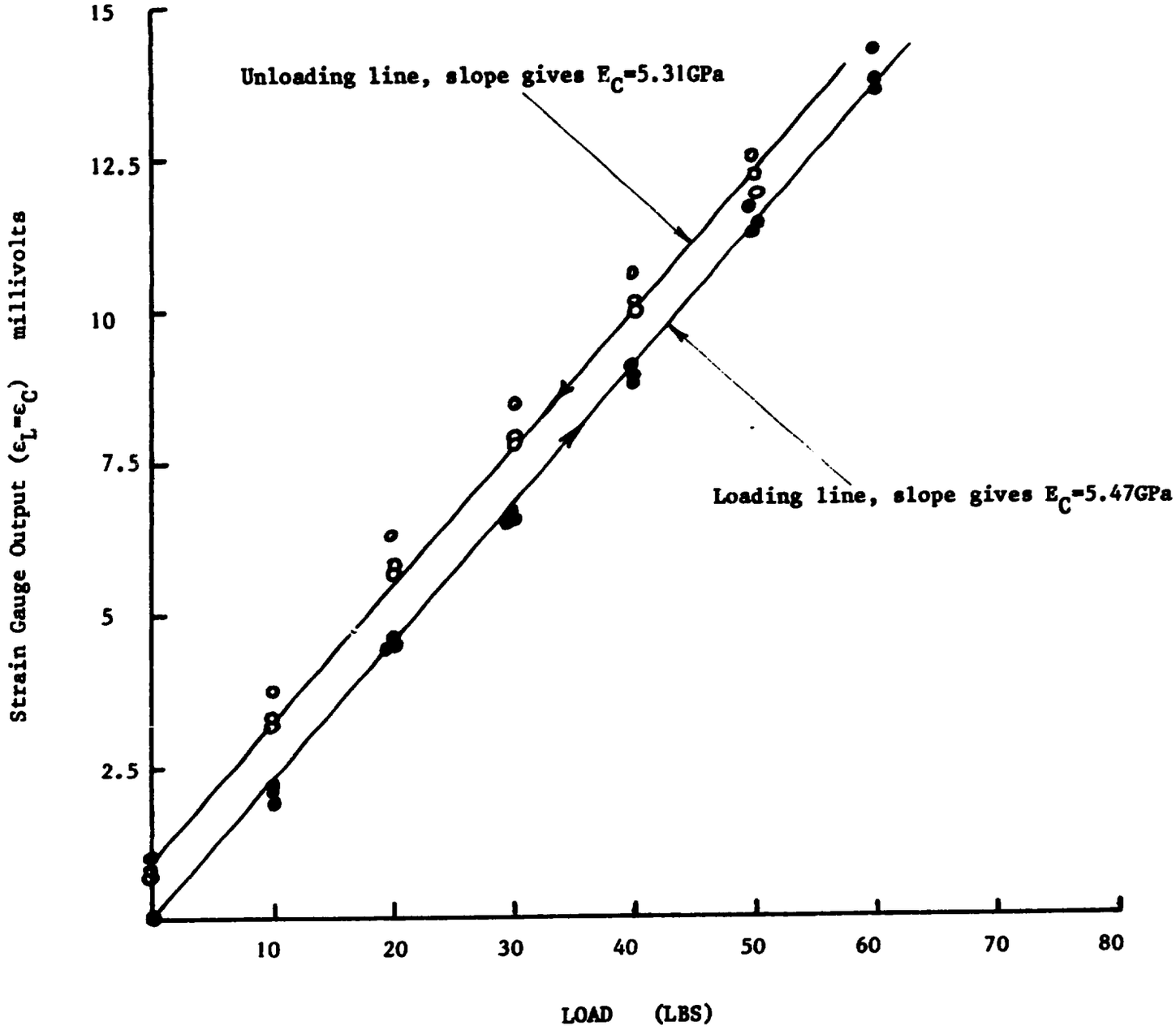

$$\varepsilon_y = \varepsilon_\alpha + \varepsilon_\beta - \varepsilon_C$$

so that equation (3) becomes

$$G_{AB} = \sigma_C/\{4\varepsilon_C - 2(\varepsilon_\alpha + \varepsilon_\beta)\} \quad (4)$$

where $\sigma_C = \sigma_x$ and $\varepsilon_C = \varepsilon_x$. Defining the 'moduli' E_α and E_β as $\sigma_C/\varepsilon_\alpha$ and $\sigma_C/\varepsilon_\beta$, respectively, this gives

$$G_{AB} = \tfrac{1}{4}\{(2/E_C) - (1/E_\alpha) - (1/E_\beta)\}^{-1}. \quad (5)$$

The variation of σ_C with both ε_α and ε_β was obtained from the three elastic reloading tests on the all-carbon parallel-sided coupon. After an initial anomalous region a linear elastic response was obtained corresponding to mean values for E_α and E_β of 67.1±4.8GPa and 161.5±13.5GPa respectively. The same specimen was subsequently loaded to failure and curves of σ_C versus ε_α and ε_β obtained, as shown in the computer plots of figs. 30 and 31, leading to further values for E_α and E_β of 72.6GPa and 162.7GPa respectively, in reasonable agreement with the reloading tests. Corresponding results were obtained in similar tests on an all-glass coupon. Using the average values derived from these various results for E_C, E_α and E_β, see Table III below, the shear modulus was determined from equation (5) and found to be 2.74GPa for the all-carbon and 1.61GPa for the all-glass laminates, respectively, about 4% greater than the value previously determined from equation (2) for the all-carbon laminate and about 2% greater for the all-glass laminate.

TABLE III Elastic Constants from Quasi-Static Tests on Parallel-Sided 45° Coupons (GPa)

	All-glass laminate			All-carbon laminate		
	E_C	E_α	E_β	E_C	E_α	E_β
Loading	5.15	27.8	62.0	9.56	68.6	158.5
	5.44	29.3	62.0	9.62	64.6	171.0
	5.35	29.7	64.4	9.54	65.0	165.9
Unloading	5.35	30.2	57.6	9.54	65.0	143.8
	5.46	29.9	55.6	9.60	74.1	163.9
	5.58	29.5	58.3	9.62	65.0	165.9
Failure test	6.41	30.8	65.7	11.30	72.6	162.7
Mean	5.53	29.6	60.8	9.83	67.8	161.7

3.4 Impact Tests on the Modified Gas Gun

Three stress-strain curves for tests similar to that described in section 2.3 on all-carbon specimens loaded in the weft direction are shown in fig. 32. Mean values for the initial modulus, maximum strength and fracture strain from these three tests and estimates of the stress and strain at the limit of the linear elastic region are compared in Table IV with similar mean values from five earlier tests using the

Fig.30 QUASI-STATIC FAILURE TEST ON AN ALL-CARBON PARALLEL-SIDED COUPON LOADED IN THE 45° DIRECTION

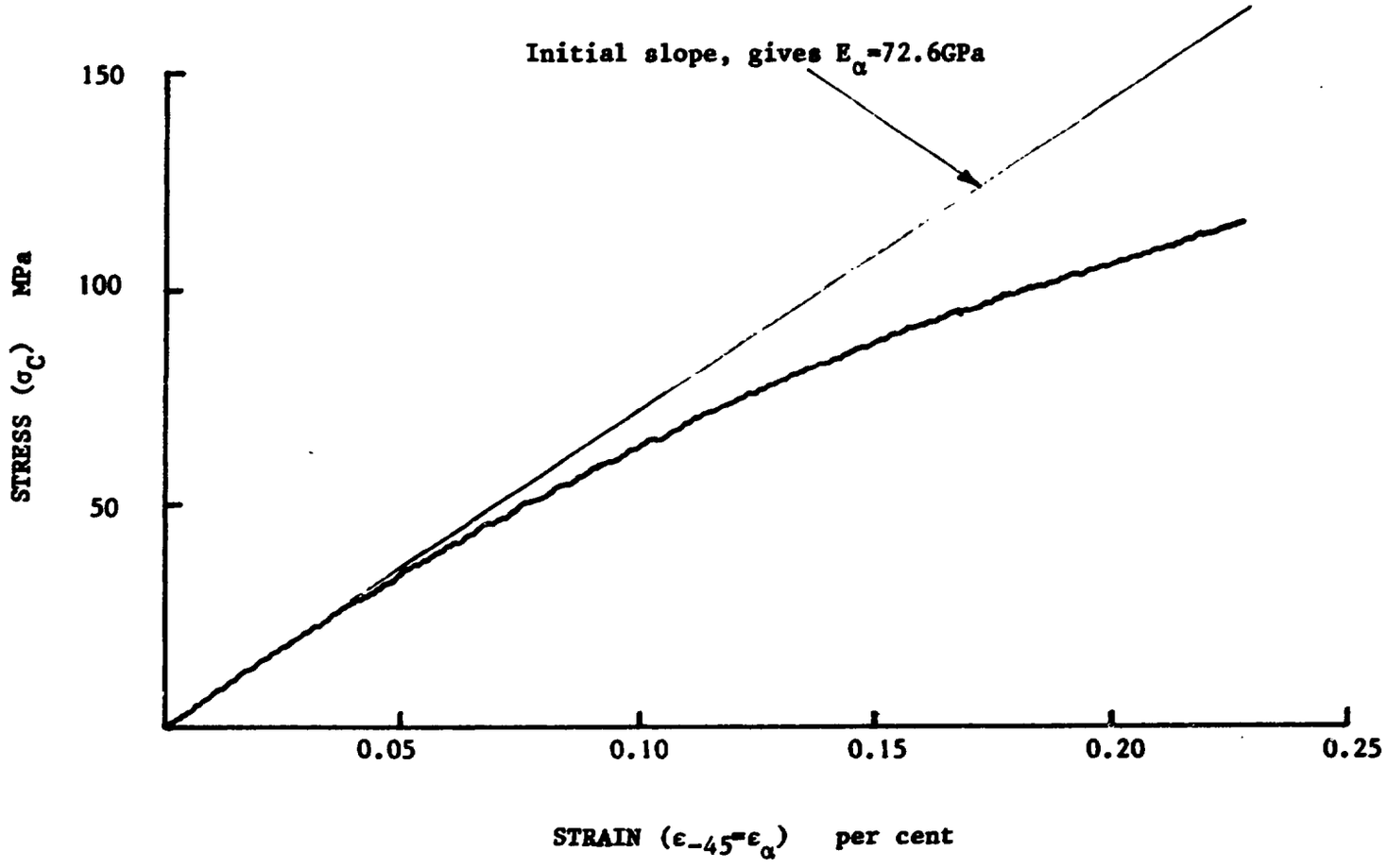

Fig.31 QUASI-STATIC FAILURE TEST ON AN ALL-CARBON PARALLEL-SIDED COUPON LOADED IN THE 45° DIRECTION

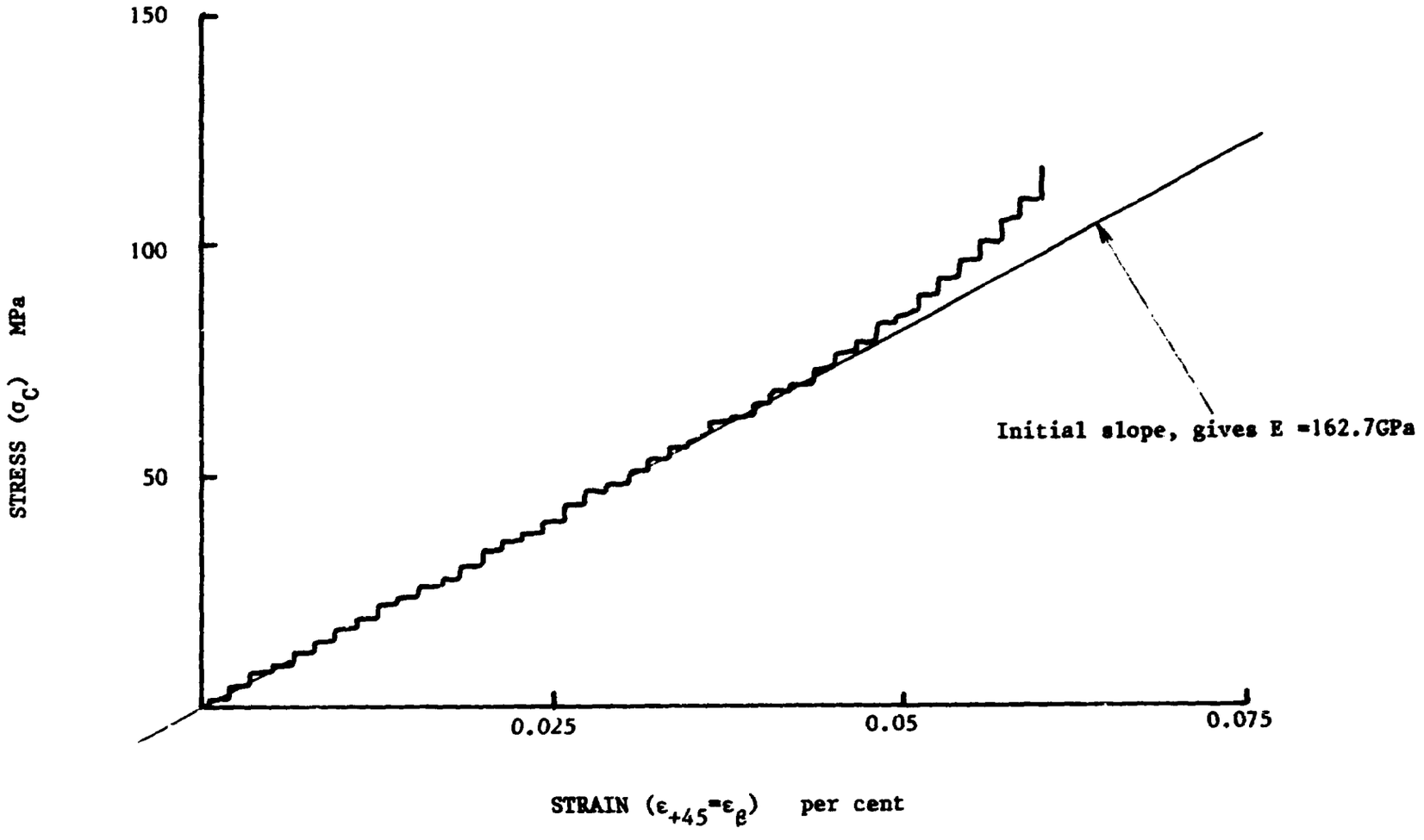

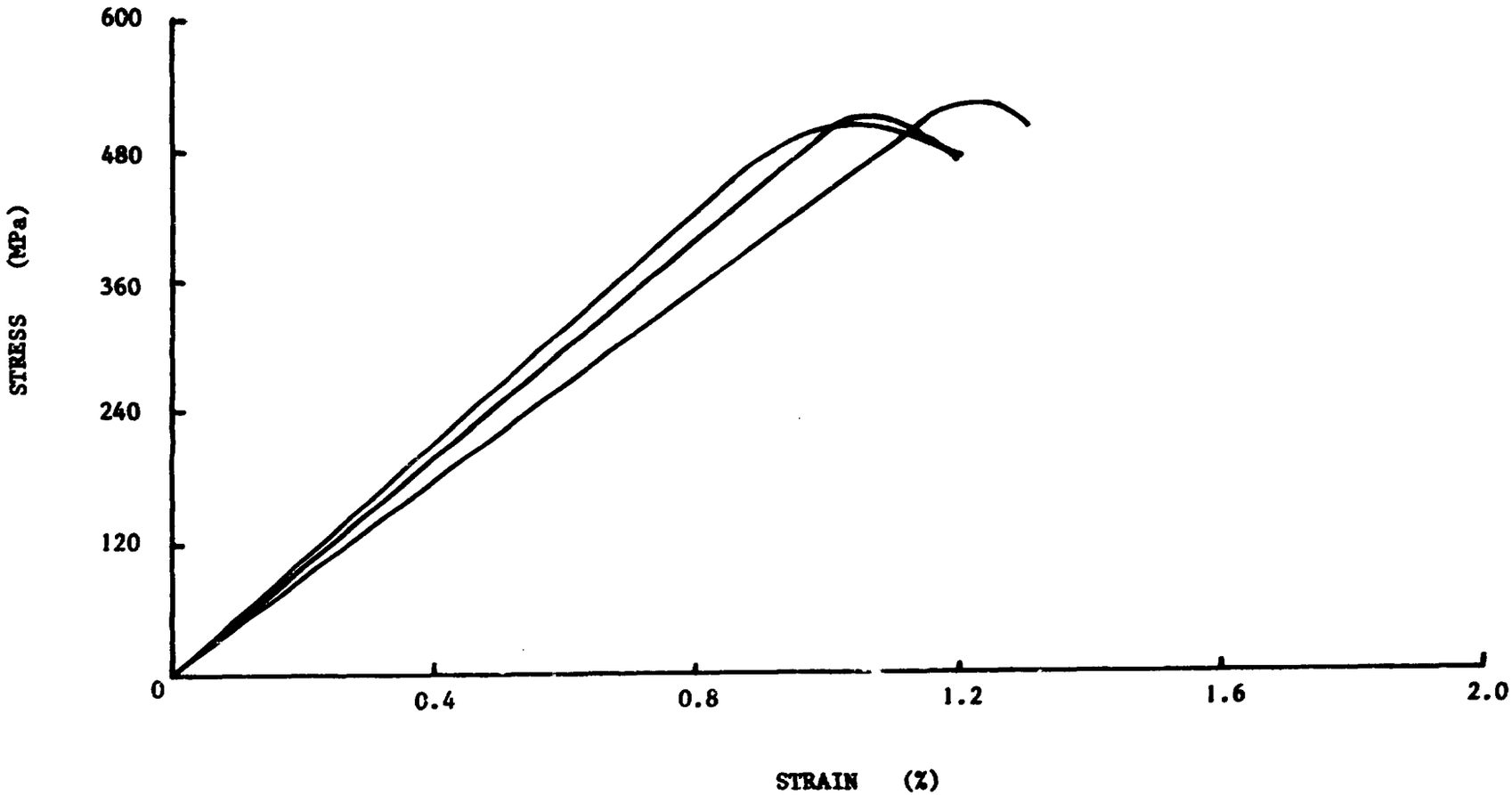

Fig. 32 IMPACT STRESS-STRAIN CURVES FOR ALL-CARBON SPECIMENS LOADED IN THE WEFT DIRECTION

unmodified gas gun on all-carbon specimens loaded in the warp direction. Mean stress-strain curves for the two sets of tests are compared in fig. 33. Although specimens cut in the warp direction show a greater strength and strain at failure no significant difference in the modulus for the two directions of loading was observed.

TABLE IV Comparison of Mechanical Properties in Warp and Weft Directions for All-Carbon Specimens under Impact Loading

Direction of loading	E (GPa)	σ_{max} (MPa)	ϵ_f (%)	σ_y (MPa)	ϵ_y (%)
Warp (A)	48.7±14%	562±7%	1.32±6%	501±6%	1.04±14%
Weft (B)	49.0±8%	508±2%	1.10±9%	482±5%	1.00±14%

Similar tests in both warp and weft directions have also been performed on all-glass specimens using the modified gun. Stress-strain curves for three specimens loaded in the warp direction are compared in fig. 34 and very close agreement is obtained. Less good agreement was observed in tests on specimens loaded in the weft direction. Stress-strain curves for two such tests are shown in fig. 35. A third test in this direction was unsuccessful and will be repeated when the opportunity occurs. Mean stress-strain curves for the warp and weft directions, taken from figs. 34 and 35, are compared in fig. 36. Here there is a significant reduction in both modulus and strength in the weft direction but a slight increase in the failure strain. These results supersede those of the earlier impact tests on all-glass specimens and strengthen the suspicion that the earlier tests were on two specimens cut in the weft direction and one cut in the warp direction.

Fig.33 COMPARISON OF IMPACT STRESS-STRAIN CURVES FOR ALL-CARBON SPECIMENS LOADED IN WARP AND WEFT DIRECTIONS

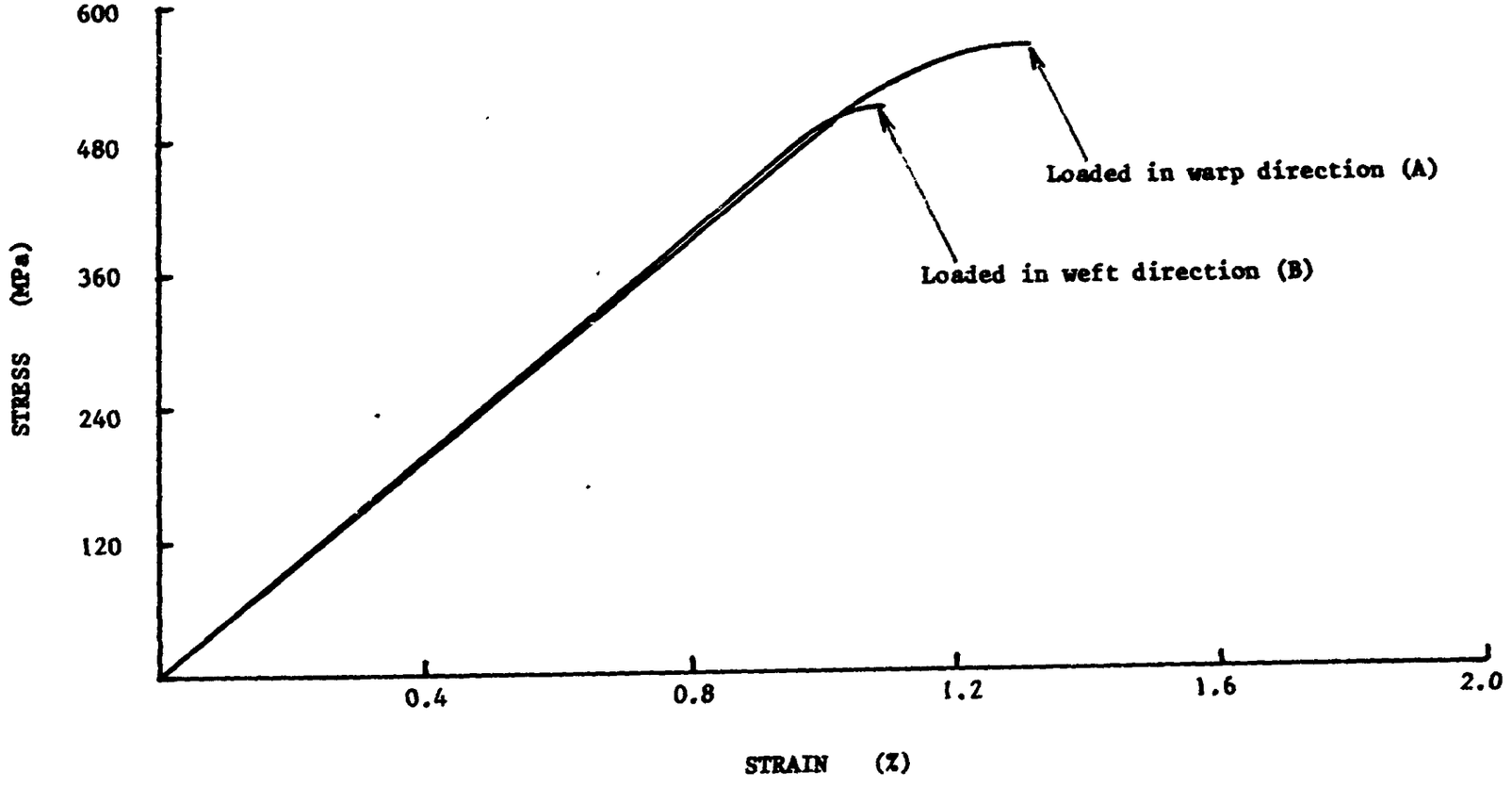

Fig.34 IMPACT STRESS-STRAIN CURVES FOR ALL-GLASS SPECIMENS LOADED IN THE WARP DIRECTION

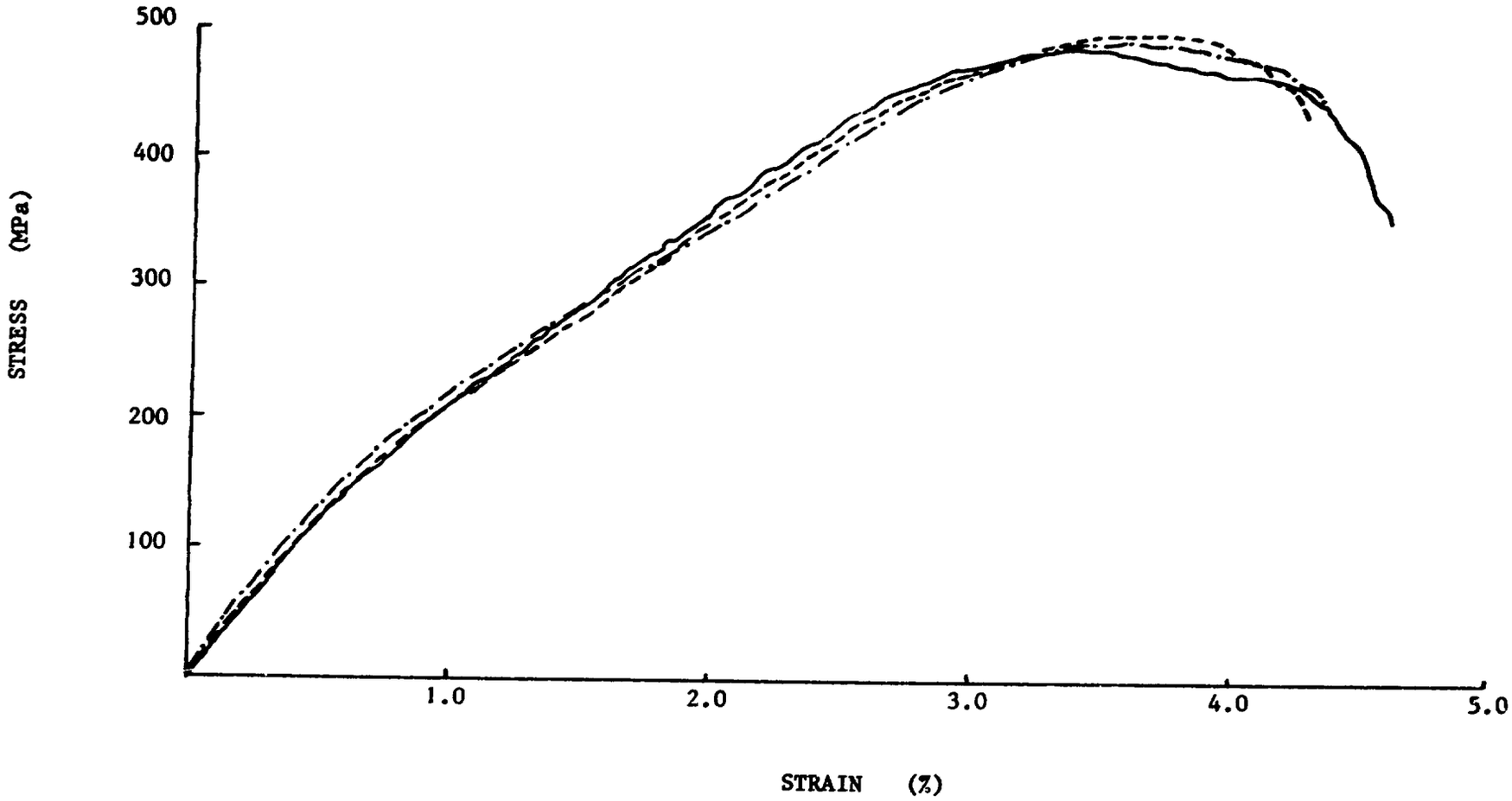

Fig.35 IMPACT STRESS-STRAIN CURVES FOR ALL-GLASS SPECIMENS LOADED IN THE WEFT DIRECTION

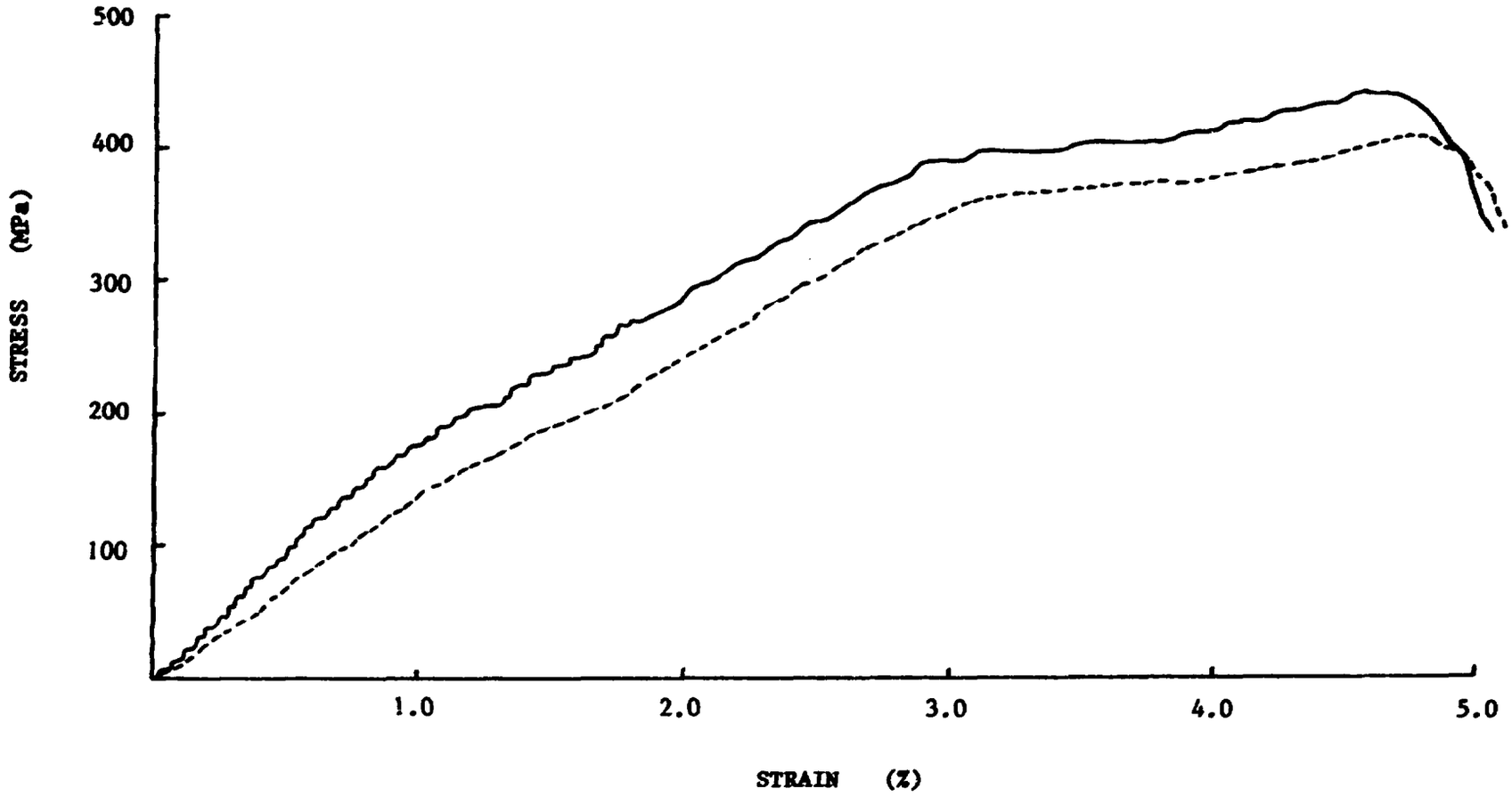

Fig.36 COMPARISON OF IMPACT STRESS-STRAIN CURVES FOR ALL-GLASS SPECIMENS LOADED IN WARP AND WEFT DIRECTIONS

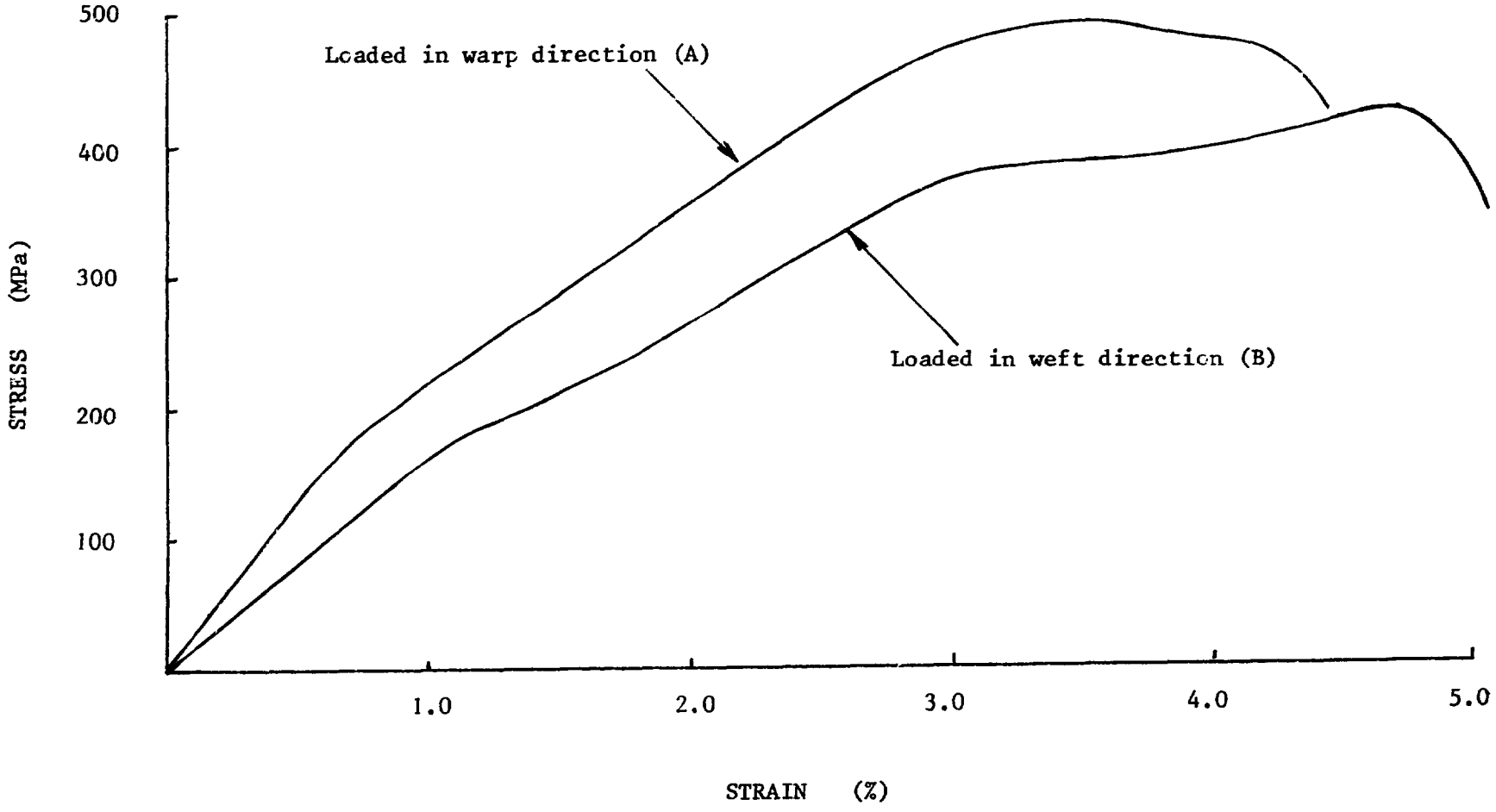

4. ANALYTICAL PREDICTION OF STIFFNESS

In an appendix to the second progress report analytical expressions for the stiffness and strength of interlaminated fabric-reinforced hybrid composites were developed, in terms of the stiffness and strength properties of the constituent plies, either carbon or glass. Since a plain-weave fabric was used in both types of reinforcing ply it was assumed that the properties in the warp and the weft directions would be the same. Subsequently, however, see section 3, experimental measurements have shown that, at least for the glass reinforcing plies, this is not the case. Analytical predictions of the hybrid stiffness have, therefore, to be modified, as outlined in section 4.1 below. The determination of the stiffness matrices for the carbon and the glass plies, based on the results of sections 3.2 and 3.3, is outlined in section 4.2 and the resulting predicted stiffness values for the hybrid specimens compared in section 4.3 with experimental results and the values obtained by a simple 'rule of mixtures' approach.

4.1 Modifications to the Analytical Predictions of Stiffness

The previous analysis assumed a balanced plain-weave reinforcement for which

$$E_L = E_T \quad \text{and} \quad \nu_{TL} = \nu_{LT}$$

where L and T refer, respectively, to the longitudinal and transverse directions and may be taken to correspond to the warp (A) and weft (B) directions in the current analysis. The stiffness matrix was given by

$$Q_{ij} = \begin{bmatrix} Q_{11} & Q_{12} & 0 \\ Q_{12} & Q_{11} & 0 \\ 0 & 0 & Q_{66} \end{bmatrix}$$

and for a laminated, symmetrically-stacked, composite material with no relative orientation between the principal material directions of the plies, the elements of the extensional stiffness matrix were given by

$$A_{ij} = \sum_{k=1}^{n} (Q_{ij})_k (h_k - h_{k-1})$$

Applied to a symmetrically-stacked hybrid with a total of n plies, of which m are of fabric 'b', each of thickness h_b, and (n−m) of fabric 'a', each of thickness h_a, the matrix A_{ij} becomes

$$A_{ij} = (n - m)h_a \begin{bmatrix} (1 + \alpha\beta)(Q_{11})_a & (1 + \alpha\lambda)(Q_{12})_a & 0 \\ (1 + \alpha\lambda)(Q_{12})_a & (1 + \alpha\beta)(Q_{11})_a & 0 \\ 0 & 0 & (1 + \alpha\eta)(Q_{66})_a \end{bmatrix}$$

where the parameters α, β, λ, and η are given by

$\alpha = (m/(n-m))(h_b/h_a)$; $\beta = (Q_{11})_b/(Q_{11})_a$; $\lambda = (Q_{12})_b/(Q_{12})_a$; and $\eta = (Q_{66})_b/(Q_{66})_a$.

Under uniaxial tension with the load applied in the x-direction this gave

$$E_x = \phi/\{(1+\alpha)(1+\alpha\beta)(Q_{11})_a\}$$

where

$$\phi = (1+\alpha\beta)^2(Q_{11})_a^2 - (1+\alpha\lambda)^2(Q_{12})_a^2$$

For the general case, however, where

$$E_L \neq E_T \quad \text{and} \quad \nu_{TL} \neq \nu_{LT}$$

this approach has to be modified. The stiffness matrix becomes

$$Q_{ij} = \begin{bmatrix} Q_{11} & Q_{12} & 0 \\ Q_{12} & Q_{22} & 0 \\ 0 & 0 & Q_{66} \end{bmatrix}$$

where $Q_{11} \neq Q_{22}$. The symmetry hypothesis, $\nu_{LT} = \nu_{TL}$, still holds and the expression for the extensional stiffness, A_{ij}, remains unaltered, but when applied to the hybrid lay-up, now has the form

$$A_{ij} = (n-m)h_a \begin{bmatrix} (1+\alpha\beta)(Q_{11})_a & (1+\alpha\lambda)(Q_{12})_a & 0 \\ (1+\alpha\lambda)(Q_{12})_a & (1+\alpha\mu)(Q_{22})_a & 0 \\ 0 & 0 & (1+\alpha\eta)(Q_{66})_a \end{bmatrix}$$

where the additional parameter, μ, is given by $(Q_{22})_b/(Q_{22})_a$. The corresponding expression for the modulus becomes

$$E_x = \phi'/\{(1+\alpha)(1+\alpha\mu)(Q_{22})_a\} \qquad (6)$$

where

$$\phi' = (1+\alpha\beta)(1+\alpha\mu)(Q_{11})_a(Q_{22})_a - (1+\alpha\lambda)^2(Q_{12})_a^2 \qquad (7)$$

4.2 Determination of the Quasi-Static Stiffness Matrices for the Carbon and the Glass Plies

Results from quasi-static tests on standard tensile specimens cut from the all-glass or the all-carbon laminates and loaded in the warp (A) or weft (B) directions were reported in section 3.2 and are summarised below.

All-glass plies: $E_A = 16.7 \pm 0.3$ GPa (3 tests)
$E_B = 13.7 \pm 0.4$ GPa (3 tests)

All-carbon plies: $E_A = 43.3 \pm 2.7$ GPa (3 tests)
$E_B = 42.5 \pm 1.3$ GPa (4 tests)

Results from quasi-static elastic tests on parallel-sided coupons cut from the same laminates with axes aligned in the warp (A), weft (B) or 45° (C) directions, each reloaded several times in the elastic range, were reported in section 3.3 and are summarised below.

All-glass plies:	E_A = 16.35 GPa	ν_{AB} = 0.164	(3 loadings)
	E_B = 13.77 GPa	ν_{BA} = 0.141	(3 loadings)
	E_C = 5.39 GPa		(3 loadings)
All-carbon plies:	E_A = 46.4 GPa	ν_{AB} = 0.144	(3 loadings)
	E_B = 43.6 GPa	ν_{BA} = 0.088	(3 loadings)
	E_C = 9.58 GPa		(3 loadings)

The same parallel-sided coupons were subsequently loaded to failure, when they pulled out of the grips, see sections 2.2 and 3.3, and a further measure of the elastic constants was obtained, as listed below.

All-glass plies:	E_A = 17.1 GPa	ν_{AB} = 0.167	(1 test)
	E_B = ----	ν_{BA} = 0.128	(1 test)
	E_C = 6.41 GPa		(1 test)
All-carbon plies:	E_A = 47.5 GPa	ν_{AB} = 0.125	(1 test)
	E_B = 45.4 GPa	ν_{BA} = 0.091	(1 test)
	E_C = 10.7 GPa		(1 test)

From the three sets of results summarised above a final set of mean values may be derived and are listed in Table V.

TABLE V Mean Quasi-Static Elastic Constants for Glass and Carbon Plies

Material	E_A (GPa)	E_B (GPa)	E_C (GPa)	ν_{AB}	ν_{BA}	ν^*_{BA}	G^{**}_{AB} (GPa)
All-glass	16.6	13.75	5.65	0.165	0.138	0.137	1.69
All-carbon	45.3	43.3	9.86	0.139	0.089	0.133	2.73

where ν^*_{BA} is determined from equation (1) and G^{**}_{AB} from equation (2), see section 3.3.

Using the mean values for E_A, E_B and ν_{AB}, the derived values for ν^*_{BA} and G^{**}_{AB} and assuming the standard expressions for the components of the stiffness matrix,

$$Q_{11} = E_A/(1 - \nu_{AB}\nu_{BA})$$

$$Q_{22} = E_B/(1 - \nu_{AB}\nu_{BA})$$

$$Q_{12} = \nu_{AB}E_B/(1 - \nu_{AB}\nu_{BA}) = \nu_{BA}E_A/(1 - \nu_{AB}\nu_{BA})$$

$$Q_{66} = G_{AB}$$

the following stiffness matrices are obtained for the all-glass and the all-carbon plies under quasi-static loading:-

$$(Q_{ij})_{GFRP} = \begin{bmatrix} 17.0 & 2.3 & 0 \\ 2.3 & 14.1 & 0 \\ 0 & 0 & 1.6 \end{bmatrix} \quad \text{and}$$

$$(Q_{ij})_{CFRP} = \begin{bmatrix} 46.2 & 6.1 & 0 \\ 6.1 & 44.1 & 0 \\ 0 & 0 & 2.7 \end{bmatrix}$$

4.3 Predicted Moduli for Hybrid Specimens

Using the stiffness matrices determined above the various parameters β, μ and λ may be obtained from

$$\beta = (Q_{11})_b/(Q_{11})_a = 0.368$$

$$\mu = (Q_{22})_b/(Q_{22})_a = 0.320 \quad \text{and}$$

$$\lambda = (Q_{12})_b/(Q_{12})_a = 0.377$$

where the suffices (a) and (b) refer to the carbon and the glass plies respectively. For each of the three hybrid lay-ups the parameter α, and hence from equation (7) also the parameter ϕ', may be determined:

Hybrid type 1 : $\alpha = 1.27$: $\phi' = 4150\ (GPa)^2$
Hybrid type 2a : $\alpha = 0.57$: $\phi' = 2869\ (GPa)^2$
Hybrid type 2b : $\alpha = 0.28$: $\phi' = 2408\ (GPa)^2$

For loading in the warp direction the predicted moduli are obtained from equation (6), giving values of 29.5GPa, 35.1GPa and 39.1GPa, respectively, for the type 1, type 2a and type 2b hybrids. A similar calculation for loading in the weft direction, for which α and ϕ' remain unaltered but for which equation (6) now becomes

$$E_y = \phi'/\{(1 + \alpha)(1 + \alpha\beta)(Q_{11})_a\} \qquad (8)$$

gives reduced values for the predicted moduli of 27.0GPa, 32.7GPa and 36.9GPa, respectively.

In an alternative 'rule of mixtures' approach, taking h_a=0.287mm for the carbon plies and h_b=0.121mm for the glass plies, a further set of predicted moduli are obtained and are listed in Table VI. The results of these two sets of predictions for the quasi-static moduli of the three hybrid types are compared, in Table VII, with the experimentally determined values. A graphical comparison is given in fig. 37. Very close agreement is observed between the predictions based on the laminate theory approach and those derived from the rule of mixtures for both warp and weft directions. The experimental measurements fall close to the predicted values for the warp direction, the biggest divergence being for the type 1 hybrids where the experimental value exceeds the analytical

Fig.37 COMPARISON BETWEEN ANALYTICAL PREDICTIONS AND EXPERIMENTALLY DETERMINED VALUES OF QUASI-STATIC HYBRID MODULI

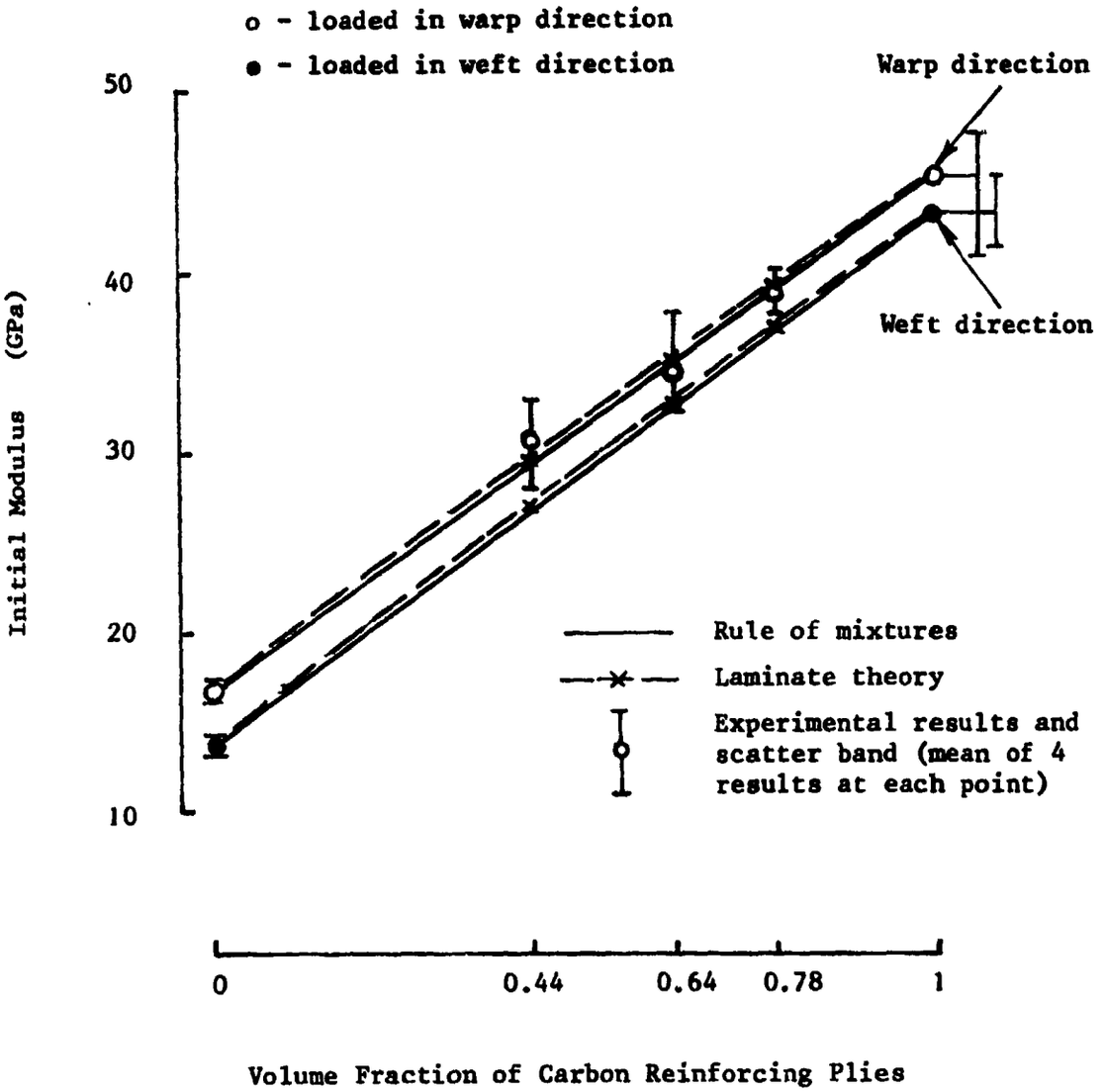

TABLE VI 'Rule of Mixtures' Predictions of Quasi-Static Hybrid Moduli

Hybrid	No. of Plies		Volume fraction of carbon, (V_f)	Predicted Moduli (GPa)	
	Carbon	Glass		Warp	Weft
Type 1	6	2	0.44	29.3	26.8
Type 2a	4	3	0.64	35.0	32.7
Type 2b	2	3	0.78	39.0	36.8

prediction by about 4%. It had been assumed that the hybrid specimens were being loaded in the warp direction. In view, however, of some of the anomalies observed in section 3.1, this will have to be checked before firm conclusions can be drawn.

TABLE VII Comparison between Analytical Predictions and Experimentally Determined Values of Quasi-Static Hybrid Moduli (GPa)

Hybrid	Warp direction (A)		Weft direction (B)		Experimental value
	Laminate theory	Rule of mixtures	Laminate theory	Rule of mixtures	
Type 1	29.5	29.3	27.0	26.8	30.6
Type 2a	35.1	35.0	32.7	32.7	34.4
Type 2b	39.1	39.0	36.9	36.8	38.9

5. DISCUSSION

5.1 Effect of Hybrid Composition on Initial Modulus

The variation of initial modulus with the volume fraction of carbon reinforcing plies in quasi-static tests was shown in fig. 37. The experimental results for the three hybrid lay-ups are seen to agree closely with the predictions of both the rule of mixtures and the laminate theory, assuming the specimens had been loaded in the warp direction. Similar results are given in figs. 38a and 38b for tests at the impact rate and the intermediate rate respectively. Fig. 38a is an amended version of fig. 32 of the second progress report, results for tests in the warp and weft directions on the all-glass and the all-carbon specimens being indicated separately here. The number of tests and the experimental scatter band is given for each testing condition and it is apparent that under impact loading the hybrid moduli fall slightly below the predictions of the rule of mixtures. In this case, however, it is the weft, rather than the warp, direction which is being studied. The laminate theory predictions for the hybrid moduli will be included in fig. 38a once the stiffness matrices for the all-glass and the all-carbon plies under impact loading have been determined.

At the intermediate rate, see fig. 38b, only the type 2a hybrid specimens were loaded in the warp direction, the remaining specimens all being loaded in the weft direction. Discounting, therefore, the results for the type 2a specimens, the opposite response is seen at the intermediate rate to that seen under impact loading, the experimentally measured moduli falling slightly above the predictions of the rule of mixtures. Some doubt is thrown on the precise signficance of the difference in response at the three rates of loading when it is seen, in fig. 38b, that the initial modulus for the type 2a hybrids loaded in the warp direction falls slightly below the experimental curve for the other hybrids loaded in the weft direction. However, as pointed out in section 4.3, a check on the assumed warp and weft directions in the hybrid specimens will have to be made before the results of figs. 37 and 38 can be properly compared.

5.2 Effect of Hybrid Composition on the Elastic Limit

The effect of an increasing volume fraction of carbon reinforcing plies on the initial yield stress and on the corresponding yield strain levels in tests at all three rates of loading is shown in figs. 39 and 40 respectively. Unlike the point of maximum stress, which is unambiguously indicated in each test, the 'yield' point, corresponding to the limit of the initial linear elastic region, is much less clearly defined and the measured values given in figs. 39 and 40 are somewhat subjective. They do, however, give a reasonably good indication of general trends in behaviour. In particular, fig. 39 shows that the elastic stress range, at all three loading rates, is approximately doubled between the all-glass specimens and the type 1 hybrids, where the volume fraction of carbon reinforcement is 0.44, but that a further increase in the proportion of carbon to glass reinforcement has very little effect.

Fig.38 COMPARISON BETWEEN ANALYTICAL PREDICTIONS AND EXPERIMENTALLY DETERMINED VALUES OF HYBRID MODULI

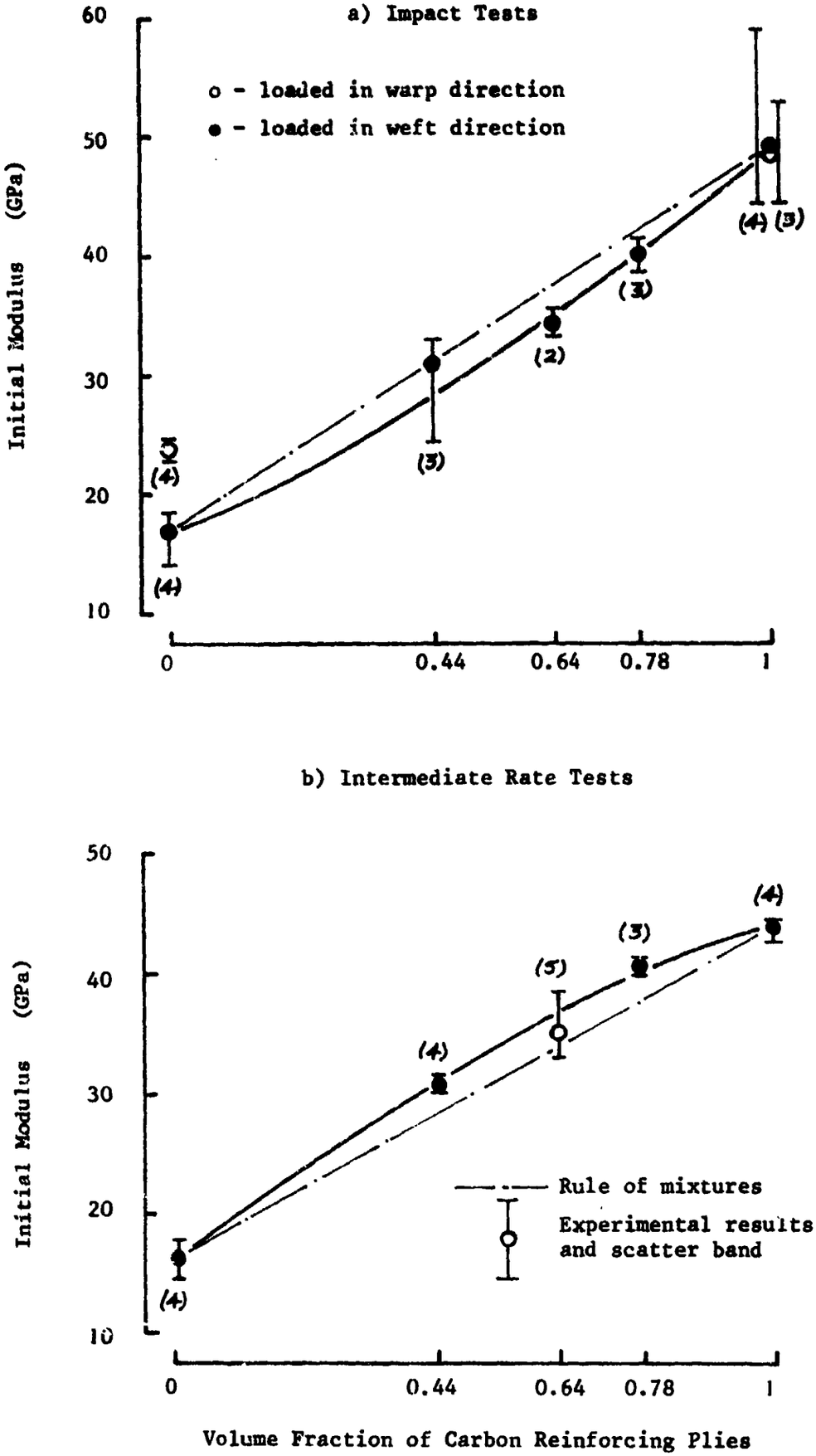

Fig.39 EFFECT OF HYBRID VOLUME FRACTION ON STRESS AT LIMIT OF LINEAR ELASTIC RESPONSE

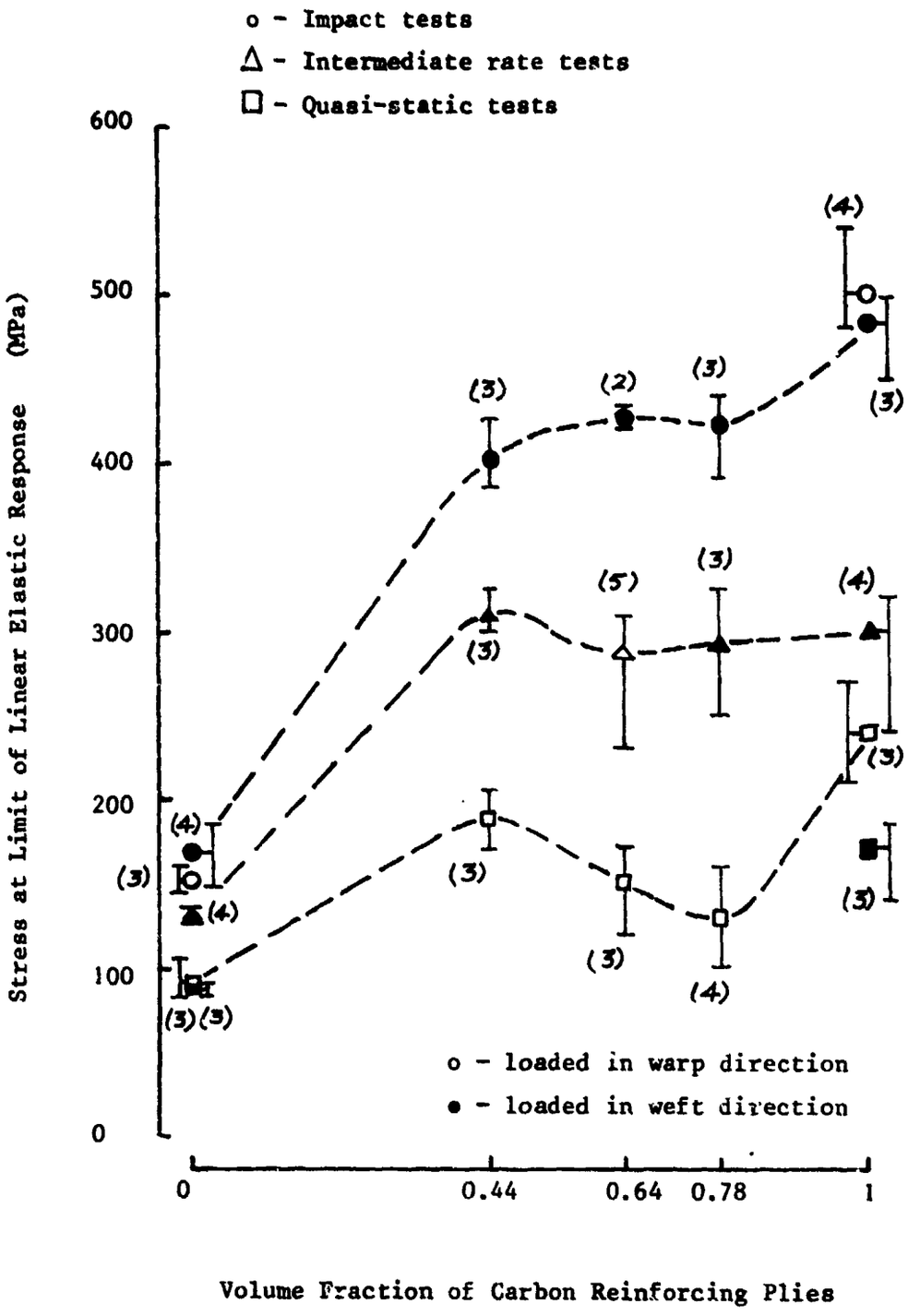

Fig.40 EFFECT OF HYBRID VOLUME FRACTION ON STRAIN AT LIMIT OF LINEAR ELASTIC RESPONSE

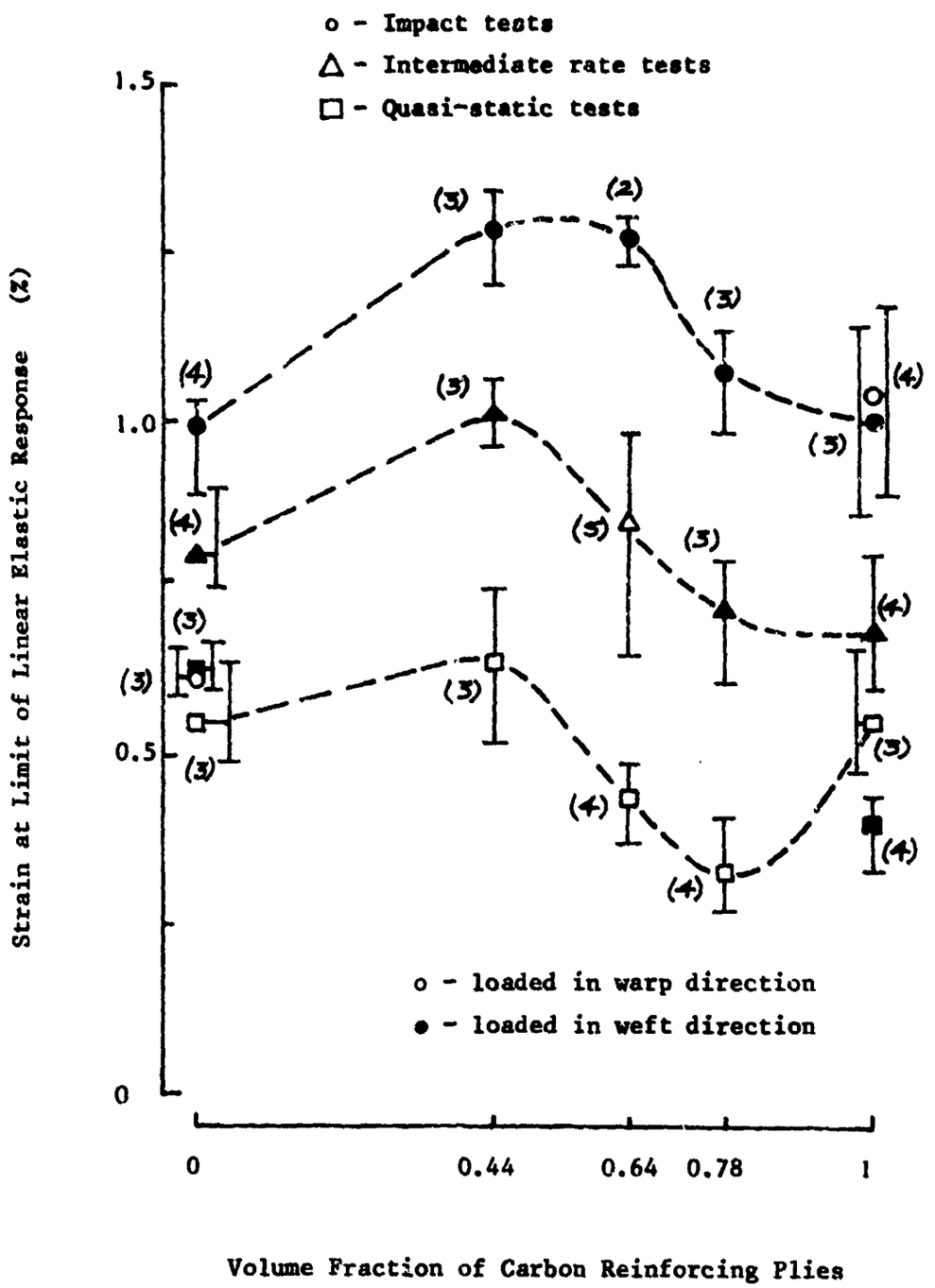

It has been suggested (10) that the yield point, i.e. the limit of the linear elastic response, in woven glass-reinforced composites corresponds to the situation where the axially-aligned fibre tows have sufficiently straightened under the applied load that, in regions of high local stress (or strain) concentration, the resin matrix develops cracks and breaks up. This is followed by a region of reduced stiffness, the 'knee' effect, until the onset of fibre fracture leads to final failure. For the woven carbon-reinforced composites the higher initial stiffness of the carbon fibre reinforcing mat leads to a higher yield point, assuming break up of the resin depends principally on a critical strain being reached. The region of reduced stiffness in the stress-strain response is correspondingly less marked, particularly as fracture of the first carbon fibre tow is more likely to lead to catastrophic failure.

In the present results, if the yield point was controlled solely by the attainment of a critical strain in the matrix, then the stress levels in fig. 39 should show the same general trends as the moduli in figs. 37 and 38. However, it is clear from fig. 40 that, although the yield strain is approximately constant at any given loading rate there are considerable fluctuations about the mean value where the hybrid specimens are concerned, e.g. 0.5%±0.2% at the quasi-static rate, 1.1%±0.2% under impact loading, leading to corresponding fluctuations in the yield stress, see fig. 39. This is not surprising in view of the different geometries of weave in the glass and the carbon reinforcement, the glass having a very fine and the carbon a much coarser weave configuration, suggesting that the critical strain at yield might be different for the two types of reinforcement. This is not borne out by the results of fig. 40, however, which show the same yield strain for the all-glass and the all-carbon plies in quasi-static tests when loaded in the warp direction and in impact tests when loaded in the weft direction and closely similar yield strains in medium rate tests also when loaded in the weft direction. The situation is confused, however, by conflicting results for quasi-static tests in the weft direction where the all-carbon plies yield at a significantly lower strain and for impact tests in the warp direction where the reverse is the case.

Despite these anomalies the general trends observed in figs. 39 and 40 at all three rates of loading and in three different testing machines are sufficiently similar to suggest that some significance may be placed on them. It should perhaps be noted that in addition to the volume fraction of carbon reinforcing plies a further difference between the three hybrid lay-ups is in the type of interlaminar regions present, both carbon/glass and glass/glass in the type 1 hybrids, only carbon/glass in the type 2a and 2b hybrids. This could have an effect on the local stress concentrations leading to the matrix break up at yield. A more detailed discussion of this possibility, however, will have to await the results of the programme to model the impact response of fibre-reinforced composites which is due to start shortly.

---

(10) Welsh, L. M. and Harding, J., "Effect of Strain Rate on the Tensile Failure of Woven-Reinforced Polyester Resin Composites", in 'Mechanical and Physical Behaviour of Materials under Dynamic Loading', Proc. DYMAT 85, J. de Physique, Colloque C5, Supplement No.8, Vol. 46, August 1985, 405-414.

5.3 Effect of Hybrid Composition on the Maximum Stress and Failure Strain

At all three loading rates the maximum stress preceding final failure increases with the carbon content, as shown in fig. 41, up to a volume fraction of about 0.8, at which point the hybrid strength exceeds that of the all carbon specimens loaded in the same direction at the same strain rate. This differs from the results as previously reported (in the second progress report, fig. 35) and is due to the distinction that has been made between the properties in the warp and the weft directions. As a consequence a clear hybrid effect is now apparent in that the failure strengths of the hybrids with carbon volume fractions between, say, 0.5 and 0.9 exceed that which would be predicted from a simple rule of mixtures based on the failure strengths of the all-glass and the all-carbon plies. The maximum increase due to this effect is small, only about 10% of the rule of mixtures prediction, but the general trend is consistent at all three rates of loading.

Similar results for the effect of carbon volume fraction on the failure strain, defined as the strain corresponding to the point of maximum stress, are given in fig. 42. A mean failure strain for the all carbon specimens of 1.31±0.3% is determined from the results of all tests on this material in both the warp and the weft directions and at all three loading rates. For each of the three hybrid lay-ups a small hybrid effect, defined as the enhancement of the failure strain of the low elongation phase, is observed, to ∿1.5%, ∿1.6% and ∿1.7% for the type 2b, the type 2a and the type 1 hybrid specimens respectively. A much more marked effect is seen in the all-glass specimens where the failure strain ranges from ∿2.5% in the quasi-static tests to more than 4% under impact loading. Evidence was presented in the second progress report to suggest that in impact tests on the hybrid specimens the relatively low overall failure strain was due to a restriction of the damage zone in the glass-reinforced plies by the limited elongation possible in the qdjacent carbon-reinforced plies. This conclusion was based on an optical and scanning electron microscopic examination of broken specimens after impact. A similar examination of the specimens tested at the two lower rates is still in progress. However, since the failure strains in the hybrids appear relatively insensitive to strain rate (see next section) it is unlikely that anything very different will come out of this further study.

Taking the results of figs. 41 and 42 together it may be seen that hybrid specimens with a carbon volume fraction of between, say, 0.6 and 0.7, at all rates of loading, show both an enhancement of the failure strain over that of the all-carbon plies and an increased failure strength over that predicted by the rule of mixtures.

5.4 Effect of Strain Rate on Hybrid Mechanical Properties

Stress-strain curves, in each case the mean of three tests, for the type 1 hybrid specimens at the three loading rates are compared in fig. 43. The negligible effect of strain rate on the modulus and strain to failure and the marked increase in 'yield' stress and subsequent stress at failure at the higher strain rates were characteristic of all three hybrid lay-ups. Unfortunately the significance of the comparison in fig.

Fig.41 EFFECT OF HYBRID VOLUME FRACTION ON MAXIMUM STRESS

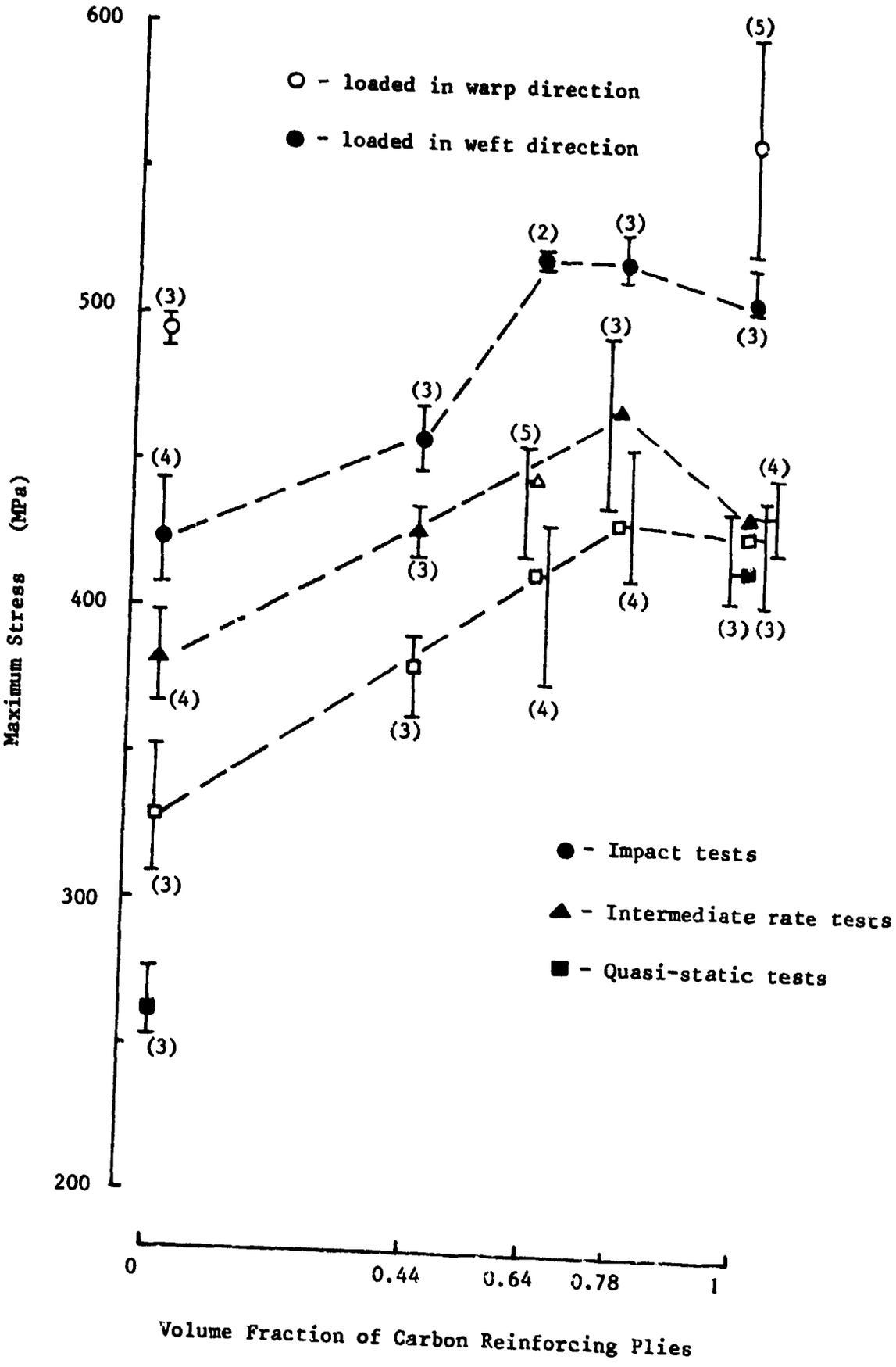

Fig.42 EFFECT OF HYBRID VOLUME FRACTION ON STRAIN AT FAILURE

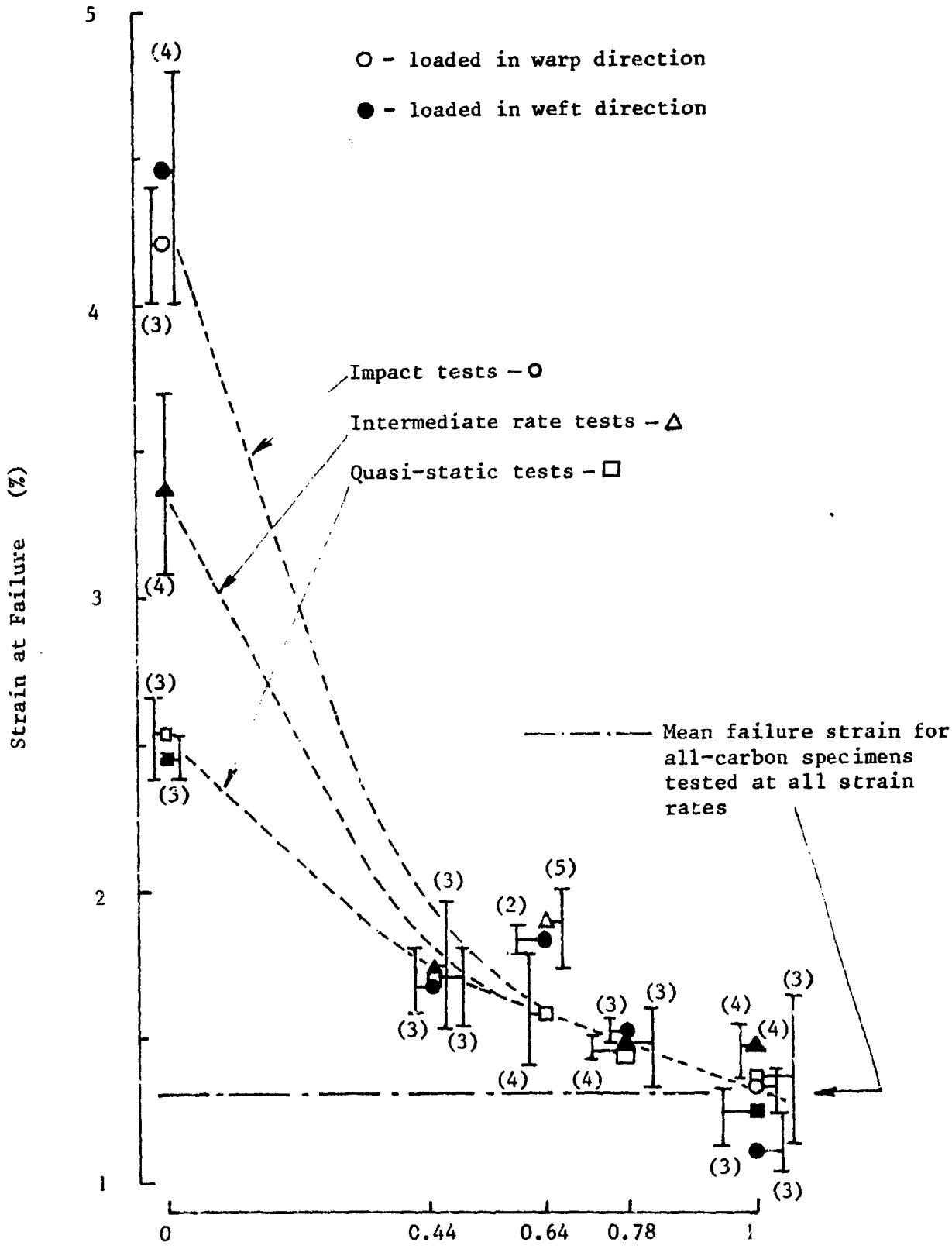

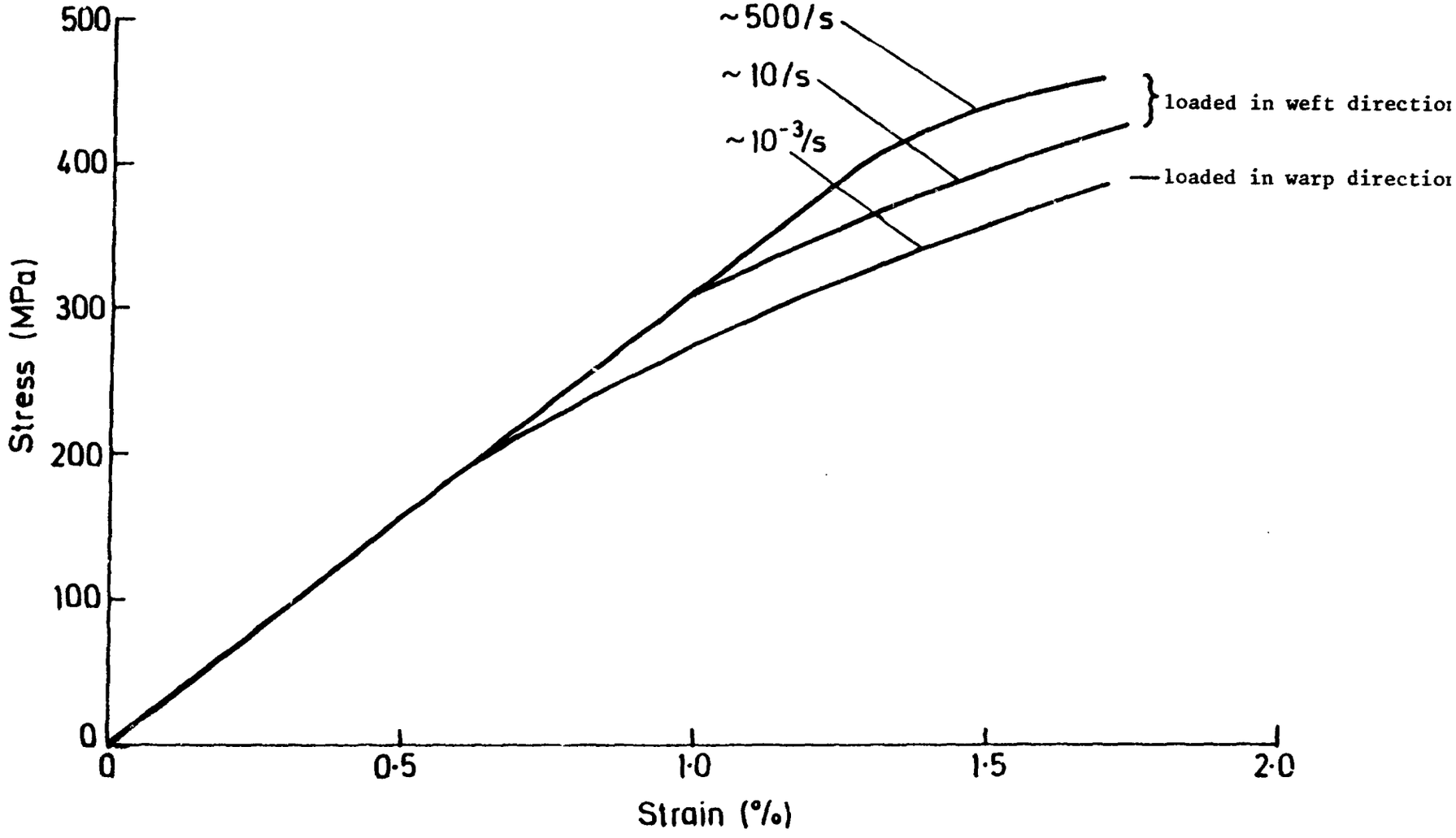

Fig.43 EFFECT OF STRAIN RATE ON STRESS-STRAIN CURVES FOR TYPE 1 HYBRID SPECIMENS

43 is reduced in that the direction of loading (warp or weft) was different at the different loading rates. This was also true of the results for the other two hybrid lay-ups, but not of those for the all-glass and the all-carbon plies. Stress-strain curves for the latter, when loaded in the weft direction, are compared in fig. 44 and here an effect of strain rate on the modulus and on the strain at failure is clearly observed. The general trends shown in fig. 44 are similar to earlier results for plain-weave glass/epoxy composites (11) except that here the rate dependence of the failure strain is more marked and of the modulus and strength rather less marked.

A more detailed description of the effect of strain rate on the mechanical response of the various specimen types is given in figs. 45 to 49. These show the variation of initial modulus, 'yield' and maximum stress and 'yield' and failure strain with the logarithm of the average strain rate for the all-glass and the all-carbon plies and the type 1, type 2a and type 2b hybrids respectively. The mean of each set of measurements, the scatter band and the number of test results obtained is indicated in each case.

For the all-glass specimens loaded in the weft direction the increase in modulus with strain rate is only a little greater than the experimental scatter. In the warp direction, however, the modulus is both greater and more clearly rate dependent. For the all-carbon specimens, fig. 46a, the modulus is the same in the warp and weft directions and there is some indication of an increase in modulus under impact loading although the experimental scatter here is much greater. For each of the three hybrid lay-ups, figs. 47a, 48a and 49a, no significant effect of strain rate on modulus is observed, although the comparison is between specimens loaded in different directions at the various strain rates. Since the hybrid moduli obey the predictions of both the rule of mixtures and the laminate theory in quasi-static tests, see fig. 37, and both the all-glass and the all-carbon plies show an increased modulus with strain rate it would seem at first sight unlikely that the hybrid moduli would reach the rule of mixtures and laminate theory predictions in the impact tests. This is confirmed in fig. 50 for the type 2a and the type 2b hybrids which have moduli falling significantly below the rule of mixtures predictions, by about 10% and about 6% respectively, but not for the type 1 hybrids where the experimentally determined modulus agrees well with the rule of mixtures prediction. Comparison with the predictions of the laminate theory, under impact loading, awaits the determination of the stiffness matrices of the all-glass and the all-carbon plies under these conditions.

For the all-glass specimens, fig. 45b, both the yield stress and the maximum stress increase continuously with strain rate, there being no effect of loading direction on the former but a significant effect on the latter (this being, in fact, the indication of which are the warp and the weft directions). In contrast, for the all-carbon specimens, fig. 46b, the maximum stress only begins to increase at the highest rate

---

(11) Harding, J. and Welsh, L. M., "A Tensile Testing Technique for Fibre-Reinforced Composites at Impact Rates of Strain", J. Mat. Sci., 18, (1983), 1810-1826.

Fig.44 EFFECT OF STRAIN RATE ON STRESS-STRAIN CURVES FOR ALL-GLASS SPECIMENS LOADED IN WEFT DIRECTION

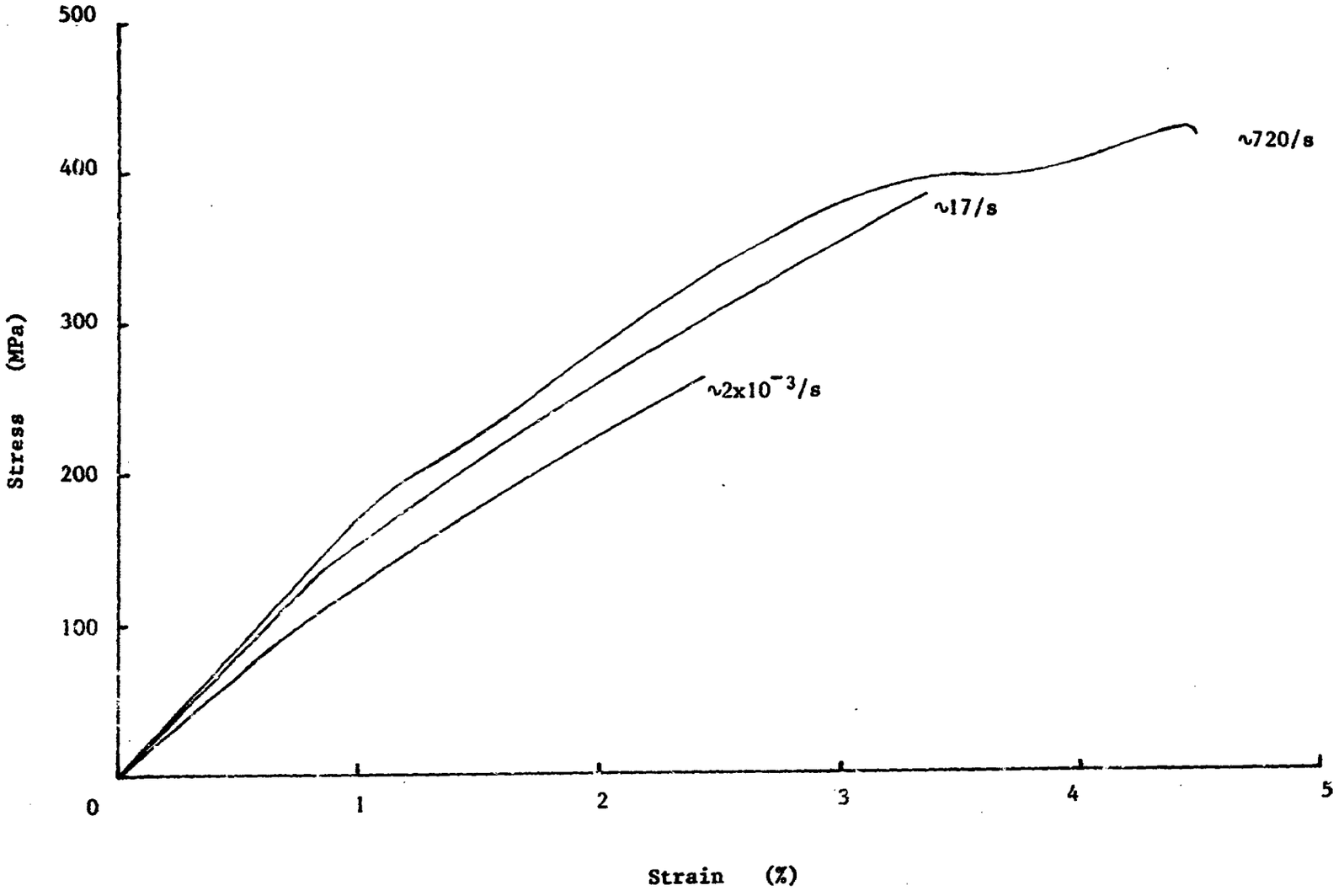

b) 'Yield' and Maximum Stress

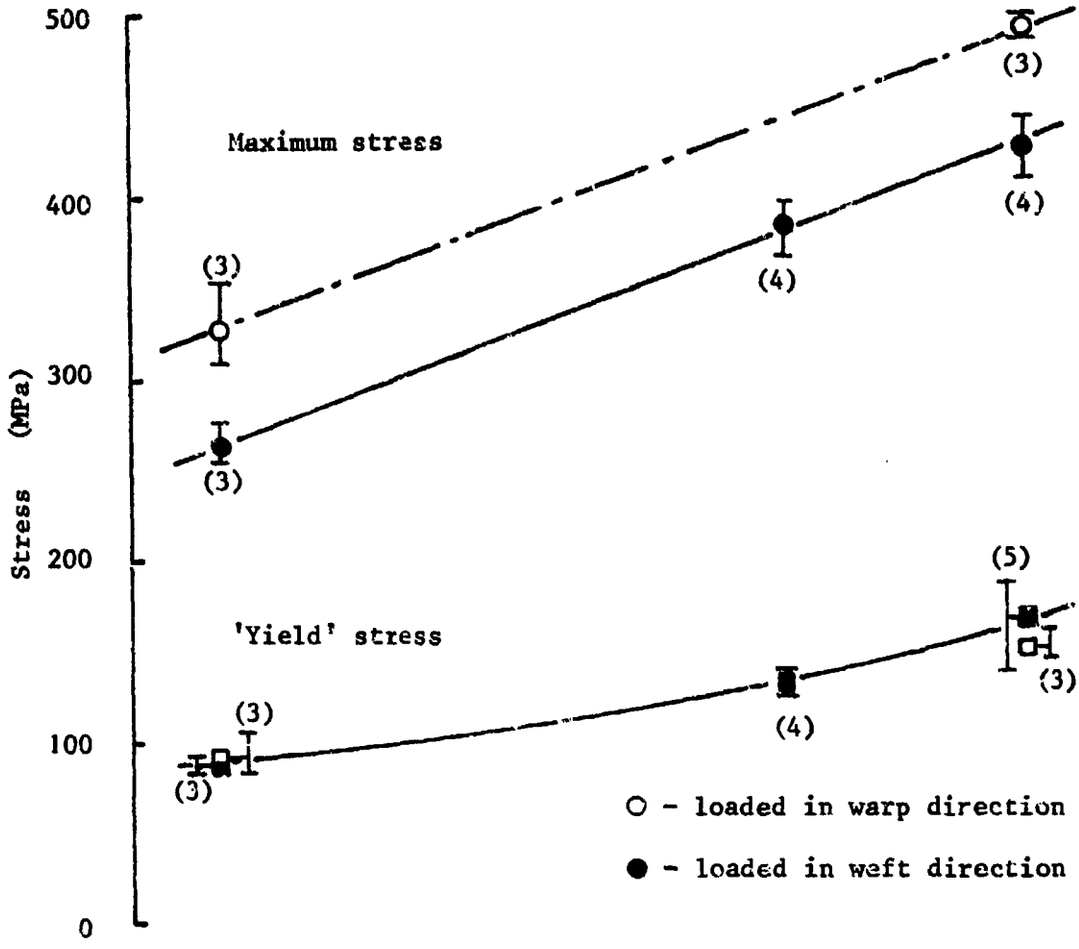

a) Initial Modulus

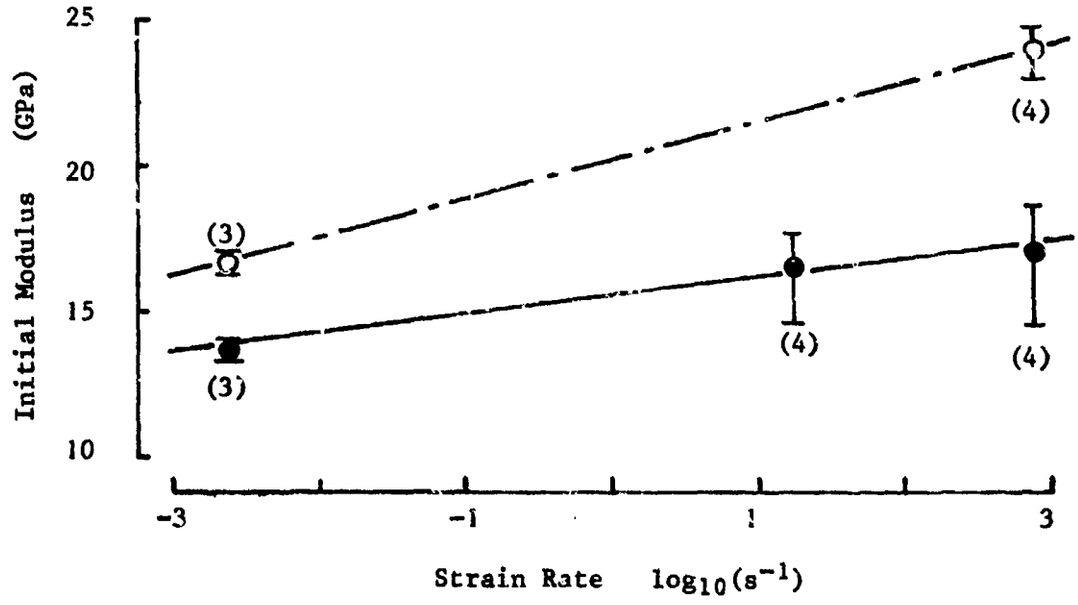

Fig.45 EFFECT OF STRAIN RATE ON TENSILE PROPERTIES OF ALL-GLASS SPECIMENS

c) 'Yield' and Failure Strain

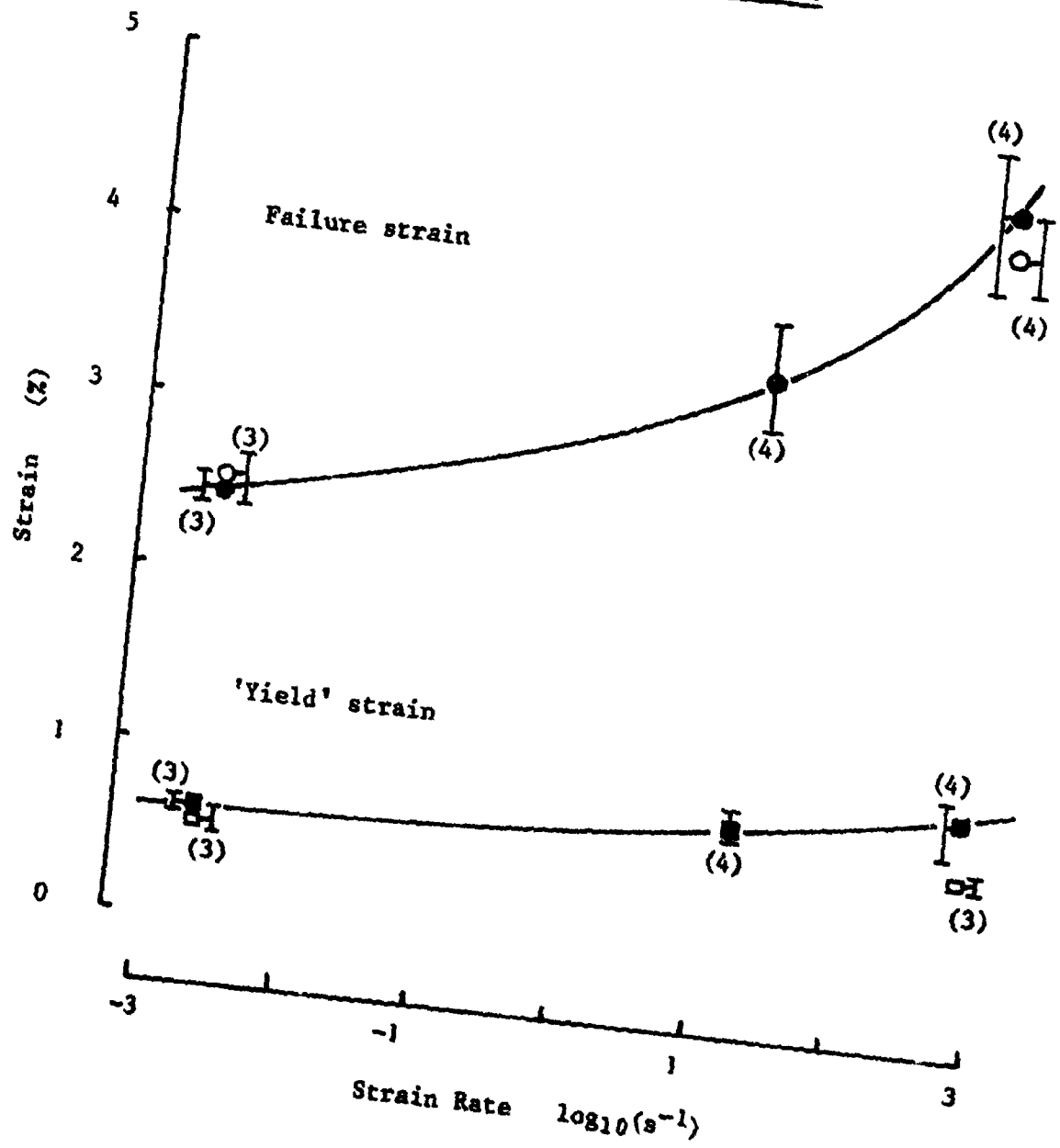

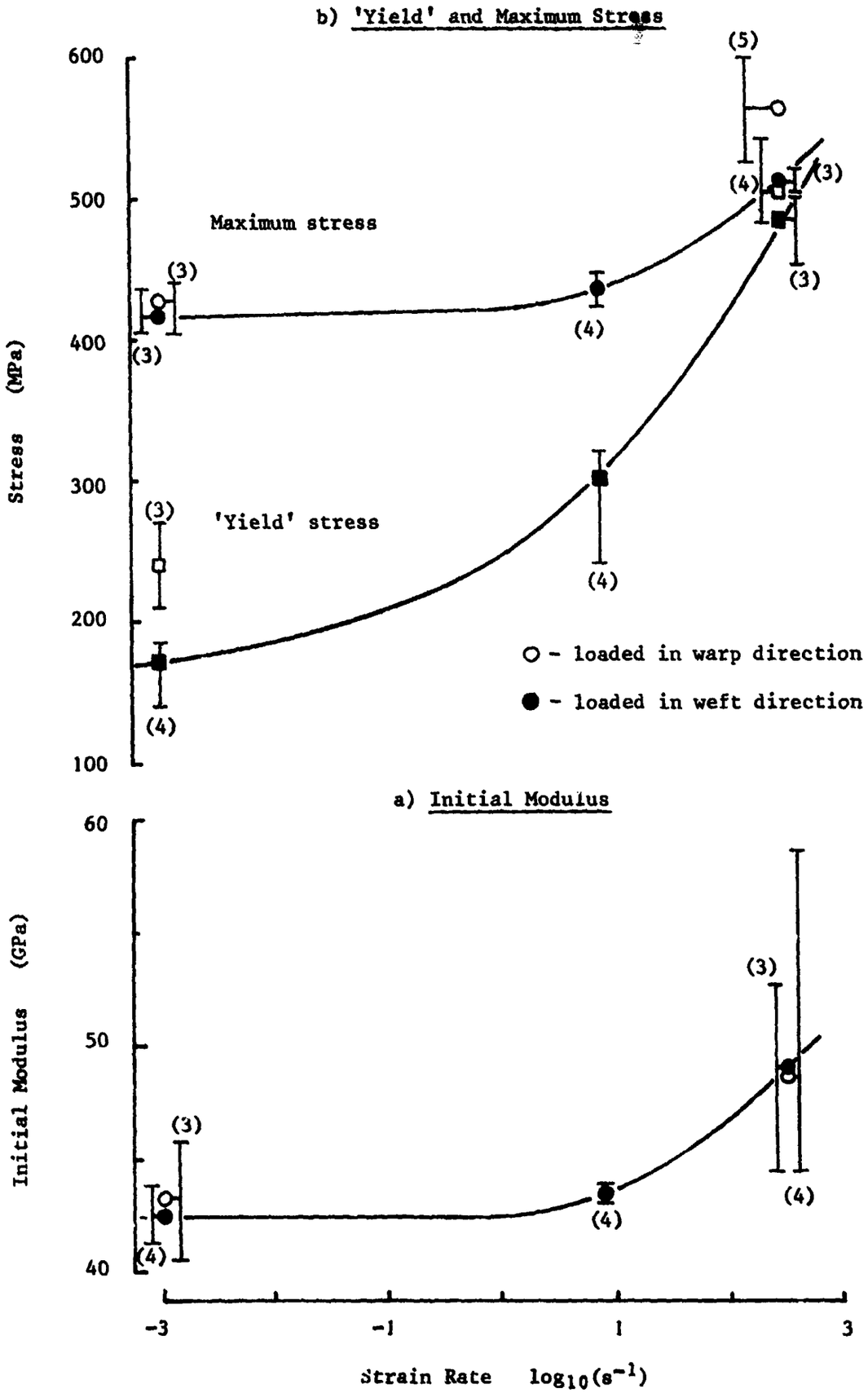

Fig.46 EFFECT OF STRAIN RATE ON TENSILE PROPERTIES OF ALL-CARBON SPECIMENS

c) 'Yield' and Failure Strain

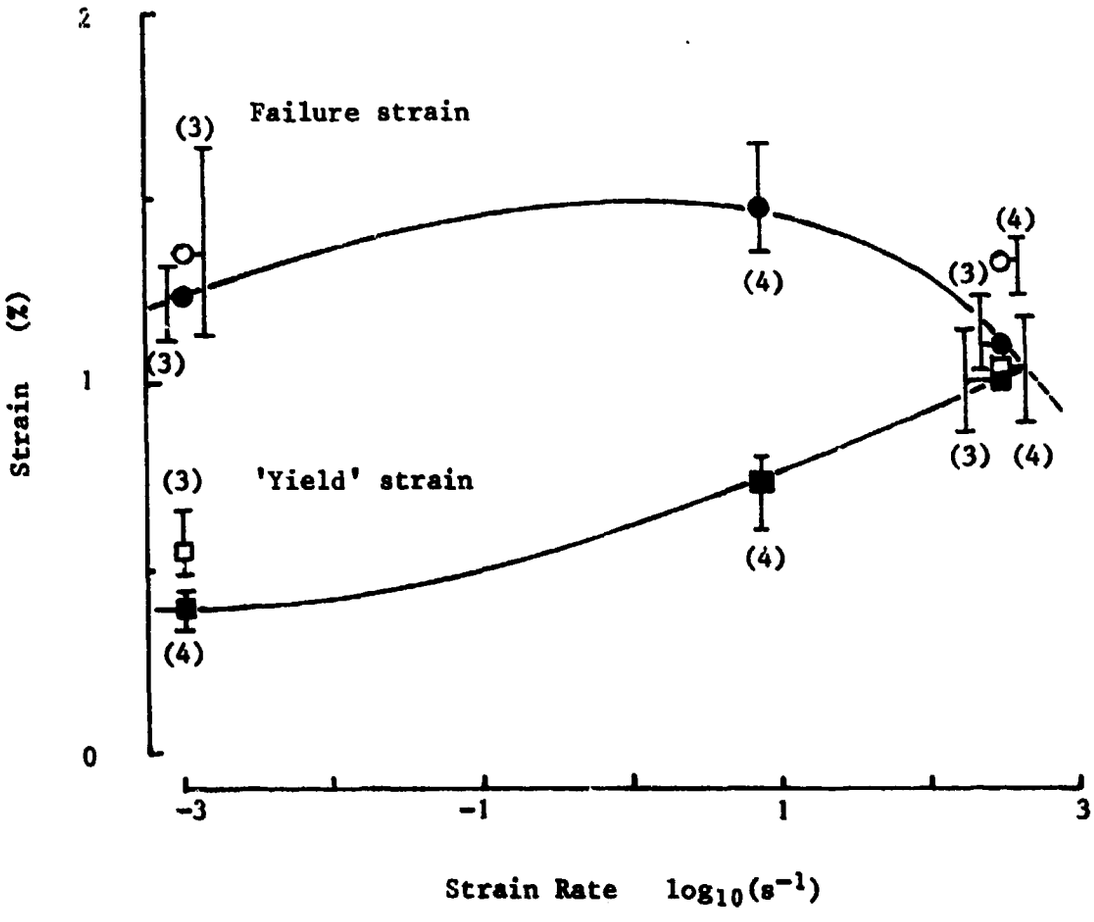

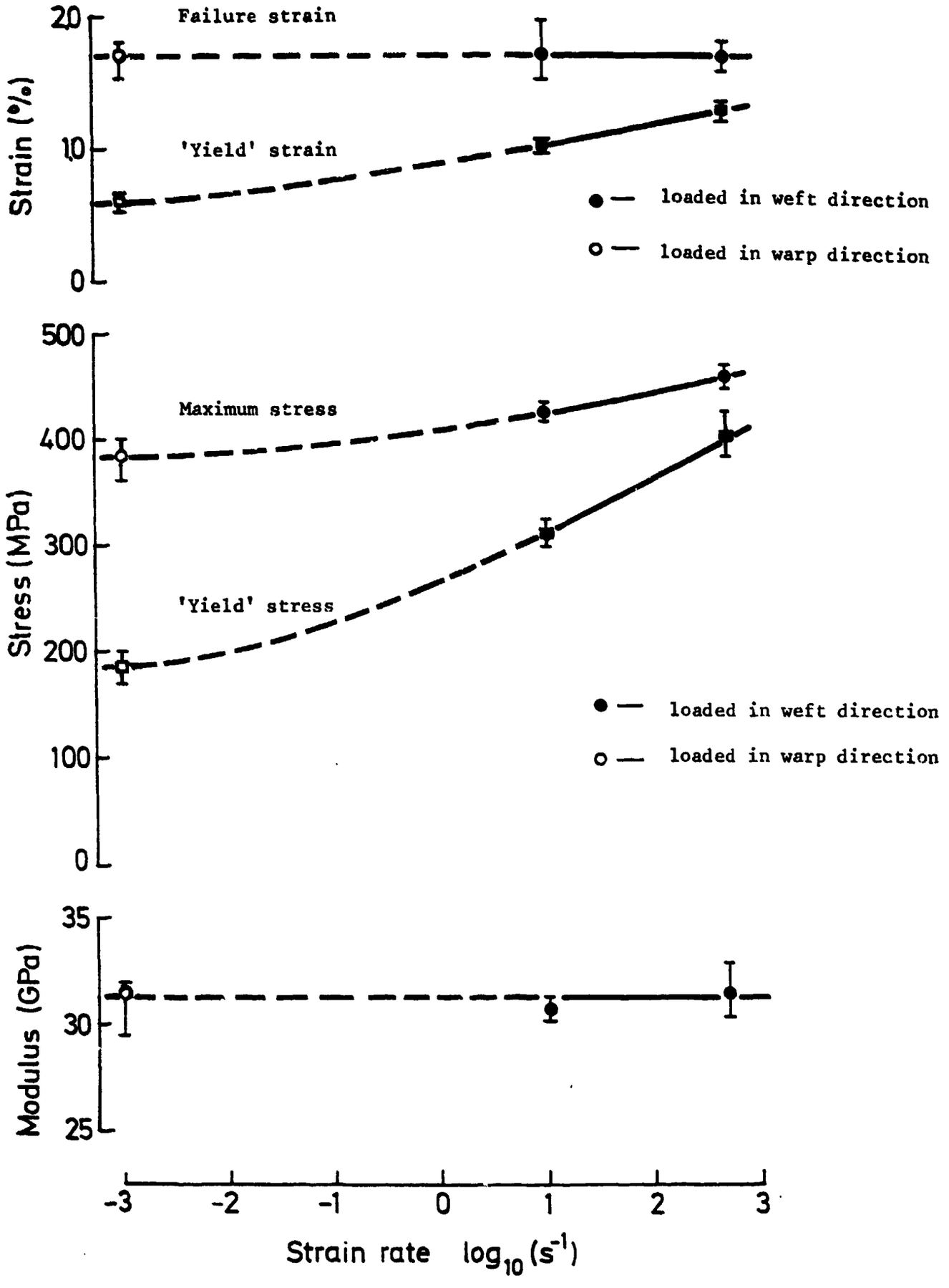

Fig.47 EFFECT OF STRAIN RATE ON TENSILE PROPERTIES OF TYPE 1 HYBRID SPECIMENS

b) 'Yield' and Maximum Stress

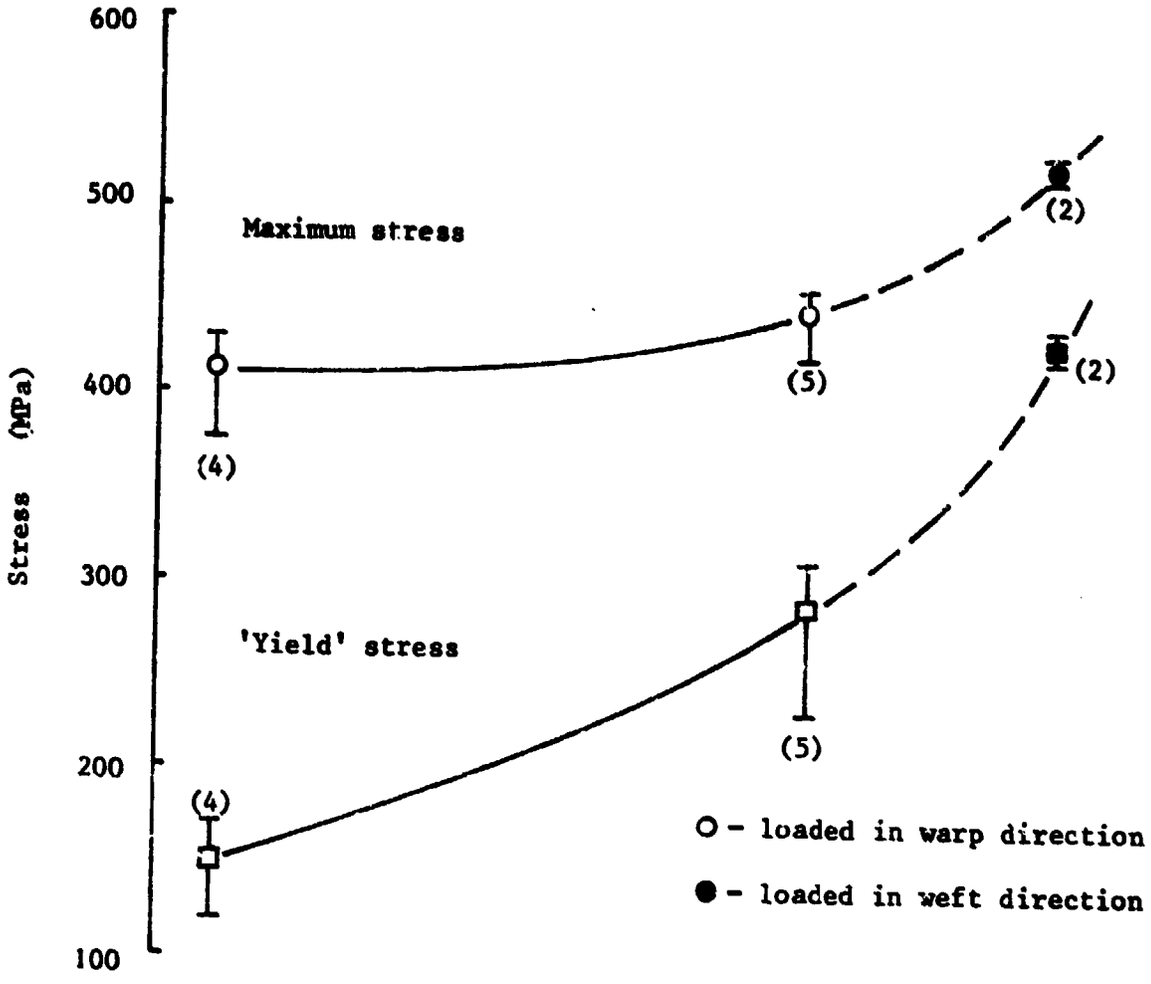

a) Initial Modulus

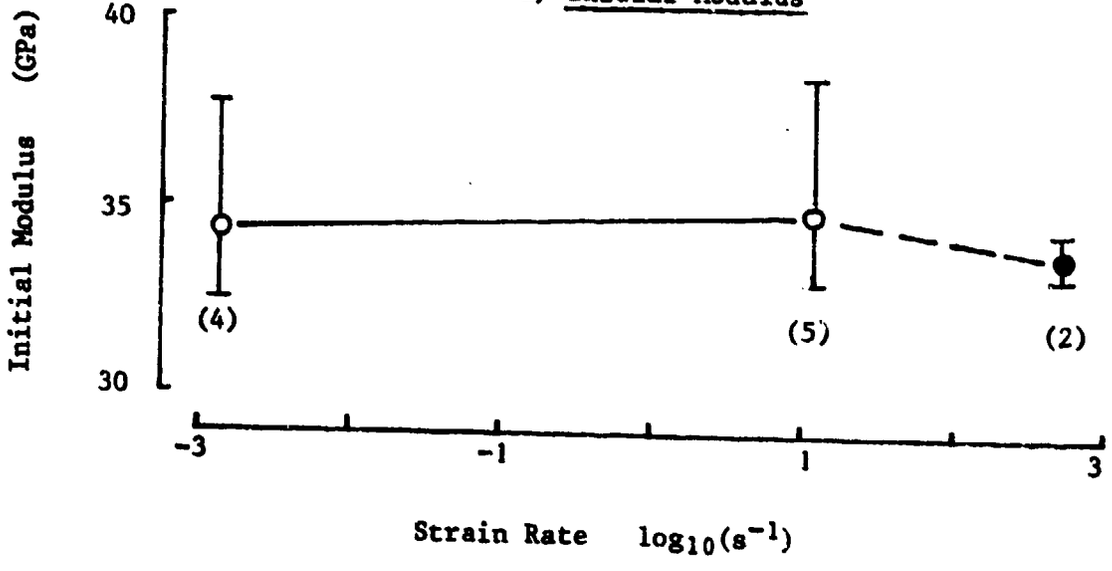

Fig.48 EFFECT OF STRAIN RATE ON TENSILE PROPERTIES OF TYPE 2a HYBRID SPECIMENS

c) 'Yield' and Failure Strain

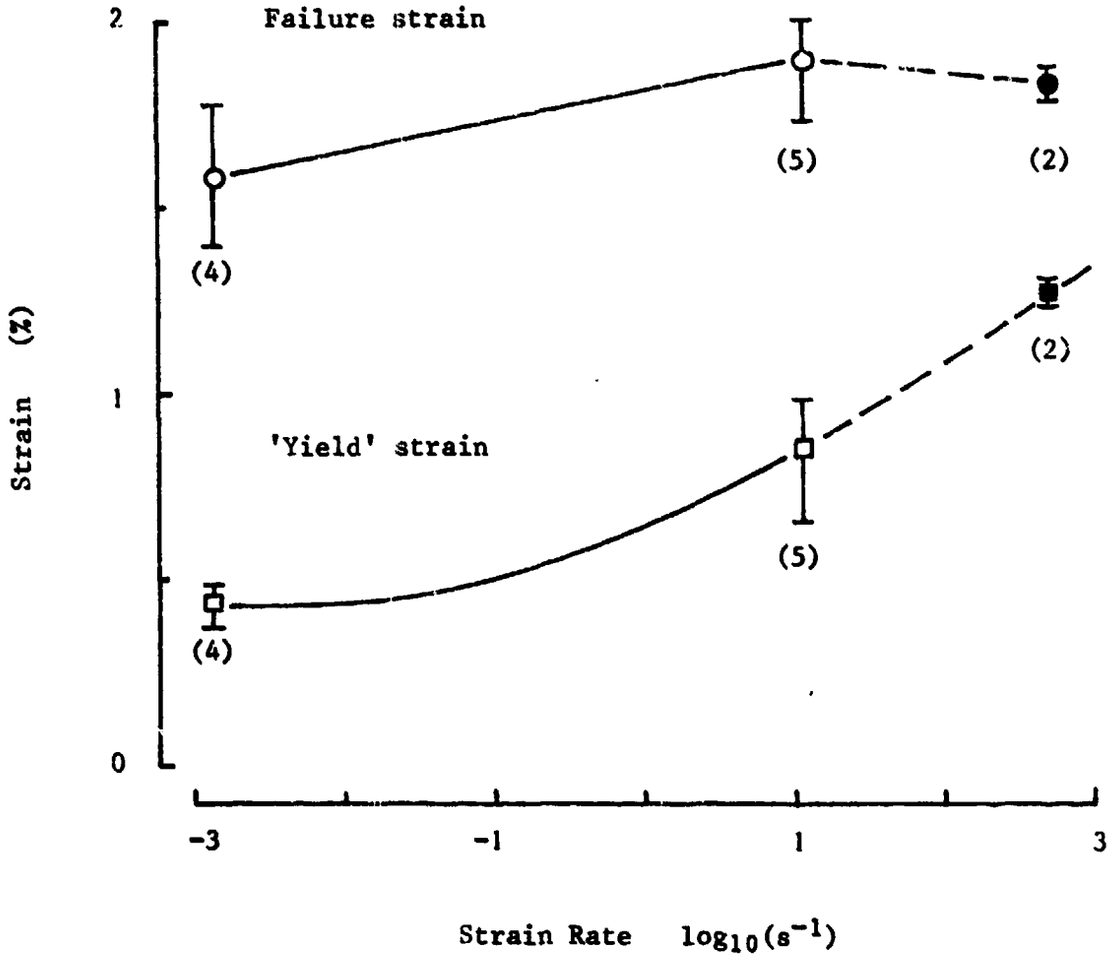

b) 'Yield' and Maximum Stress

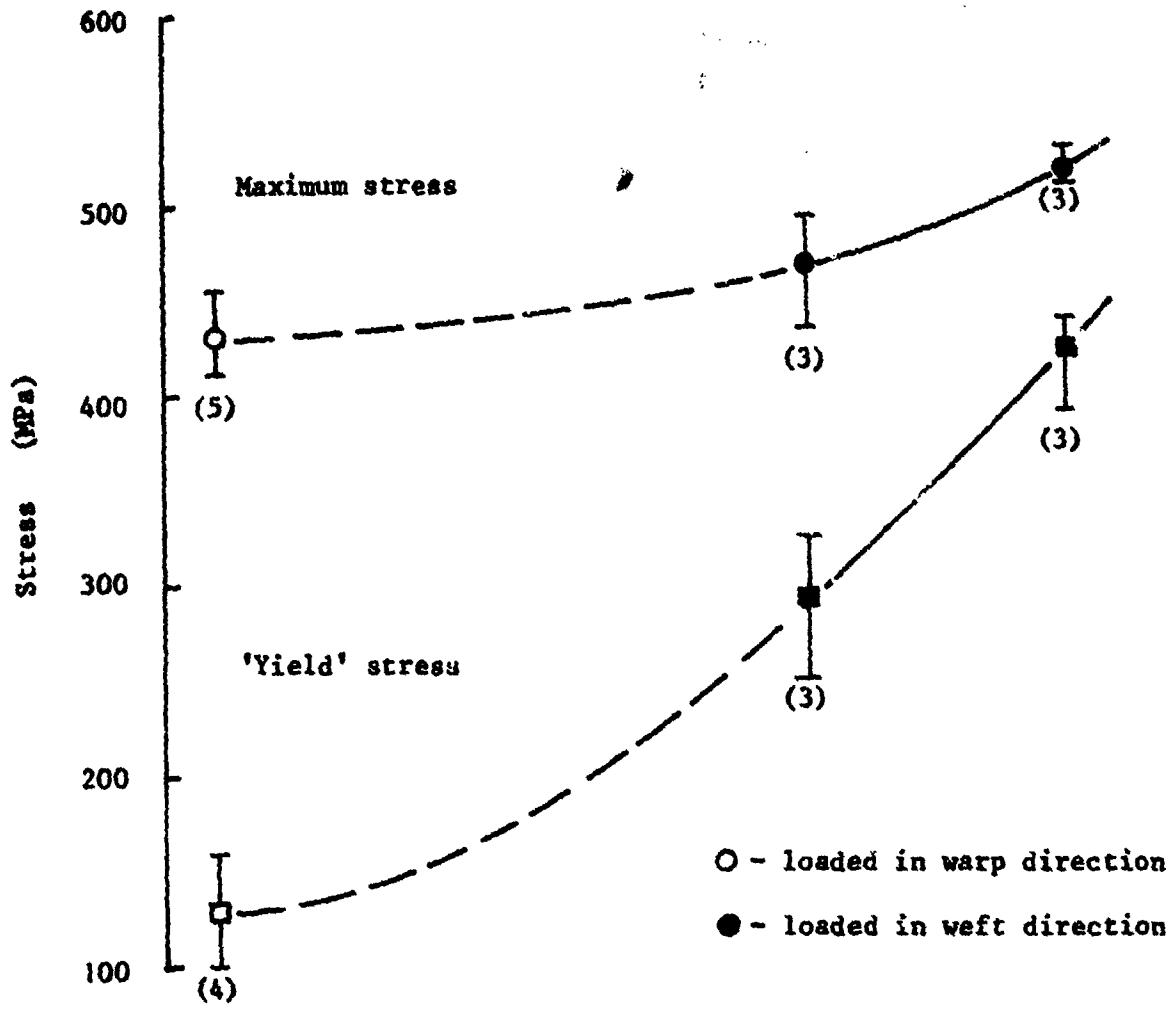

a) Initial Modulus

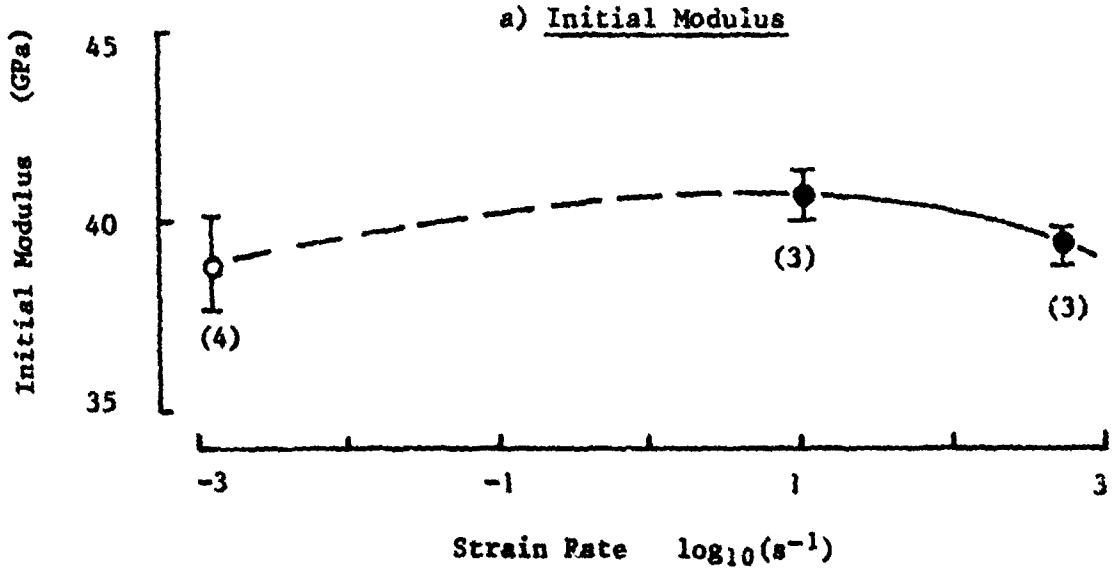

Fig.49 EFFECT OF STRAIN RATE ON TENSILE PROPERTIES OF TYPE 2b HYBRID SPECIMENS

c) 'Yield' and Failure Strain

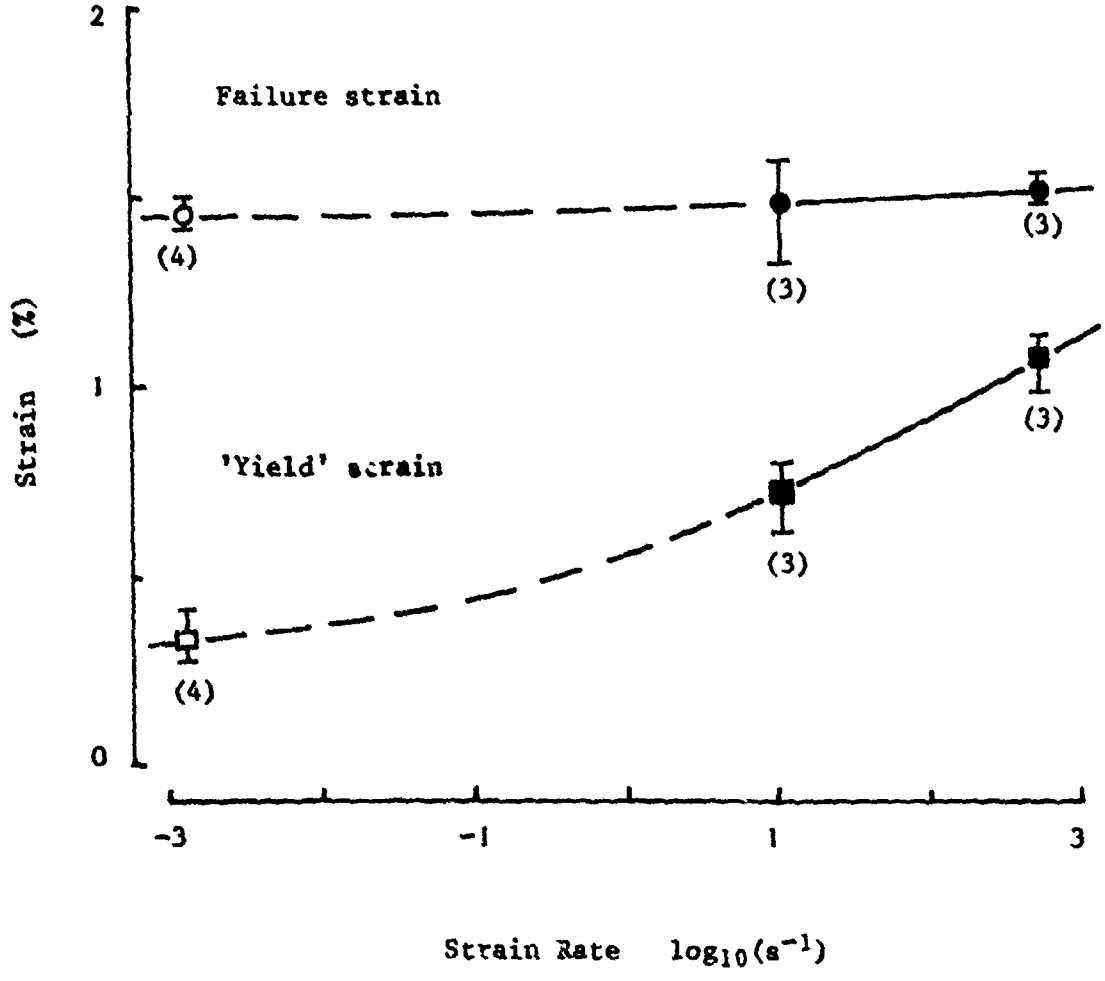

Fig.50 COMPARISON OF HYBRID MODULI UNDER IMPACT LOADING WITH RULE OF MIXTURES PREDICTIONS

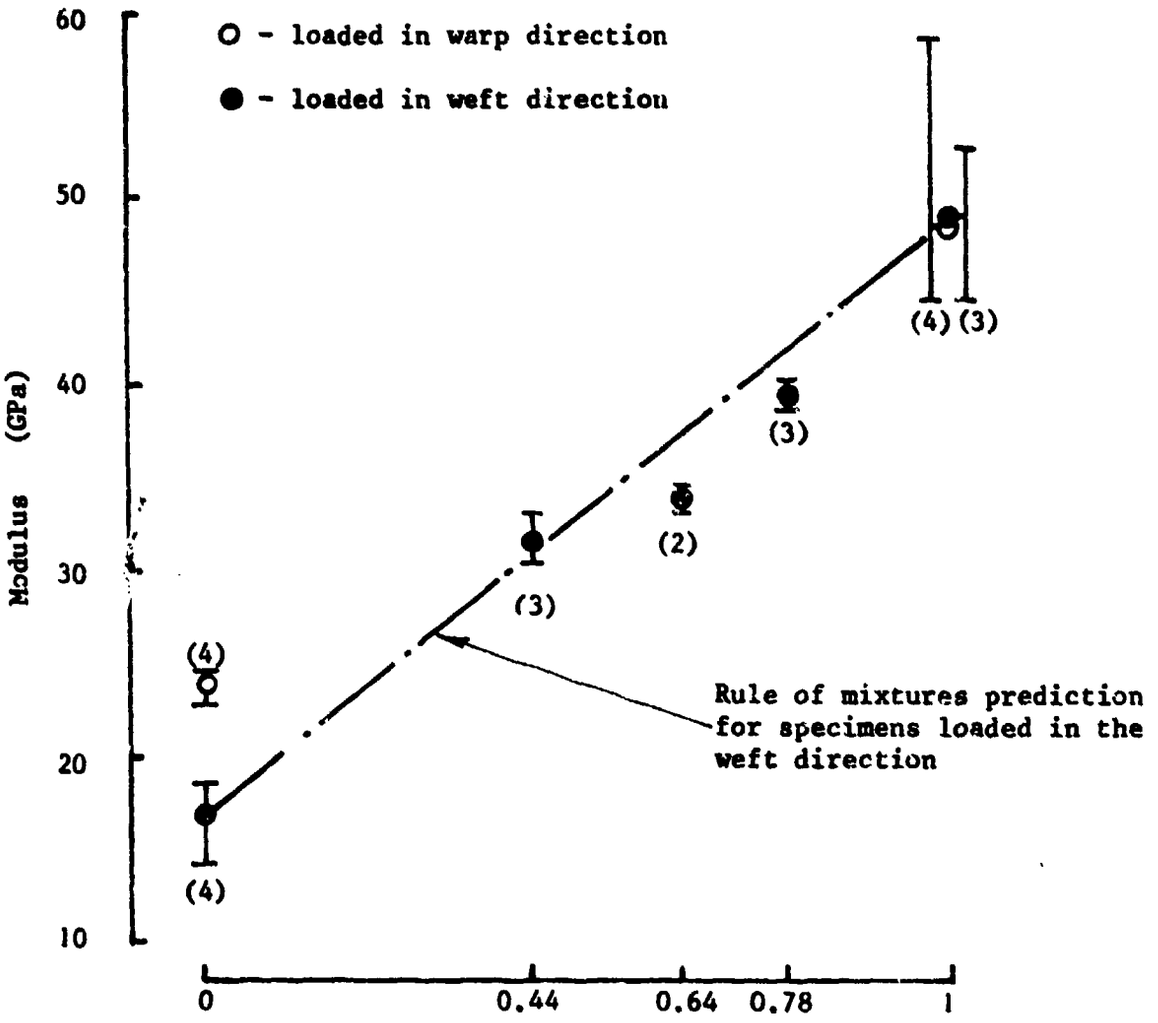

of strain while the yield stress shows a much more marked increase with strain rate at all rates. Thus, while for the all-glass specimens there is a modest increase in the elastic range and a much greater increase in the extent of the subsequent deformation as the strain rate is raised, the all-carbon specimens show the opposite effect with a markedly increased elastic range and a reduced anelastic deformation leading, at the highest strain rates, to a stress-strain curve which is linear-elastic almost through to final failure. The hybrid specimens, as might be expected, showed a response intermediate between these two extremes but tending towards that of the all-carbon specimens. With increasing carbon content the yield stress becomes more markedly strain rate dependent while the maximum stress only exhibits a significant rate dependence at the higher strain rates.

A similar contrast is apparent when considering the effect of strain rate on the strain at yield and at fracture. Thus, for all-glass specimens, fig. 45c, the failure strain is almost doubled between the quasi-static and the impact tests, closely similar results being obtained for the warp and weft directions, while the yield strain increases only very slightly with strain rate. For the all-carbon specimens, however, fig. 46c, it is the yield strain which is doubled while the failure strain shows a slight decrease at the highest strain rates, although the large experimental scatter prevents any great significance from being placed on this observation. Again all three hybrids, figs. 47c, 48c and 49c, show a behaviour tending towards that of the all-carbon specimens with a significantly rate dependent yield strain but, apart from hybrid type 2a, no effect of strain rate on the failure strain. This reinforces the previous conclusion that, at least under uniaxial tensile loading, the failure strain in the hybrids is controlled by the same process as in the all-carbon specimens even though the presence of the glass-reinforced plies allows some increase in the absolute value of failure strain, see fig. 42.

6. CONCLUSIONS

1. The programme of tests on epoxy specimens reinforced with plain-weave fabrics of carbon or glass in various lay-ups to give five different weight fractions, from all-carbon to all-glass, has been continued. Tests at an intermediate rate of $\sim$10/s have been completed and a further set of results for tests at a quasi-static rate of $\sim 10^{-3}$/s, has been obtained.

2. Following suggestions that the mechanical behaviour of the all-glass and the all-carbon specimens in the warp and weft directions might be different, tests have been performed in each of these directions at both the quasi-static rate and, using the modified gas-gun, also under impact loading and some variation in behaviour observed.

3. In the light of these tests previous results obtained at an impact rate of $\sim$1000/s (2) have been modified to distinguish between specimens loaded in the warp and the weft directions.

4. The complete set of results for the five types of specimen tested at the three different loading rates has been analysed and the data collated to show the effect of both hybrid composition (volume fraction of carbon reinforced plies) and applied strain rate on the initial modulus, the stress and strain at the limit of the linear elastic response and the stress and strain at failure (corresponding to the point of maximum load on the stress-strain curve). A limited hybrid effect is observed in specimens with a carbon volume fraction in the range 0.6 to 0.7. At all strain rates there is an enhancement of the failure strain over that for the all-carbon plies and an increased failure strength, most marked in the impact tests, over that predicted by the rule of mixtures.

5. Elastic quasi-static tests have been performed on all-glass and all-carbon specimens loaded in both the warp and the weft directions and in a direction at 45° to both warp and weft directions and values of the Poisson's ratio and the shear modulus obtained. Using these results the quasi-static two-dimensional stiffness matrix has been derived for each type of reinforcing ply.

6. Analytical predictions of the hybrid stiffness based on classical laminate theory and assuming the same properties in the warp and weft directions were developed in the second progress report. These have been modified to allow for the different moduli now observed in those two directions and using the experimentally determined stiffness matrices for the all-glass and the all-carbon plies predicted hybrid moduli have been obtained. These were found to agree well with both the experimental values of hybrid moduli and the rule of mixtures predictions.

7. FUTURE WORK

The present report describes progress on a programme of work under Research Grant No. AFOSR-85-0218. This programme continues for a further six months and then will be succeeded by a new Research Grant No. AFOSR-86-0031 entitled "Modelling of the Impact Response of Fibre-Reinforced Composites" which will combine a continuation of the experimental programme described in the present report with attempts to model the experimental results by numerical techniques, thus allowing the impact response to be predicted.

The next stages in the experimental programme under the present Research Grant will involve:

1. A determination of the quasi-static compressive strengths of the all-glass and the all-carbon plies, to allow a check on the analytical predictions of strength developed in the second progress report. It will also be necessary to confirm, probably in quasi-static tests, which are the warp and the weft directions in the two hybrid laminates.

2. A determination of both the stiffness matrices and the compressive strengths of the all-glass and all-carbon plies under impact loading. This will allow the check on the analytical predictions of strength and stiffness to be extended to composite response at these very high rates of strain.

Under the new Research Grant it is anticipated that the experimental programme will develop both as an extension of the present work and also along lines related to the analytical results from the numerical modelling studies. Amongst the former possible developments include:

1. A parallel series of tests to those described in the present report, at impact, intermediate and quasi-static strain rates, on specimens reinforced with plain-weave fabrics of carbon and kevlar and an examination of the failure processes by optical and scanning electron microscopy.

2. A study of the effects of different hybrid lay-ups with the same overall hybrid weight fraction on the tensile impact response and, in particular, to determine whether improved properties are obtained when the surface layers are glass rather than carbon reinforced.

3. A study of the effect of temperature on the tensile impact response of the various carbon/glass hybrids.

whilst amongst the latter it is hoped to undertake as soon as the analytical data are available,

4. An experimental study of the effects of variations in specimen design and in the loading-bar/specimen fixing arrangement in the light of analytical studies of the associated stress concentration factors with the aim of optimising the load transfer from the loading bars to the specimen, in particular for specimens with a unidirectional reinforcement geometry, so as to make possible the tensile impact testing of such materials.

8. ACKNOWLEDGMENT

This research was sponsored by the Air Force Office of Scientific Research, Air Force Systems Command, USAF, under Grant No. AFOSR-85-0218.